INVESTIGATION OF TSUNAMI INDUCED HAZARDS IN THE FLOATING DOCKS OF SEFERIHISAR SIGACIK MARINA BY NUMERICAL MODELING

A Thesis Submitted to
the Graduate School of
İzmir Institute of Technology
in Partial Fulfillment of the Requirements for Degree of

MASTER OF SCIENCE

In Civil Engineering

by

Hilal ÇELİK

September 2023
İZMİR

We approve the thesis of **Hilal ÇELİK**

Examining Committee Members:

Assoc. Prof. Dr. Bergüzar ÖZBAHÇECİ
Department of Civil Engineering, İzmir Institute of Technology

Prof. Dr. Utku KANOĞLU
Department of Aerospace Engineering, Dokuz Eylül University

Asst. Prof. Dr. Doğan KISACIK
Department of Civil Engineering, İzmir Institute of Technology

18 September 2023

Assoc. Prof. Dr. Bergüzar ÖZBAHÇECİ
Supervisor
Department of Civil Engineering
İzmir Institute of Technology

Prof. Dr. Cemalettin DÖNMEZ
Head of the Department of Civil Engineering

Prof. Dr. Mehtap EANES
Dean of the Graduate School

ACKNOWLEDGEMENTS

In the beginning, I must forward my deepest thanks to every person and organization that contributed to this thesis. They deserve my sincere thanks and respect for contributing significantly to the completion of this thesis.

First and foremost, I owe my supervisor a debt of gratitude, Assoc. Prof. Dr. Bergüzar Özbahçeci, whose unwavering guidance, expertise, and support have been instrumental throughout this research odyssey. Your insightful comments, constructive criticism, and commitment to excellence have influenced this thesis and my development as a researcher.

I would like to thank Prof. Dr. Ahmet Cevdet Yalçıner, Dr. Gözde Güney Doğan, Dr. Işıkhan Güler, Kadir Aktaş and Yağız Arda Çiçek for their contributions to my study.

I also extend my sincere thanks to the members of my thesis committee Asst. Prof. Dr. Doğan Kısacık and Prof. Dr. Utku Kanoğlu. Your valuable judgement, scholarly expertise, and constructive suggestions have enhanced this work and contributed to its overall quality. I appreciate the time and work you put into reading, analyzing, and contributing this thesis.

I would like to thank Yüksel Alkarem and Elif Girgin for their helps about Ansys AQWA.

I would like to express my sincere thanks to the staff and faculty at İzmir Institute of Technology. Their dedication to fostering a vibrant academic community, providing access to invaluable resources, and creating an environment that supports intellectual growth has been most appreciated throughout my studies.

I would also like to thank for the financial support in this research provided by TÜBİTAK. I was able to conduct the required research and finish this thesis with the help of this funding.

I am grateful to my friends, İbrahim Can Akgül, Deniz Özdoğan and Rabia Karagöz for their help and understanding.

I would also like to thank my dear friend Ekin Gültepe for her endless support and encouragement during the challenging moments of this research journey.

I also want to thank my husband Göktürk Karaca for his endless support in this thesis and being on my side on all the steps of this academic adventure.

I am deeply thankful to my family; my mother Sebahat Çay and her husband Celal Çay, my brother Alpagu Çelik and my father Orhan Çelik for their unconditional love, support, and encouragement during this thesis process. Their confidence in my abilities and constant motivation has been the driving force behind my academic pursuits.

In conclusion, without the amazing assistance and support from the people and institutions mentioned above, the completion of this thesis would not have been achievable. I am incredibly appreciative of their consistent encouragement, wisdom, and faith in my skills. Their combined efforts have shaped both this thesis and my own academic development.

ABSTRACT

INVESTIGATION OF TSUNAMI INDUCED HAZARDS IN THE FLOATING DOCKS OF SEFERIHISAR SIGACIK MARINA BY NUMERICAL MODELING

Tsunamis can cause significant damage to structures within the harbor due to the water level changes and strong currents they generate. The 6.6 Mw earthquake occurred near Samos Island on 30 October 2020 caused a tsunami due to vertical deformation of the sea floor. The tsunami caused heavy damage to the floating pontoons at Sigacik (Teos) Marina in Seferihisar. While there are numerous studies regarding the propagation of tsunamis, their run-up, and inundation distances, the damage caused by tsunami-induced water level changes and currents on floating pontoon docks with mooring chains has not been investigated yet. Numerical modeling is an important tool to calculate the loads and tensions acting on the floating structures in the time domain. In this study, dock A, which is the most damaged floating dock in Teos Marina, was numerically modeled using a mid-fidelity hydrodynamic model, ANSYS™ AQWA®. Initially, the stability of the floating dock was examined without the tsunami. Subsequently, the tsunami-induced water level changes and currents were introduced to the model. Displacements and rotations of the pontoons, tensions in the chains, and forces on the connections between pontoons were calculated. The safety factors for sliding and uplifting of the concrete anchorage blocks were examined and the stability conditions were checked. Results were compared with the observations of the Marina officials, eyewitnesses, captured photographs. Consequently, it was shown that chain breakages, pontoon connection failures, and the uplift of the concrete anchorage blocks could be simulated in the model.

ÖZET

SEFERİHİSAR SIĞACIK MARİNA YÜZER İSKELELERİNDE TSUNAMI KAYNAKLI HASARLARIN SAYISAL MODEL İLE ARAŞTIRILMASI

Tsunamiler neden oldukları su seviyesi değişimleri ve güçlü akıntılar nedeniyle liman içindeki yapılarda önemli hasarlar meydana getirebilirler. 30 Ekim 2020 tarihinde Sisam (Samos) Adası kuzeyinde meydana gelen 6.6 Mw büyüklüğündeki deprem, deniz tabanındaki düşey deformasyona bağlı olarak tsunamiye yol açmıştır. Tsunami Seferihisar'daki Teos Marina yüzer iskele pontonlarında ağır hasarlara neden olmuştur. Literatürde tsunaminin denizde ilerlemesi, kıyıda tırmanması ve baskın mesafeleri ile ilgili çok sayıda çalışma olmasına rağmen tsunami kaynaklı su seviyesi değişimlerinin ve akıntının, zincirlerle tabandaki tonozlara ve birbirlerine bağlı yüzer iskele pontonlarında oluşturduğu hasarın henüz incelenmediği görülmüştür. Tsunaminin yapılar üzerindeki hasar seviyesinin tespit edilmesi ve azaltılması için sayısal modelleme oldukça önem taşımaktadır. Bu çalışmada, Teos Marinada yer alan ve en çok hasar gören yüzer iskele olan A iskelesi orta doğruluklu hidrodinamik model, ANSYS™ AQWA® kullanılarak sayısal olarak modellenmiştir. Çalışmada öncelikle tsunami etkileri olmaksızın yüzer iskelenin stabilitesine bakılmıştır. Daha sonra tsunamiden dolayı oluşan su seviyesi değişimleri ve akıntı etkileri modelde yapıya etki ettirilmiştir. Yapının deplasman ve rotasyonları incelenmiş, zincirlerin gerilmeleri, ve pontonlar arasındaki bağlantılar üzerindeki kuvvetler hesaplanmıştır. Tonozlar için kayma ve yukarı kalkma güvenlik katsayılarına bakılmış ve stabilite durumları kontrol edilmiştir. Tüm bu sonuçlar tsunami sırasında ve sonrasında Marina yetkililerinin ve görgü tanıklarının gözlemleri, çekilen fotoğraflar ve yapılan ölçümlerle karşılaştırılmıştır. Buna göre, tsunami sırasında gözlendiği gibi, pontonların yükselip alçalması, zincirlerin kopması, ponton bağlantılarının kopması, tonozların yukarı çıkması modelde de simüle edilebilmiştir.

TABLE OF CONTENTS

LIST OF FIGURES

Figure **Page**

Figure **Page**

Figure **Page**

LIST OF TABLES

Table **Page**

CHAPTER 1

INTRODUCTION

1.1. Research Background and Problem Statement

Tsunami is a natural disaster that can have devastating effects. Since ancient times, tsunamis have been observed in the seas around Turkey, in fact, at least 96 tsunami waves have occurred in the past 36 centuries. These tsunamis mostly occurred in the Marmara Sea, the Aegean Sea and the Southwest Mediterranean. The impacts of the tsunami were further highlighted by the Kocaeli earthquake in 1999. Also, the Bodrum-Kos seismic tsunami was a significant event because of its increasing awareness of the tsunami threat in the Aegean Sea (Doğan et al., 2019). More recently the İzmir earthquake which occurred on 30.10.2020 in the north of Samos Island with a magnitude of 6.6 Mw (AFAD), generated a tsunami by creating a vertical strike-slip fracture. The tsunami impacts the west of İzmir which are Seferihisar, Urla, Çeşme, Karaburun and Güzelbahçe. According to the eyewitnesses, the tsunami causes the shoreline recedes up to 5-6 meters and afterward, it leads to the increasing free surface elevation in shallow water wave characterization and acting like an inundation and entering at a high speed. The tsunami resulted in significant coastal and port damage and caused the loss of one life.

Teos Marina in Seferihisar was severely impacted by this tsunami event. Teos Marina is one of the most important marinas in the Aegean Sea. The Marina consists of six floating docks moored with catenary chains, concrete block-type quay walls and a short rubble mound breakwater. Although there was almost no tsunami-induced damage in the quay walls and the breakwater, the floating docks in Teos Marina, were highly damaged due to tsunami hydrodynamic forces (GEER, 2020). It was observed that the mooring chains and fairleads were broken, and the pontoons were dragged offshore and were severely damaged as can be seen in Figure 1.1. Moreover, the aluminum frames of docks and the moored ships were drifted and damaged as can be seen in Figure 1.2.

Figure 1.1. Damaged pontoon due to the drifting.

Figure 1.2. Drifted floating dock and moored ships after the tsunami, in Teos Marina.

In recent years, application areas and uses of floating structures in marinas are significantly increased. Marinas are ports where marine vessels, and yachts can moor and provide for their needs. Marina construction not only contributes to increasing revenue from tourism, but it also provides the improvement of the nearby region, it offers business and job opportunities, new lifestyle and social amenities (Özkan, 2008).

Floating structures are designed against extreme forces due to the waves, winds, storms, and currents. Tsunami is one of the extreme conditions for floating structures and the structures are exposed to ultimate pressure and moments due to the tsunami. In the case of the marinas, tsunami can cause severe damage to structures and vessels, as well as being a risk to human life and safety.

The numerical modeling of the tsunami has a vital role for assessment of the hazards on floating structures, mooring lines and concrete blocks making connections from the chains to seabed. The numerical modeling can provide to determine the design conditions against tsunami impacts.

Despite the importance of numerical modeling for estimating tsunami hazards on floating structures, there is a lack of studies focusing on floating docks, particularly with mooring lines of chains. The literature survey shows that there is not any study that calculates damages on the floating docks with connected units and the mooring lines and the assessment of the damage due to the tsunami-induced currents using a hydrodynamic numerical model.

1.2. Aim and Scope of the Thesis

This study aims to investigate the hydrodynamic behavior of floating docks in Teos Marina under tsunami induced water level changes and currents using a numerical model

The main objectives of the thesis are:

1. Numerical hydrodynamic modeling of a floating dock in Teos Marina with connected units (pontoons) and the mooring lines,
2. Calculation of the responses and forces due to tsunami-induced currents and water level changes using the hydrodynamic numerical model .
3. Comparison of the calculated and observed damages and verification of the numerical model .

1.3. Outline of the Thesis

This thesis is structured as 6 chapters; Introduction, Literature Survey, Methodology, Numerical Modeling of Floating Pontoons in Teos Marina Under Tsunami

Induced Water Level Changes and Currents, Numerical Model Results and Discussions, and Conclusions.

A literature review of tsunami, floating docks, and floating docks hazards due to tsunami events are mentioned in Chapter 2.

The study area, properties of floating pontoons in Teos Marina, numerical modeling of the floating pontoons, and information about the numerical modeling tool ANSYS™ AQWA® is explained in Chapter 3.

How creates the tsunami effects which are water level changes and currents due to the tsunami, on the numerical model are expressed in Chapter 4.

Results and discussion from the numerical model are explained in Chapter 5, and conclusions are presented in Chapter 6, respectively.

CHAPTER 2

LITERATURE SURVEY

2.1. Tsunami

The Japanese word “tsunami” word is the composition of “tsu” and “nami” where “tsu” means that harbor and “nami” means that wave in Japanese language, so the “tsunami” word means that wave in harbor.

Some features and parameters of the tsunami is specified such as tsunami wave height, tsunami period, run-up height, inundation height, inundation travelling path inland, sea bottom topography and distance to the epicenter. The properties in past tsunamis are vital for the assessment of hazard and for planning and to take the precaution against the possible tsunami (Borrero et al., 2015).

Tsunami can be generated from the earthquakes, volcanic eruptions and submarine explosions like landslides, meteorite collisions (Kanoğlu et al., 2015). The earthquakes generally caused the tsunami by reverse fault type (Gupta and Gahalut, 2013, 2). The location, magnitude and depth of the earthquake is important for tsunami generation. The deformations in the sea bottoms cause the displacement of water mass which propagates as waves that refer as “tsunami”. The wave orthogonal spread and one part develops to the closest shore which is referred as local tsunami and other part propagates to offshore which is called tele tsunami (Lander et al., 2002). The tsunami in the deep water is noticed hardly due to the smaller wave height (Regina and Mohamed, 2022). The radiation of the waves causes spreading the energy from tsunami source.

The tsunami waves are different from the wind waves because there is translational motion which is the motion of a water mass; there is no oscillatory motion as the wind wave water particles do (Levin and Nosov, 2009, 82). As tsunami begins to propagate, the linear long wave theory can be considered for the waves (Sumer et al. 2007). When the waves start to come closer the shore, the wave height increases, the wave

celerity and wave length reduces and the waves start to feel the sea bottom and as a result, non-linear effects in the waves become more significant. The waves analyzed with nonlinear shallow water equations. In deep water, nonlinear terms can be neglected (Shuto, 1991).

The length of the fault rupture and slip determine the amplitude tectonic tsunamis. Typically, the energy from tectonic tsunamis radiates in a direction perpendicular to the length of the generating fault (Sumer et al., 2007).

According to the Technical Standards and Commentaries for Port and Harbor Facilities in Japan (2002), tsunami wave height can be estimated with employing the zero-upcrossing method like wind waves. For this case the estimated tide level is considered as the zero line and the wave height for every tsunami wave can be estimated by determining distance between the crest and the trough as shown in Figure 2.1.

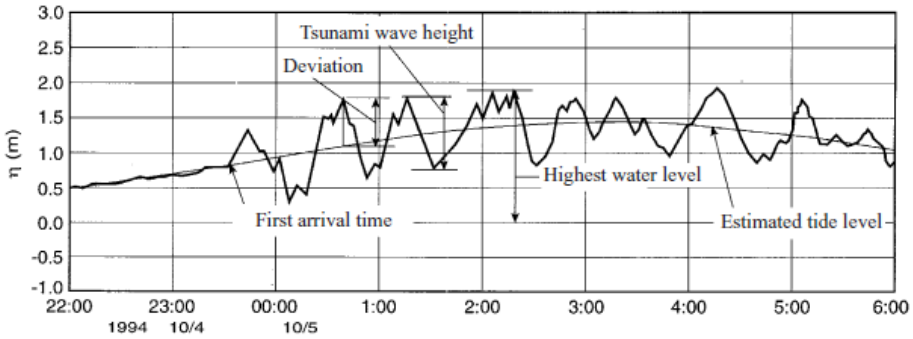

Figure 2.1. Tsunami wave height description (Source: OCDI, 2002)

The period of tsunamis is in a range between 5 and 60 minutes. Tsunami periods depend on the distance to epicenter, magnitude of the earthquake and also resonance properties of the harbor. It is essential to analyze tsunami with period that match the natural period of the harbor or bay in the design process. (OCDI, 2002). The matching of the periods and the transformations causes amplifications in tsunami height and more damages. The natural period of enclosed or partly enclosed basin, such bay, harbor or lake depends on its geometry.

According to the Technical Standards and Commentaries for Port and Harbor Facilities in Japan (2002), the tsunami waves experience mainly the wave transformations having significant changes such increase in wave height and flow velocity brought on by

a decrease in cross section area towards the bay's end and an increase in wave height owing to a seiche in the bay.

Tsunami waves have long wave periods and long wave lengths which are larger than water depths so it can be considered shallow water wave. When the tsunami waves start to close to coastline, their initial properties are predicted by linear long wave theory as definition in study of Synoklasis and Skjelbreia (1993). Nonlinear effects become prominent for the tsunami waves as increasing in the wave height and decreasing in the wave length.

Tsunami wave propagates by transmitting the energy between the water particles (Regina and Mohamed, 2022). Tsunami waves have higher wave length relative to water depth and this makes it defined as shallow water wave (González, 1999). As the tsunami wave comes to shallower regions, since the wave speed and wave length decrease, the transferring energy is obliged to hold in short wave length and it leads to increasing wave height (OCDI, 2002; Regina and Mohamed, 2022). Some part of the energy is disappeared.

The tsunami modeling is obtained by two ways which are shallow water equations and Boussinesq approach. The shallow water equations depend on Navier-Stokes equations. The water surface changes, and depth-averaged water particle velocities are determined by these equations. These equations suppose that there is pressure distribution as hydrostatic pressure all over and the distribution does not vary with respect to the depth (Özer and Yalçıner, 2011). It is observed that the vertical motions of the water particles do not impact on the pressure distribution and according to shallow water theory, the vertical acceleration of water particles in is neglected (Imamura et al., 2006). The governing equations of this theory are composed of conservation of mass and momentum, and they are described as,

$$\frac{\partial \eta}{\partial t} + \frac{\partial u}{\partial x} + \frac{\partial v}{\partial y} + \frac{\partial w}{\partial z} = 0 \tag{2.1}$$

$$\frac{\partial u}{\partial t} + u\frac{\partial u}{\partial x} + v\frac{\partial u}{\partial y} + w\frac{\partial u}{\partial z} + \frac{1}{\rho}\frac{\partial p}{\partial x} + \frac{1}{\rho}\left(\frac{\partial \tau_{xx}}{\partial x} + \frac{\partial \tau_{xy}}{\partial y} + \frac{\partial \tau_{xz}}{\partial z}\right) = 0 \tag{2.2}$$

$$\frac{\partial v}{\partial t} + u\frac{\partial v}{\partial x} + v\frac{\partial v}{\partial y} + w\frac{\partial v}{\partial z} + \frac{1}{\rho}\frac{\partial p}{\partial y} + \frac{1}{\rho}\left(\frac{\partial \tau_{xy}}{\partial x} + \frac{\partial \tau_{yy}}{\partial y} + \frac{\partial \tau_{yz}}{\partial z}\right) = 0 \qquad (2.3)$$

$$g + \frac{1}{\rho}\frac{\partial \rho}{\partial x} = 0 \qquad (2.4)$$

where; x and y are directions in horizontal and z represents vertical axis, u, v and w represent velocities of water particle in x, y and z directions, respectively, t is time, η is displacement of surface above the still water level in vertical direction, g is gravitational acceleration and τ_{ij} illustrates tangential or normal shear stress in the direction of i and on the normal plane j.

The governing equations can be solved by using boundary conditions. The boundary conditions are dynamic and kinematic conditions, and they are described as for free surface and bottom,

For $z = \eta$

$$p = 0 \qquad (2.5)$$

For $z = \eta$

$$w = \frac{\partial \eta}{\partial t} + u\frac{\partial \eta}{\partial x} + v\frac{\partial \eta}{\partial y} \qquad (2.6)$$

For $z = -h$

$$w = -u\frac{\partial h}{\partial x} - v\frac{\partial h}{\partial y} \qquad (2.7)$$

where h is water depth.

When employing the boundary conditions following equations are obtained:

$$\frac{\partial \eta}{\partial t} + \frac{\partial M}{\partial x} + \frac{\partial N}{\partial y} = 0 \qquad (2.8)$$

$$\frac{\partial M}{\partial t}+\frac{\partial}{\partial x}\left(\frac{M^2}{D}\right)+\frac{\partial}{\partial y}\left(\frac{MN}{D}\right)+gD\frac{\partial \eta}{\partial x}+\frac{\tau_x}{\rho}=A\left(\frac{\partial^2 M}{\partial x^2}+\frac{\partial^2 M}{\partial y^2}\right) \quad (2.9)$$

$$\frac{\partial N}{\partial t}+\frac{\partial}{\partial x}\left(\frac{MN}{D}\right)+\frac{\partial}{\partial y}\left(\frac{N^2}{D}\right)+gD\frac{\partial \eta}{\partial y}+\frac{\tau_y}{\rho}=A\left(\frac{\partial^2 N}{\partial x^2}+\frac{\partial^2 N}{\partial y^2}\right) \quad (2.10)$$

where D equals summation of h and η, M and N are discharge fluxes in x and y directions, respectively, τ_x and τ_y represent the bottom friction in x and y directions and A is the eddy viscosity (Imamura et al., 2006).

The fluid is assumed to be incompressible, inviscid and the surface tension is ignored.

The M and N, discharge fluxes are given as (Imamura et al., 2006),

$$M=\int_{-h}^{\eta} u dz = u(h+\eta)=uD \quad (2.11)$$

$$N=\int_{-h}^{\eta} v dz = v(h+\eta)=vD \quad (2.12)$$

Nowadays, utilizing the Nonlinear Shallow Water (NSW) equations has become the most popular method for tsunami modeling (Özer and Yalçıner., 2011).

Boussinesq approximation is the other method for tsunami modeling, and it can be utilized on nonlinear shallow water waves. Its condition is the wave length is bigger than seven times of water depth and the base advantages are that considering nonlinearities and dispersion effects (Regina and Mohamed, 2022). The nonlinearities in Boussinesq approximation can be explained by Ursell Number and it is given as (Barthélemy, 2004),

$$Ur=\frac{\varepsilon}{\sigma^2}=\frac{HL^2}{d^3} \quad (2.13)$$

where d is water depth, L is wave length and H represents wave height.

The Boussines equation with nonlinearities and involving the dispersive effects,

$$\frac{\partial^2 \eta}{\partial t^2} - gd\frac{\partial^2 \eta}{\partial x^2} - gd\frac{\partial^2}{\partial x^2}\left(\frac{3}{2}\frac{\eta^2}{d} + \frac{1}{3}d^2\frac{\partial^2 \eta}{\partial x^2}\right) = 0 \tag{2.14}$$

where η represents tsunami wave amplitude, t is time, g is gravitational acceleration and d is water depth (Regina and Mohamed, 2022).

The relation of dispersion can be described as,

$$C = C_s\left(1 - \frac{1}{3}(kd^2)\right) \tag{2.15}$$

where C represents local speed and equals to $\sqrt{gh}$ and C_s is speed of solitary wave and last part of the equation $\left(\frac{1}{3}(kd^2)\right)$ illustrates the relation of dispersive. According to Regina and Mohamed (2020) the wave celerity for shallow water is described as,

$$C = \sqrt{g(h+H)} \tag{2.16}$$

Boussinesq equations can be explained in several ways. Whitham (1974) obtains an equation which is derived from the original version of this approximation of Boussinesq (1872) with utilizing velocity potential. The approximation depends on Euler equations (Barthélemy, 2004).

It is assumed as,

$$\sigma^2 \ll 1 \tag{2.17}$$

However,

$$\sigma^2 \sim \varepsilon \text{ and } Ur \sim 1 \tag{2.18}$$

The equation is given as,

$$\eta_t + (h\bar{u})_x = 0 \tag{2.19}$$

$$\bar{u}_t + u\bar{u}_x + g\eta_x = \frac{h_0^2}{3}\bar{u}_{xxt} \tag{2.20}$$

The nonlinear, dispersive waves is offered by the Boussinesq equation,

$$u_{tt} - u_{xx} - u_{xxxx} + 2(u^3)_{xx} = 0 \tag{2.21}$$

The equation is defined the long waves motions in shallow water region and in one dimension with nonlinearities, is offered by Wazwaz (2007), (Jawad et al., 2013).

2.1.1. Tsunami Events in the History

The tsunami events worldwide have been devastating in many harbors, vessels, floating structures, and properties. The history indicates that some tsunami events especially have a catastrophic effect in the world. In 1755 Lisbon tsunami, which is one of the most devastating tsunamis in history, occurs in the Atlantic Ocean, and it was generated by an earthquake within the range of 8.5 Mw and 9.0 Mw (Gupta and Gahalaut, 2013, 21). It is estimated that the tsunami causes the loss of 10000 lives, and this is extremely high when considering the growing of the city (Baptista, 1996).

In 1868 a tsunami is generated in Arica (new Chile) due to an earthquake with a magnitude of 9.0 Mw and it has been severely damaged in this region. It also causes damage to New Zealand after the crossing over the Pacific Ocean and the effects in Lyttelton, New Zealand mentioned at Lyttelton Times under the caption "The Earthquake Wave at Lyttelton, 1868"which is cited by Lost Christchurch (Borrero et al., 2015).

The Peru-Chile border region has recently suffered many devastating tsunamis like the 1960 tsunami, all of which have a negative impact on the New Zealand Coast. (Goring and Borrero, 2015). The tsunami generated an earthquake with a magnitude of 9.5 Mw and a report was written about the devastating event, which destroyed Ancud, Maullin, and Corral harbors (Sievers, 1963). The disadvantage of these ports is to have more open bays than others. Horikawa's study involves the consequences of the 1960 Chile tsunami in Japan and mentions how the event's effects differed from near-field disasters. The difference is explained with resonance because of a match between the period of this tsunami and the base period of the relevant harbor in the report.

An earthquake with a magnitude of 9.2 occurred in the Prince William Sound region of Alaska in 1964 (Zhang et al, 2011). Seventy percent of the deaths in southern Alaska are due to the tsunami which was generated by enormous subsurface landslides (Brocher et al., 2014). The tsunami mainly affected the coastal region of Kodiak, Valdez, Seward, Cordova, Whittier, and there was severe damage to the infrastructure of this entire region (Wood and Peters, 2014).

The 2004 Indian Ocean tsunami which is generated by an earthquake with a magnitude of 9.0, is a devastating transoceanic tsunami and spreads outward in all directions. The devastating tsunami causes severe destruction of coastal communities in severel countries bordering the Indian Ocean. Indonesia, Thailand, Sri Lanka, India, Maldives, and Somalia were the nations profoundly affected by these tremendous events, resulting in the loss of more than 200 000 human lives (Fritz et al., 2006).

On 15 November 2006, an earthquake with a magnitude of 8.3 Mw happened in the center of Kuril Island and the tsunami was generated in Crescent City, California. The study of Dengler et al. (2009), mentions the powerful current due to the tsunami has a velocity of approximately more than 5m/s.

The trans-oceanic 2010 and 2011 tsunamis had a tremendous impact on harbors around the Pacific. On 26 February 2010 an earthquake of 8.8 magnitude in Maule, Chile. According to a study by Wilson et al. (2013), the earthquake generated tsunamis with a range between 0.6 and 2.8-meter tsunami wave heights on the California coast. The most affected regions from the destroying the 2010 tsunami are south part of Santa Cruz, Santa Barbara, Ventura, Mission Bay and Shelter Island, San Diego.

On 11 March 2011 an earthquake with a magnitude of 9.0 occurred on the east coast of Tohoku, Japan and the great earthquake generates a devastating tsunami that can reach a 39 m wave height and the highest inundation height is 19.5 m (Mori et al., 2011). The Japanese National Police Agency declared that totally of 15,854 people were died and 3,274 people presumed dead in March 2012 (Koshimura et al., 2014). At least 90% of this death is caused by the tsunami.

1755 Lisbon tsunami, the 2004 Indian Ocean tsunami and the 2011 Tohoku tsunami causes of lives and properties, so they make history with their immense damages.

As investigate the geographical distribution of tsunamis worldwide, it is recognized that most of them occur in the Pacific Ocean. It is stated in the study of Altınok and Ersoy (2000) that, more than 800 tsunami events were generated in the Pacific between A.D. 684 and 1994.

Tsunamis in the Atlantic and Indian Ocean also happened and caused immense damage such 1755 Lisbon tsunami, the 2004 Indian Ocean tsunami.

In addition, the eastern Mediterranean has experienced several destructive tsunamis in history. The Minoan Civilization was destroyed due to the tsunami which was generated by a volcanic eruption in Santorini (Altınok and Ersoy, 2000). The devastating eastern Mediterranean tsunamis have been the subject of many studies: Antonopoulos, 1979 Papadopoulos and Chalkis, 1983; Papazachos et al. 1985 (Altınok and Ersoy, 2000).

Most of the eastern Mediterranean tsunamis occurred in the Aegean Sea on Turkish shores. Turkey has been exposed often devastate earthquakes and their generating tsunamis with having coasts longer than 8000 km (Altınok, Ersoy, 1997).

Tsunamis in Turkey have also occurred in inland seas; the Marmara Sea and the Black Sea (Alpar et al.,2005). The tsunami generated by the İstanbul earthquake in 1509, in 1894, the eastern Marmara tsunami in 1963, and the İzmit Gulf tsunami (Yalçıner, 1999) can be given as examples of destructive tsunamis in the Marmara Sea. The tsunamis in the Marmara Sea are investigated for the last 2000 years in the study of Ambraseys (2002). The history of significant tsunamis in the Marmara Sea is also the subject of study by Yalçıner et al. (2002).

The Black Sea is the other inland sea on the Turkish coast. This region is exposed to tsunamis in history. These destructive tsunamis are namely of Black Sea tsunami in 1598, the Fatsa tsunami in 1939, Amasra tsunami in 1968. The Erzincan earthquake in 1939 generated a tsunami in the Black Sea even though its epicenter was not located in the Black Sea, which was determined by the Russian tide gauge during the earthquake (Alpar et al., 2005).

The list of tsunamis on the Turkish coast and tsunamis which have effects on Turkish shores is available in Altınok (2005). It is known that in the last 1000 years, 11

tsunamis in the Marmara Sea, 35 tsunamis in the Aegean Sea and 17 tsunamis in the eastern Mediterranean Sea happened (Ambraseys, 1962).

The 2017 Bodrum-Kos tsunami is a reminder of the risk of tsunamis in the Mediterranean Sea (Doğan et al., 2019).

The other recent reminder of the risk of tsunamis is the tsunami in Sığacık Bay, Aegean Sea, on 30 October 2020. The normal faulting earthquake which has a magnitude of 6.6 Mw (AFAD, 2020) in the north of Samos Island, generated a tsunami. The tsunami hit the Sığacık Coast and Samos Island and its strong currents caused to loss of one life and many injured people in Turkey (Anadolu Agency, 2020).

Damages caused by the tsunami and tsunami observations are described in a report about the Aegean Sea earthquake (GEER, 2020). The mentioned field survey involves determining the inundation height, tsunami run-up, and inundation distance and the purpose of the field observations is to state the tsunami effects on the coasts of İzmir and Samos Island. The tsunami has effects on Azmak Bay in Alaçatı, Zeytineli, Demircili, Altınköy, Sığacık, Akarca, Tepecik and Gümüldür. According to the eyewitnesses, the most damaged locations are Akarca region, Sığacık Bay and Teos Marina, Sığacık (Doğan et al., 2021(b)).

The field survey results contain tsunami inundation depths and distance, run-up measurements and hazards on the coastal structures (Doğan et al., 2021(b)). The maximum flood distance inland is estimated as 285 m in Akarca where the maximum run-up height was found as 3.82 m due to the tsunami. There is severe damage in the small fishing port. The maximum inundation distance is 415 m in Sığacık area and 552 m in Teos Ancient City, and the maximum inundation height was determined in Kaleiçi, Sığacık Bay, which was 2.31 m.

The tsunami effects were amplified in Teos Marina because the small bays with narrow entrances cause the amplification of tsunamis (Doğan et al., 2021(b)).

The flow depth in Teos Marina is estimated as 2.1 m which is based on watermarks on a garden fence as seen in Figure 2.2 that is taken from the field survey.

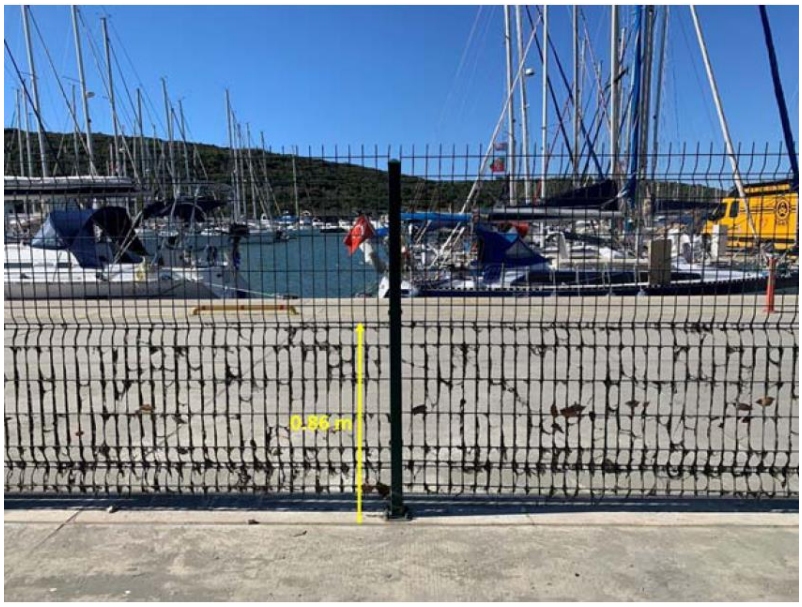

Figure 2.2. Tsunami marks on the garden fence in Teos Marina (Source: Doğan et al., 2020).

The Aegean Sea tsunami is numerically modelled by Heidarzadeh et al., 2021 and this model is compared with actual data in that study.

After the tsunami event, oscillations continued more than one day. This is described an unusual situation in the study of Doğan et al., (2021(b)). The other unusual case is that run-up heights during the tsunami reached to 3.8 m in Akarca. Normally, it is unexpected that tsunami generated by an earthquake with a magnitude of 6.6 Mw (AFAD, 2020) does not make this much run-up height (Heiderzadeh et al., 2021).

Heidarzadeh et al. (2021) claimed that the partially enclosed basin and abundance of islands in the Aegean Sea may cause to numerous wave reflections and long-lasting tsunami oscillations. Heidarzadeh et al. (2021) also recognize that duration of the tsunami is more than relatively expected for this much magnitude earthquake and the long oscillations and the late arriving of the big tsunami waves also contribute to have moe damaged on the coastal structures .

2.2. Floating Pontoons

Floating structures have started to take significant place in marine sector and coastal engineering. The pontoon-style floating structures are lighter, cheaper than the conventional fixed structure. They have also easier, quick and practical installation process, carrying and removing rather than the conventional. Since the condition of the soil or seafloor has no effects on these floating structures, differential settlement does not affect them arranged they are easily movable (Tajali, Shafieefar, 2011).They can handle hard environmental and marine conditions and offer an alternative of arrange the draft depth. Especially, floating pontoons can be useful where the exposed to tide wave because of arrangement their draft. They have many different uses in offshore projects, including offshore platforms, floating bridges (FB), floating piers (FP), floating breakwater (FBW), etc. These structures can composed of one or more pontoons which are connected by hinged or cables each other (Chen et al., 2016).

Williams et at. (2000) analyzed the motion of the submerged, moored and rectangular shape floating breakwater composing of two pontoons and the fluid motion solves in two dimension, with boundary integralequation method by utilizing Green's function. They investigate hydrodynamic properties under the assumption of linear wave and small amplitude wave theory and it is deduced that the reflection mainly depends on the draft and width of the pontoons, spacing between the pontoons and stiffness of the mooring line.

Tajali and Shafieefar (2011) investigate that hydrodynamic analysis of a floating multi-body pier having interaction with incident waves in frequency domain and motions caused the waves and response of the structure are analyzed with irregular wave concept. In this study single-body pontoon pier and several-body pontoons pier which are connected each other by hinge joints, are compared in different incident wave angles, wave frequencies and wave heights. The pontoons are mainly exposed to short waves. The study involves that determining mooring system and draft depth effects on response of the structure.

2.3. Damage of Floating Pontoons due to Tsunami Attacks

Coastal structures have been exposed and damaged due to tsunamis in history. Floating docks, that can be considered as remarkable structure today, can also be damaged due to the tsunamis.

Usage of the floating pontoons are continuously increased and they carry a vital role to make marine operations easier. Despite these important roles and increased usage of the floating pontoons, they should not be damaged by the tsunamis when sustainability is an important topic nowadays. In addition, if people are on the floating pontoons or in a marine vessel moored at the floating dock during the tsunami and if the floating dock is not designed with regarding the possible tsunami effects, the people may be injured or killed.

The one example of the damaged floating docks due to tsunamis in Kuji Port where is on the north-east of Japan. Floating docks had been damaged and partially sunken due to 2011 tsunami in Japan, which is generated by Great Eastern Japan earthquake in 2011 (Wiśniewski and Wolski, 2012).

The other example can be given in Santa Cruz Harbor. The floating docks in the Santa Cruz Harbor has been damaged due to 2011 Tohoku tele tsunami. It is observed floating dock system in Santa Cruz Harbor that typical hazards which involve loss and weak floatation, fractured whalers, cleats being dragged out from the pier and damaged pile guides (Keen et al., 2017).

The floating docks in Teos Marina were severely damaged due to the 2020 Aegean Sea tsunami. Especially the first floating dock located near to the entrance of the harbour affected more like the damaged floating dock near the entrance of harbour due to tremendous currents caused by 2006 Crescent City tsunami (Borrero et al., 2015). On the other hand, reasons of significant hazards on the floating docks at Crescent City, may be older docks and insufficient height of piles (Borrero et al., 2015) for the current loads due to the tsunami.

The field survey results which are given in Doğan et al. (2021), involve observations the damages to coastal structures such as ports, fishing ports and marinas. The observations in Teos Marina are important because comparison between the real data and acquired data from the numerical model is essential. There are six floating docks in Teos Marina. During this tsunami event four floating docks have been damaged, some of the concrete anchorage blocks which hold the mooring lines at the seabed, floated, some chains were broken as can be seen in Fig 2.3., most of the vessels sunk or were dragged..

Figure 2.3. Broken chain in Teos Marina due to the tsunami.

Floating docks of Teos Marina before and after the tsunami event are shown in Figure 2.4 and Figure 2.5.

Figure 2.4. Teos Marina before the tsunami (Source: Google Earth, Google Inc; received in 2023).

Figure 2.5. Teos Marina after the tsunami (Source: Doğan et al., 2021; photograph is taken from a ship owner).

Executive manager of the marina states that the marina was exposed to oscillations with taking approximately 4-5 hours and amplitude of 0.7 meters. He observed that sea receded 15 minutes following the earthquake and sea bed was seen at some locations. According to the eyewitnesses, the ropes that connects vessels to the docks, were broken and this created tremendous blasts. Some of the boats were aground and 5 minutes after the receding, huge waves made the severe currents and vortexes occurred in the marina. 25 minutes after the earthquake, water level increased by 2 meters' height above the still water level in the marina. The manager also mentioned that results of second wave were more destructive and had more severe damages (Doğan et al., 2021).

Keen et al. (2017) aimed at the estimation of hazard levels at the floating dock system in Santa Cruz Harbor, California, and their piles by using a "physics-based tool". This study is conducted with the concern of tsunami threat for small boat harbors on the West Coast of the United States after the 2010 Chile and 2011 Tohoku tsunamis. Their methodology depends on the demands and capacity of the floating docks, mooring elements, and moored vessels. Monte Carlo Based approach is used in that study to assess indefinite parameters such as current speed and direction and remain structural capacity of the system.

Keen et al. (2017) analyze the floating dock system with pile guides, and the demands and capacities of this system are calculated under the tsunami impacts. Damages of floating pontoons connected with chains under tsunami effects have not been studied. The thesis study aims to fill this gap in the literature.

2.4. Hydrodynamic Modeling Under Tsunami

In hydrodynamic Modeling, the modeling tools can be separated into three categories according to their fidelities. Low and mid-fidelity modeling tools use Potential Flow Theory.

For the early design stages, simple low-fidelity frequency-domain models can be used to simulate linear dynamics. Capytaine, WAMIT, HAMS can be given as examples of the low fidelity modeling tools.

Mid-fidelity software, often referred to as engineering tools, is used for global dynamics analysis, both in linear and nonlinear loads. Potential flow theory is used in the time domain. They allow the simulation of nonlinear subsystems. WEC—Sim, ANSYS AQWA are examples of the tools.

High-fidelity is generally used to solve specific nonlinear problems such as slamming loads due to extreme wave events and complex flow patterns. Navier-Stokes equations are used in these modeling tools with either grid-based or particle-based. Simulation of shallow water, nonlinear waves, breaking waves, complex fluid-structure interaction (FSI), and more accurate profiles can be obtained by these tools. OpenFOAM, DualSPHysics, Star-CCM+ are examples of these tools.

As given in Fig. 2.6 when the fidelity increases, the computational cost also increases.

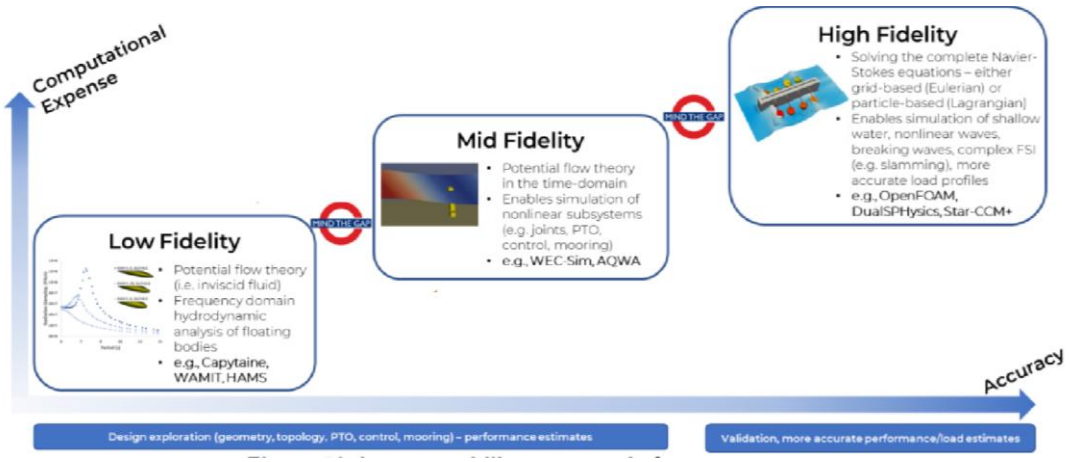

Figure 2.6. Description of low, mid, and high-fidelity hydrodynamic tools (Source: NREL, 2023).

In the literature, there are many works about hydrodynamic modeling under tsunami by using low and high-fidelity tools. Keen et al. (2017) is considered an example of low-fidelity work. In that study, the governing equations were used for the transverse and longitudinal forces on vessels to calculate the demand from the tsunami current and assess the damage. For high-fidelity works study of Pringgana et al. (2016) and Nistor et al. (2010) can be given as examples. In the study of Pringgana et al. (2016) SPH (Smoothed particle hydrodynamics)-based software DualSPHyics is employed with FE (Finite Element) analysis to simulate interactions between a tsunami bore and a timber structure. The impact pressure distribution is provided very specifically by the SPH models. The numerical pressure forecasts were also contrasted with semi-empirical design code pressure predictions. In the study of Nistor et al. (2010) SPH numerical model results and experimental results of extreme hydrodynamic impacts were compared. The goal of this research is to accurately estimate loads, propose and derive new formulations for the design of structures along the shore in tsunami-prone coastal areas, as well as to understand complicated hydrodynamic mechanics of the impact of high loadings on buildings.

However, there is no hydrodynamic modeling of tsunamis in mid-fidelity hydrodynamic modeling tool. Ansys AQWA is one of the mid-fidelity models. The accuracy of Ansys AQWA has been proved in various studies. There are many studies of modeling the Floating Offshore Wind Turbine (FOWT) by using Ansys AQWA. The study of Alkarem and Özbahçeci (2021) demonstrates enhanced agreement between the wave loading-calibrated model and the experimental data, especially in the LF (low frequency) region, according to the validation results. Ghafari and Dardel (2018) modeled a semi-submersible floating platform in Ansys AQWA under regular wave conditions. In that study, numerical results from AQWA and experimental results are compared, and it is stated that the results are in good consistent. In the research of Aktaş et al. (2018), AQWA created a hydrodynamic model of floating offshore platforms that are both semi-submersible and spar buoy platforms. The results were then compared to actual experiments and other simulation models. Results indicate that modeling can employ AQWA. In a study of Karimirad and Moan (2012) and Kim et al., (2015) Ansys AQWA also was used to model FOWT.

There are many studies modeling floating breakwaters with Ansys AQWA. In the study of Özbahçeci et al. (2018), floating breakwater performances were investigated with numerical modeling by using Ansys AQWA, and the numerical results were compared with the experimental results. This numerical model performs better in terms of economy and hydrodynamics.

It has been made known that it can be applied to the design of breakwaters. Samaei et al. (2016) compare the experimental results and numerical results from Ansys AQWA. In that study, there are two different models of floating breakwater (one of them includes simple and the other one includes step pontoon). The research shows a good correlation between numerical and experimental results. Zheng et al. (2023) verified the accuracy of the numerical simulation using Ansys AQWA by the verification of the amplitude response operator, mooring box, porous floating breakwater, and wave energy conversion device breakwater.

CHAPTER 3

RESEARCH METHODOLOGY: NUMERICAL MODEL SET-UP

3.1. Study Area

Teos Marina is in the coastal town of Seferihisar which is about 45 kilometers southwest of İzmir. Teos Marina, which is located on the Aegean Sea shore, provides expansive views of the coast and the surrounding landscape. The facility offers its residents a marina, a private beach, swimming pools, restaurants, cafes, a fitness center, a spa and other leisure amenities. Because of its luxury amenities, picturesque setting and proximity to historical monuments and natural attractions.

Teos Marina is a well-liked choice for people looking for a high-quality coastal living experience in Turkey so it has an important place for tourism. (Teos Marina, https://www.teosmarina.com.tr/kurumsal.html).

Teos Marina has a capacity of 400 ships, at sea and 80 ships on land. With a 75 tons travel lift, the boatyard at the marina provides towing and launching services for vessels up to 7.25 meters in width (Teos Marina, https://www.teosmarina.com.tr/teknik-servisler.html)

There are six floating docks such as A, B, C, D, E and F with 8000 m^2 lifting and launching area of Teos Marina (Teos Marina, https://www.teosmarina.com.tr/teknik-servisler.html) as seen in the general layout given in Figure 3.1.

Figure 3.1. The general layout of Teos Marina.

3.2. Properties of the Floating Pontoons

The floating docks can be produced in two forms; monobloc and multi-units. These can be made of reinforced concrete, steel, aluminum and polyethylene. The floating docks in Teos Marina are composed of multi-units called pontoons connected to each other by hinge type connections. The pontoons properties are provided by Turkish Ministry of Transport, General Directorate of Infrastructure Investments which was responsible from the design and the construction of Teos Marina. However, it is realized that Teos Marina was renovated in 2012 during a technical visit of Teos Marina. Although there were 5 floating docks with aluminium pontoons at the beginning, a new floating dock (Dock B) with concrete pontoons was added in 2012. In this thesis, floating dock A with aluminium pontoons is investigated since it was the most damaged one.

As can be seen in Figure 3.2, the pontoons are 2.5-m width and 11.5-m length. The total height of the pontoons is 0.598 m and their draft is 0.0859 m it is shown in Figure 3.5. Figure 3.3, 3.4 and 3.5 show the floaters from the bottom and sides. There are 12 floaters which have sizes of 1.829 meter and 0.61 meter and height of 0.406 meter. The floaters are kept together by aluminum frame and profiles. Wood is used as a deck

material on the aluminum dock as can be seen in Fig3.2. The floaters filled with polystyrene and their shell are made of polyethylene. The using polystyrene has a unit mass of 16 kg/m^3 and their compression resistance at 10% deformation is in a range of 160-224 kg/m^3. The shell material (polyethylene for rotational moulding) of the floaters has a tensile strength of 17.9 MPa and density of this material is 939 kg/m^3. The last (seventh) pontoon is shorter than other pontoons as seen in Figure 3.6 but it has same cross sectional geometry with others.

Figure 3.2. A pontoon used in teos marina.

The main compounds of floating docks are gangway, mooring chains and anchorages. The gangways are connection between the docks and quay walls. The mooring lines are chains in catenary configuration and concrete anchorage blocks are used for the anchorage system.

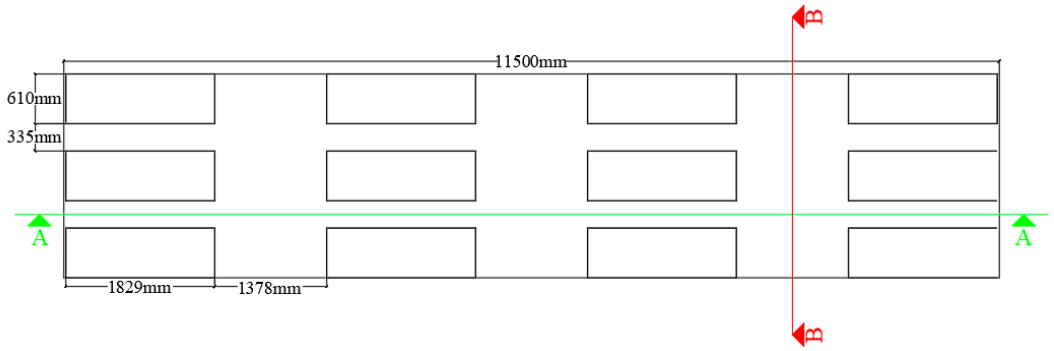

Figure 3.3. View of pontoon from the bottom.

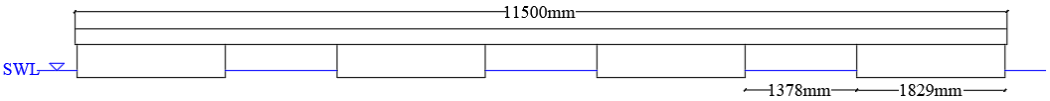

Figure 3.4. Sectional view of the pontoon from cutting plane A.

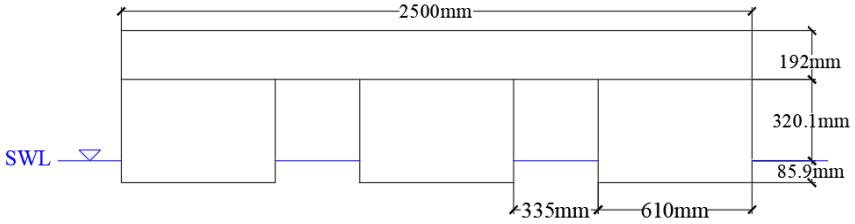

Figure 3.5. Sectional view of the pontoon from cutting plane B.

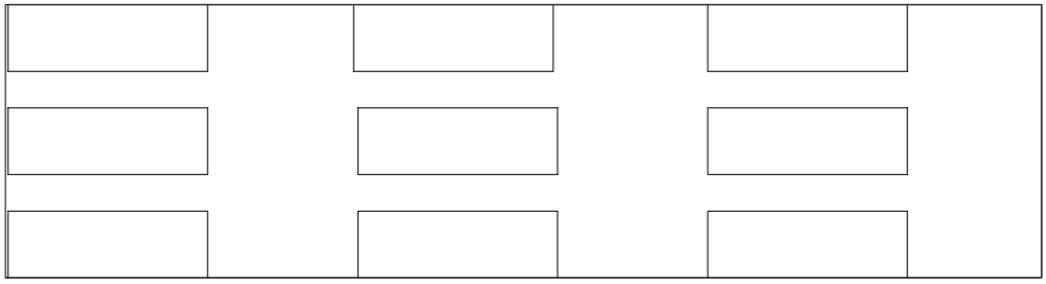

Figure 3.6. View of the seventh (the last) pontoon from the bottom.

As a mooring line, DIN763-studless chains with a diameter of Φ28 were used in the catenary configuration in Teos Marina as it shown in Figure 3.7. Their break load is 300 kN.

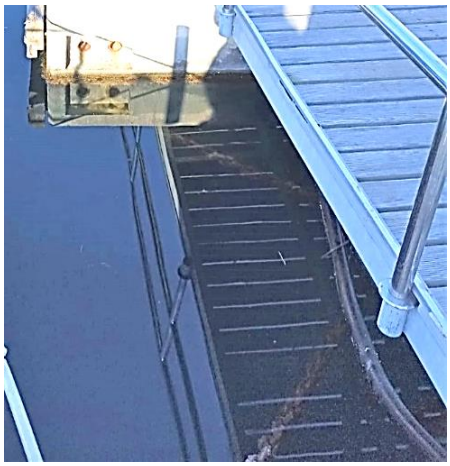

Figure 3.7. Mooring chains in Teos Marina.

As a mooring anchorage, 26 concrete anchorage blocks are used. Their horizontal dimensions are 2.438 m and 2.438 m and height of 0.305 m. The mass of the concrete anchorage blocks is 4532 kg, and details of used concrete anchorage block in Teos Marina are given in Figure 3.8.

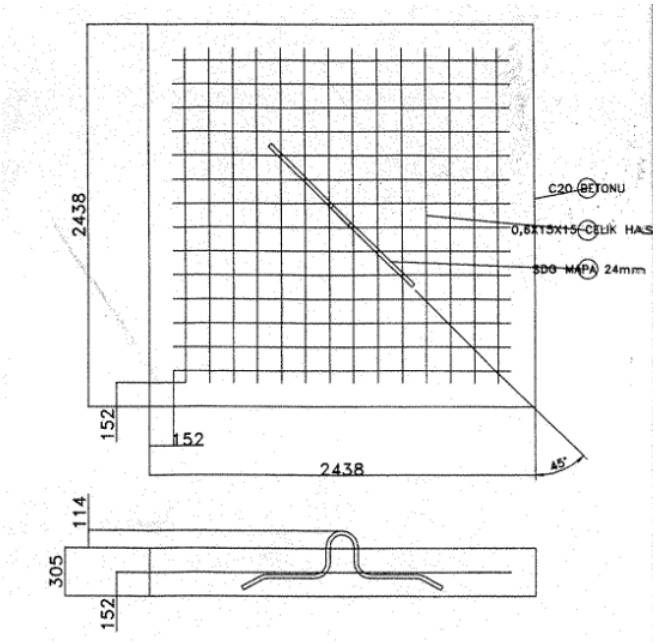

Figure 3.8. Details of the concrete anchorage blocks.

Steel ropes of 26mm called 6x36 (6 bundels, each of them has 36 wires as seen in Figure 3.9) are used to connect the pontoons. The break load of the ropes is given as 426 kN. Their stiffness is not known but calculated by assuming the maximum allowed rotation as 10° in the y-direction for the numerical model.

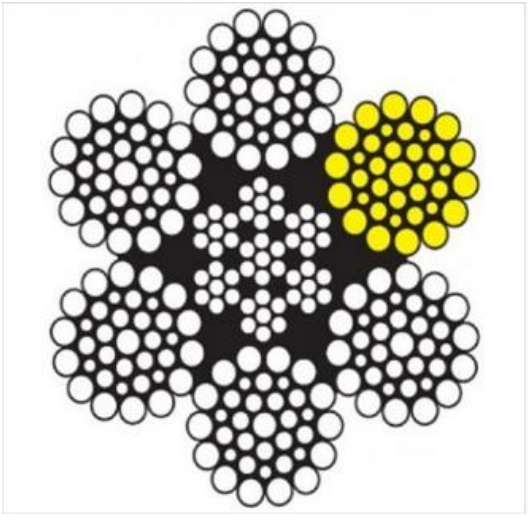

Figure 3.9. Steel ropes called 6x36 used for the connection of the pontoons.

3.3. Current states of the docks

Dock A is at the entrance of the marina, so it has the most damaged one due to the tsunami. Its length is 78.74 meters and it has seven pontoons. The first six pontoons' length is 11.5 meters and the last one is 9.5 meters. The width of all is 2.5 meters.

The fenders at this pontoon are made from wood and the distance between the pontoons is about 40 millimeters. The chains are connected to concrete anchorage blocks in catenary form. The pontoons are also attached to quay wall by chains as seen in Figure 3.10.

Figure 3.10. Gangway and connection chain between the quay and a floating pontoon.

After the tsunami aluminum pontoons in Dock A are replaced with concrete pontoons as shown in Figure 3.11. The reason may be that the dock B with concrete pontoons has the lowest damage caused by the tsunami. The new sizes of the concrete pontoon are 15 and 3 meters.

Figure 3.11. Renewed pontoon A after the tsunami.

Dock B is constructed in 2012 with concrete pontoons. It is the only dock without any damage caused by the tsunami. Plastic fenders which are about 30-35 millimeters, are used and the width of the pontoon is 2.4 meters. The general view of the dock B from the seaside is given in Figure 3.12.

Figure 3.12. Dock B from the sea.

Dock C has the same properties as the dock A and it is also replaced with concrete floating pontoons. Figure 3.13 shows the current view of the dock C.

Figure 3.13. Dock C.

After the damage due to the tsunami, docks D,E and F were repaired using the undamaged parts the old docks A and C which were replaced with the concerete pontoon units and chains were added. Pontoon's materials and geometrical properties are preserved.

The docks, D, E and F have the same geometry and materials, all properties remain identical as seen in Figure 3.14 and 3.15. Still these pontoons have wood covering on the aluminum dock with same draft and floaters and their widths are 2.5 meters.

The damaged dock parts have been repaired and assembled by the marina technical team, and a floating dock has been formed from these parts, as seen in Figure 3.16.

Figure 3.14. Dock D from the quay side.

Figure 3.15. Dock F from the sea side.

Figure 3.16. Repaired Dock with aluminum pontoons.

3.4. Hydrodynamic Modeling of Dock A using ANSYS™ AQWA®

ANSYS™ AQWA® is a suite of engineering software that are used to estimate the impact of waves, wind and currents on the floating or fixed structures and the response the structure due to these effects. It can be used to analyze structures such as spars, floating production storage (FPSO) systems, semi submersibles, tension leg platforms (TLP), marine vessels, renewable energy systems and coastal protection structures like breakwater design (Çekirdekçi, 2015). Engineers and designers use the software to simulate and optimize the performance of these structures, ensuring that to make an endurable structure design to harsh marine and environmental conditions (ANSYS Inc., 2020). The software also can simulate motions of the structure in time domain and frequency domain and the study consists of stability and dynamic analysis in time domain. The general utilizing formulas for time domain and frequency domain analysis is defined as,

$$[-\omega^2 M - i\omega C + K]U = F(\omega) \tag{3.1}$$

$$M\ddot{U} = F(t) \tag{3.2}$$

where M, C, and K are the structural mass, damping, and stiffness matrix in the size of 6×6, respectively and F is the combination matrix in the size of the 6×1 of all external forces as a function of frequency ω or time t. Also, U is the displacement matrix in the size of 6×1 and $\ddot{U}$ illustrates acceleration matrix .

Environmental conditions are crucial for design and analysis of coastal structures. These conditions are wave, wind and current.

In ANSYS™ AQWA® irregular or regular wave concept can be used. Regular wave data must involves wave period and wave amplitude. In deep and finite water ANSYS™ AQWA® can simulate by using Stokes Wave Theory and Airy Wave Theory. Regular waves which have a constant wave and period are the most fundamental type of monochromatic waves, according to Linearized Airy Wave Theory. The nonlinear terms and boundary conditions are neglected in Airy Wave Theory. Under the simplifications and assumptions that fluid is irrotational, inviscid and incompressible, the wave profile solution is obtained using the Laplace equation for an ideal fluid. The Laplace equation is divergence of gradient the velocity potential and it is described as,

$$\nabla \cdot \nabla\phi = \nabla^2\phi = \frac{\partial^2\phi}{\partial x^2} + \frac{\partial^2\phi}{\partial y^2} + \frac{\partial^2\phi}{\partial z^2} = 0 \tag{3.3}$$

The wave profile, η is described as:

$$\eta(x,t) = a\cos(kx - \omega t + \epsilon_0) \tag{3.4}$$

where, a is the wave amplitude, L is the wavelength, T is the wave period, t is the time, x is the cartesian coordinate in the horizontal axis, and ϵ_0 is the initial phase of the wave, k is the wavenumber, ω is the wave angular frequency and k and ω are decribed as,

$$k = \frac{2\pi}{L};\ \ \omega = \frac{2\pi}{T} \tag{3.5}$$

Analysis of irregular waves is difficult due to the complexity of irregular waves so considering that the irregular waves are composed of the infinite number of regular waves, is helpful to solution. It is represented the superposition the regular waves with different amplitudes and frequencies as mathematically in sinusoidal Equation 3.6

(Young, 1999, 20). The variance in the wave energy can explained by wave spectra concept. The energy distribution on the waves can be represented in frequency or in direction, it is called “frequency spectrum” and “directional spectrum”, respectively (Goda, 2000, 26). The spectrum deals with the incident how much waves in a direction or a frequency not when.

$$\eta(t) = \sum_{i=1}^{N} a_i \sin\left(w_i t + \Phi_i\right) \tag{3.6}$$

where a_i is the wave amplitude, w_i is the angular frequency which equals to ratio of 2π over wave period (T) and Φ_i is the wave phase angle. This Equation 3.6 yields on the sine function in time domain.

Irregular wave can be introduced to AQWA by entering characteristic wave height, period and wave spectra. The wave spectra can be defined by “Formulated Wave Spectra” such as; JONSWAP Spectrum, Pierson-Moskowitz Spectrum and Gaussian Spectrum or by “User Defined Wave-Spectrum”.

When the required spectrum is not yet accessible in AQWA, user defined wave spectra can be used (Ansys Inc., 2020). The inputs are arranged to frequency and corresponding spectral ordinate.

Irregular waves can also be introduced as surface profiles defined as a water level changes data in a time series .

According to Goda (2000, 257), the frequency spectrum, S(f) can be defined as,

$$S(f)df = \sum_{f}^{f+df} \frac{{a_i}^2}{2} \tag{3.7}$$

The time domain data convert to frequency domain and frequency spectrum is obtained by employing of the Fourier Transform Method (Massel, 2001).

The wave surface profile η in a time series can be adopted in the Fourier model as,

$$\eta(t) = \int_{-\infty}^{\infty} X(f) e^{iwt} dt \tag{3.8}$$

where X(f) is Fourier transform of wave surface profile and Euler's formula is described as,

$$\mathrm{e}^{\mathrm{iwt}} = \cos w\,t + i \sin w\,t \tag{3.9}$$

$$\eta(t) = \int_{-\infty}^{\infty} X(f)(\cos wt + i \sin wt) dt \tag{3.10}$$

The X(f), Fourier transform model can be described as,

$$X(f) = \int_{-\infty}^{\infty} \eta(t)(\cos wt - i \sin wt) dt \tag{3.11}$$

In addition to wave, wind data can also be entered as a constant wind or as a spectrum. A wind spectrum can be used to represent the frequency distribution of the varitions of wind speed. AQWA also allows, importing a time history of wind speed amplitude and wind direction (Ansys Inc., 2020).

Another environmental condition is the current which can bring about severe loads on coastal structures and moored vessels. Both uniform (constant current speed and direction in water depth) and profiled current data (varies current speed and direction in water depth) is available in AQWA (Ansys Inc., 2020).

ANSYS™ AQWA® can make a stability analysis as the structure in equilibrium position, involving static and dynamic aspects. The software consists of one or more floating structures which are affected by forces such as mooring lines, steady current and wind thrusters and wave drifting.

AQWA can compute the movements of structures in 6 degrees of freedoms which are composed of the three displacements (surge X, sway Y, heave Z) and three rotations (roll RX, pitch RY, yaw RZ), under the influence of gravity, hydrostatic, hydrodynamic,

wind, mooring and current loads in frequency and time domain. In equilibrium state, there are three translational and three rotational directions that should be checked with respect to origin at fixed reference axis for the structure. ANSYS™ AQWA® can produce a time-based simulation that comprises the motions of floating model connected by articulations or mooring lines. The six degrees of freedom of a pontoon in the project is given in Figure 3.17. The simulation considers the impacts of wave, wind and current forces and obtains the position and velocity of the structure at each step by integrating accelerations caused by certain time related forces. (ANSYS Inc., 2020)

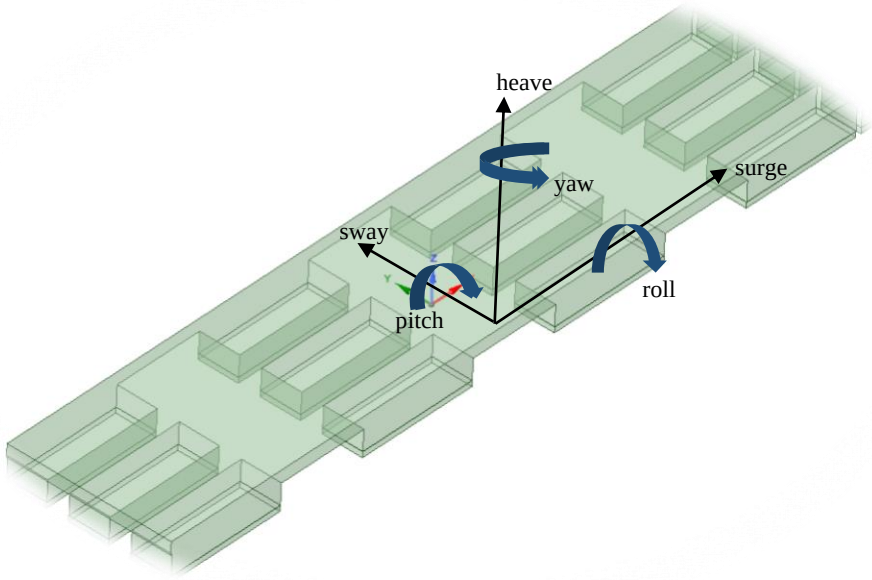

Figure 3.17. Degrees of freedom for one pontoon.

ANSYS™ AQWA® is formed by two solution systems; they are hydrodynamic diffraction and hydrodynamic response system. In hydrodynamic diffraction solution, hydrodynamic effects of more than one floating structure can be analyzed in three dimensions. Hydrodynamic response solution system uses data provided by diffraction analysis and hydrodynamic analysis of floating model is completed in frequency and time domain.

AQWA functionally involves calculation of diffraction and radiation forces, static and dynamic initial balance, analysis and design the effects of mooring systems, calculation of wave-induced shear force and bending moments, solutions with irregular waves in time domain.

Source Distribution Method

A coastal structure is exposed to hydrodynamic forces which are mainly composed of the body motions, water wave particles kinematics and the interactions with waves. The hydrodynamic forces can be separated as wave-induced loads, inertia loads and drag loads on a marine structure.

The wave exciting forces are considered as linear wave exciting forces and second order wave exciting forces. The linear wave exciting forces on a fluid can be separated into active and reactive forces. The active forces are wave-induced forces that are diffraction force and Froude-Krylov force. The reactive force is caused by the body resulting from motions radiation waves; it is referred as radiation force.

Froude-Krylov force is resulted the pressure impacts by undisturbed incident waves. Diffraction force results from pressure effects due to existence of the structure in the fluid-flow domain. The pressure effects caused by motion of body components in an ideal fluid creates hydrodynamic added mass and potential damping forces. Viscous drag force is a result of the pressure effects which are caused by the difference in velocity of the water particles and the body components (Chandrasekaran, 2018, 83).

Radiation forces are results from disturbed waves due to the structure motions (Ansys Inc., 2020).

The applied assumptions and conditions in ANSYS™ AQWA® are explained below.

The fluid is assumed to be Newtonian fluid that is inviscid, irrotational and incompressible fluid. Flow is irrotational when the vorticity equals to zero. The vorticity is curl of the velocity, it is described as,

$$\vec{\nabla} \times \vec{V} = \begin{vmatrix} \vec{\imath} & \vec{J} & \vec{k} \\ \frac{\partial}{\partial x} & \frac{\partial}{\partial y} & \frac{\partial}{\partial z} \\ u & v & w \end{vmatrix} = \left(\frac{\partial w}{\partial y} - \frac{\partial v}{\partial z}\right)\vec{\imath} - \left(\frac{\partial w}{\partial x} - \frac{\partial u}{\partial z}\right)\vec{J} + \left(\frac{\partial v}{\partial x} - \frac{\partial u}{\partial y}\right)\vec{k} \tag{3.12}$$

If the volumetric strain rate is zero, the flow is incompressible, it can be explained mathematically as,

$$\frac{1}{V}\frac{\Delta V}{\Delta t} = \frac{1}{V}\frac{dV}{dt} = \varepsilon_{xx} + \varepsilon_{yy} + \varepsilon_{zz} = \frac{\partial u}{\partial x} + \frac{\partial v}{\partial y} + \frac{\partial w}{\partial z} \tag{3.13}$$

To analyses the radiation and diffraction, the Linear Potential Flow theory is employed.

The motions are considered in the first order and in small amplitude. Employing the assumption of irrotational and incompressible fluid, it makes the continuity equation is provided by velocity potential. (Dean and Dalrymple, 1984, 43).

The physical states for every boundary are defined by velocity of fluids. The boundary conditions employing the small amplitude wave theory, are expressed below. If the conditions deal with water particle kinematics, then it is referred to kinematic boundary conditions.

The kinematic boundary condition is described as,

$$\mathrm{u} \cdot \mathrm{n} = \frac{-\frac{\partial F}{\partial t}}{|\nabla F|} \Big|_{F(x,y,z,t)=0} \tag{3.14}$$

$$|\nabla F| = \sqrt{\left(\frac{\partial F}{\partial x}\right)^2 + \left(\frac{\partial F}{\partial y}\right)^2 + \left(\frac{\partial F}{\partial z}\right)^2}$$

where F represents $F(x, y, z, t)$ which is mathematical definition of any surface and $\mathrm{u} \cdot \mathrm{n}$ is velocity component of the fluid in direction of normal to the surface. The kinematic boundary condition tells that when move with the surface the derivative of the surface with respect to time does not change.

If the seabed is considered impermeable, the velocity of bottom surface is zero $(\mathrm{u} \cdot \mathrm{n} = 0)$ whereas sometimes like when earthquake happens, the velocity must be involved. The bottom surface equation $F(x, z) = z + h(x) = 0$ for the two dimensions. The normal to the surface, n is defined for bottom boundary condition,

$$\mathrm{n} = \frac{\nabla F}{|\nabla F|} \Big|_{F(x,z)=z+h(x)=0} = \frac{\frac{dh}{dx}i + 1k}{\sqrt{\left(\frac{dh}{dx}\right)^2 + 1}} \tag{3.15}$$

Bottom boundary condition can be described as,

$$w = -u\frac{dh}{dx} \Big|_{z=-h(x)} \tag{3.16}$$

Free surface of waves is represented as equation of $F(x, y, z, t) = z - \eta(x, y, t) = 0$, where $\eta(x, y, t)$ is the wave profile. For the free surface kinematic free surface boundary condition is described as,

$$\mathrm{u} \cdot \mathrm{n} = \frac{\frac{\partial \eta}{\partial t}}{\sqrt{\left(\frac{\partial \eta}{\partial x}\right)^2 + \left(\frac{\partial \eta}{\partial y}\right)^2 + 1}} \Big|_{z=\eta(x,y,t)} \tag{3.17}$$

where n is,

$$\mathrm{n} = \frac{-\frac{\partial \eta}{\partial x}i + -\frac{\partial \eta}{\partial y}j + 1k}{\sqrt{\left(\frac{\partial \eta}{\partial x}\right)^2 + \left(\frac{\partial \eta}{\partial y}\right)^2 + 1}} \Big|_{z=\eta(x,y,t)} \tag{3.18}$$

The kinematic free surface boundary condition is obtained by the dot product of u · n,

$$w = \frac{\partial \eta}{\partial t} + u\frac{\partial \eta}{\partial x} + v\frac{\partial \eta}{\partial y} \Big|_{z=\eta(x,y,t)} \tag{3.19}$$

Dynamic boundary condition makes essential that the pressure on the free surface be uniform along the wave profile and it is stated with Bernoulli's equation,

$$-\frac{\partial \phi}{\partial t} + \frac{p_n}{\rho} + \frac{1}{2}\left[\left(\frac{\partial \phi}{\partial x}\right)^2 + \left(\frac{\partial \phi}{\partial z}\right)^2\right] + gz = C(t) \Big|_{z=\eta(x,t)} \tag{3.20}$$

where p_n has a constant value and mostly equals the gage pressure and it is taken as zero.

The lateral boundaries can be expressed with periodicity condition in space and time for waves, it is defined as,

$$\phi(x,t) = \phi(x+L,t) \tag{3.21}$$

$$\phi(x,t) = \phi(x,t+T) \tag{3.22}$$

where L is the wave length and T is the wave period.

For more details, study of Dean and Dalrymple can be read (Dean and Dalrymple, 1984, 41-69.)

The total potential velocity provides Laplace equation and boundary conditions. It is described as,

$$\phi(X,t) = \phi_I(X,t) + \phi_D(X,t) + \sum_{j=1}^{6} \zeta_j \phi_{R_j}(X,t) \tag{3.23}$$

where $\phi_I(X,t)$ is incident wave potential, $\phi_D(X,t)$ is wave potential from diffraction ζ_j is displacement of motion, $\phi_{R_j}(X,t)$ is wave potential due to radiation and j is for the six degrees of freedom which are surge, sway, heave, roll, pitch and yaw and X represents coordinates (Lin and Yang, 2020).

First order potential theory is used to compute active and reactive forces on floating or fixed structure. In ANSYS™ AQWA®, the velocity potential is mathematically represented as,

$$\phi(\vec{X},t) = a_w \varphi(\vec{X}) e^{-i\omega t} \tag{3.24}$$

where a_w is amplitude of incident wave, $\varphi(X)$ is space-dependent component, $\vec{X}$ is vector notations of the coordinates and ω is the incident wave frequency. The total velocity potential in the software is described as,

$$\varphi(\vec{X})e^{-i\omega t} = \left(\varphi_I + \varphi_d + \sum_{j=1}^{6} \varphi_{r_j} x_j \right) e^{-i\omega t} \tag{3.25}$$

where φ_I incident wave potential, φ_d wave potential due to the diffraction, φ_{r_j} is wave potential from the radiation due to motion of j[th] and x_j is three translational and three rotational motions of the center of gravity of the body due to the incident wave.

The incident wave potential for finite depth is expressed as in the AQWA,

$$\varphi_I(\vec{X})e^{-i\omega t} = -\frac{iga_\omega \cosh(k(Z+d))}{\omega \cosh(kd)} e^{i(-\omega t + k(X\cos\chi + Y\sin\chi) + a)} \tag{3.26}$$

The first order pressure hydrodynamic pressure can be found by utilizing linearized Bernoulli's equation,

$$p^{(1)} = -\rho \frac{\partial \phi(\vec{X}, t)}{\partial t} = i\omega\rho\varphi(\vec{X})e^{-i\omega t} \tag{3.27}$$

In AQWA the first-order hydrodynamic force and moment are mathematically defined as,

$$F_j e^{-i\omega t} = -\int_{S_0} p^1 n_j dS = \left[-i\omega\rho \int_{S_0} \varphi(\vec{X}) n_j dS \right] e^{-i\omega t} \tag{3.28}$$

where S_0 is wetted structure surface and n can be defined as,

$$\begin{aligned} \vec{n} &= (n_1, n_2, n_3) \\ \overrightarrow{r \times \vec{n}} &= (n_4, n_5, n_6) \end{aligned} \tag{3.29}$$

The total first order hydrodynamic force is,

$$F_j = (F_{Ij} + F_{dj}) + \sum_{k=1}^{6} F_{rjk} x_k, \qquad j = 1{,}6 \tag{3.30}$$

F_{Ij} is j[th] Froude-Krylov force caused the incident wave and it can be expressed as,

$$F_{Ij} = -i\omega\rho \int_{S_0} \varphi_I(\vec{X}) n_j dS \tag{3.31}$$

F_{dj} is j[th] diffraction force caused the diffraction wave and it can be expressed as,

$$F_{dj} = -i\omega\rho \int_{S_0} \varphi_d(\vec{X}) n_j dS \tag{3.32}$$

F_{rjk} is j[th] radiation force caused the radiation wave due to the k[th] rigid motion of the body and it can be expressed as,

$$F_{rjk} = -i\omega\rho \int_{S_0} \varphi_{rk}(\vec{X}) n_j dS \tag{3.33}$$

The total wave velocity potential depends on linear wave theory and the Laplace equation can be solved by employing Green's function. In the source distribution method, the floating structure model is divided into several equal grids (Lin et al., 2019).

In unstable hydrodynamic analyzing of floating structures utilizing a boundary-integral formulation, the presence of the irregular frequencies, leads to significant inaccuracies in the solution throughout a wide frequency range surrounding these frequencies (Ansys Inc., 2020). These inaccurasies result in sudden variations when the hydrodynamic coefficients are computed (Du et al.,2011). The situation is especially important if there are multiple structures having hydrodynamic interactions each other. There is no physical explanation for the irregular frequencies of the source distribution method, which coincide with the eigenvalues of the interior Dirichlet problem (Ansys Inc., 2020). The irregular frequencies causes the numerical problems because of these reasons, the irregular frequency must be taken out. To prevent the irregular frequency problem internal lid method is utilized in AQWA.

Mesh

The element size parameter determines the overall density of the created mesh. The results will be less precise when the larger element size is used. Nevertheless in Hydrodynamic Diffraction calculation, required memory and computational cost rise with the square of the quantity of the diffracting elements. Finding a balance between accuracy and processing expense may be necessary as a result. Whether the proper mesh properties are taken or not can be understood by controlling with volumetric displacements. AQWA calculate actual and equivalent volumetric displacements for modeled body. Both represent the displaced water volume by the body. The actual volumetric displacement depends on the mesh quality of diffracting body. Computation of the equivalent volumetric displacement is based on equivalence of buoyancy force and weight of the body. This can be described as,

$$\frac{W}{F_B} = \frac{\sum V_{body}\,\rho_{body}}{V_d\,\rho_{water}} = 1 \tag{3.34}$$

where W is total weight of the body, F_B is the buoyancy force, V_d is the submerged volume of the body. The displaced water volume equals to V_d,

$$V_{water} = V_d = \frac{\sum V_{body}\,\rho_{body}}{\rho_{water}} \tag{3.35}$$

The mesh quality influences the hydrostatic and hydrodynamic results of the model.

The model surface must be divided adequate number of quadrilateral or triangular panels. The panels have to completely cover the hull surface, specifically the portion of the mean wetted surface with no gaps or overlaps. The maximum panel size should be smaller than the one-seventh of the wave length (Ansys Inc., 2020).

There are a maximum of 60,000 nodes and 40,000 elements in the 64-bit Aqwa solver, of which 30,000 may be diffracting (Ansys Inc., 2020).

Hydrodynamic Second Order Wave Exciting Forces

The second order wave exciting forces are obtained by employing the Taylor series expansion of hydrodynamic pressure with second-order terms. The

$$p = p^{(0)} + p^{(1)} + p^{(2)} + O(\varepsilon)^{(3)} = -\rho \frac{\partial \phi}{\partial t} - \frac{1}{2}\rho \nabla\phi \cdot \nabla\phi - \rho g z \tag{3.36}$$

where $p^{(0)}$, $p^{(1)}$ and $p^{(2)}$ are expressed as,

$$p^{(0)} = -\rho g X_3^{(0)} \tag{3.37}$$

$$p^{(1)} = -\rho g X_3^{(1)} - \rho \frac{\partial \phi^{(1)}}{\partial t} \tag{3.38}$$

$$p^{(2)} = -\frac{1}{2}\rho \nabla\phi^{(1)} \cdot \nabla\phi^{(1)} - \rho \vec{X}^{(1)} \cdot \nabla \frac{\partial \phi^{(1)}}{\partial t} - \rho \frac{\partial \phi^{(2)}}{\partial t} - \rho g X_3^{(2)} \tag{3.39}$$

where the X_3 represents wave surface profile (η).

The total force and moment about the center of gravity of the structure is described as,

$$\vec{F}(t) = -\iint_{S(t)} p\vec{N}\, dS \tag{3.40}$$

$$\vec{M}(t) = -\iint_{S(t)} p(\vec{X} - \vec{X}_g) \times \vec{N}\, dS \tag{3.41}$$

where $S(t)$ is instant wetted body surface and $\vec{X}_g$ represents vector of center of gravity coordinates of the structure.

3.5. Benchmark Study

Before using the AQWA to model the floating dock under tsunami induced loads some benchmark study was performed.

The software is also used to model a floating pool shown in Figure 3.18. This structure is designed using 60 catenary chains with diameter of 36 mm. the orientation of the chains is given in Figure 3.19. The water depth is 8 m, and the tidal levels are ±0.4 m. Chains are designed for LWL (Low Water Level) which corresponds to 7.6m and they are tensioned at SWL (Still Water Level) and HWL (High Water Level) corresponding to 8m and 8.4m, respectively. The buoyancy forces and the average tensions at some critical chains for SWL condition are calculated using basic equations and the results are given in Table 3.1. Similar calculations are performed using Ansys AQWA and the force in the z direction and tension results are tabulated in Table 3.2 and Table 3.3, respectively.

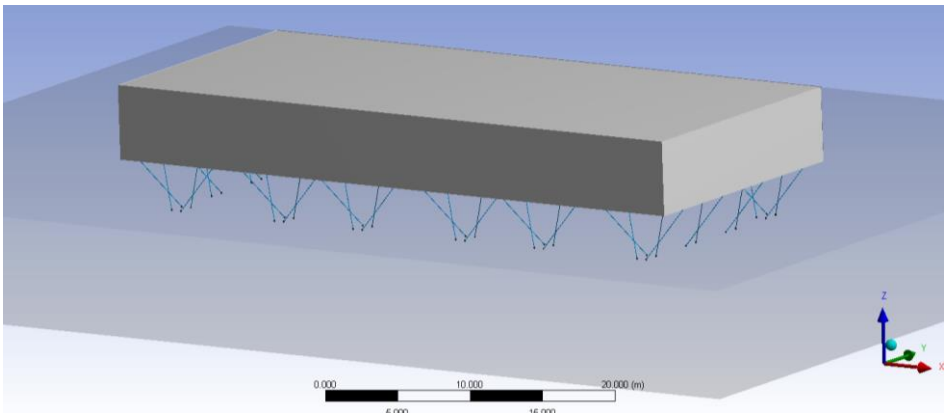

Figure 3.18. Modeled floating pool in Ansys AQWA.

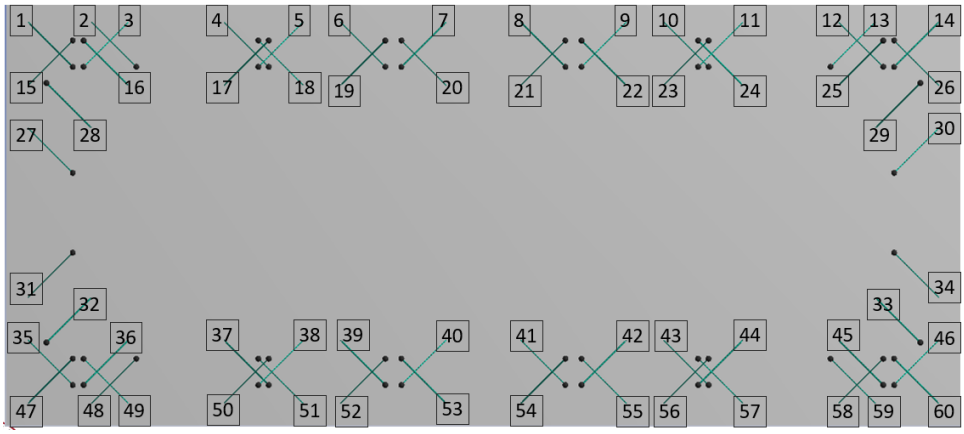

Figure 3.19. Orientation of chains and chain numbers of the floating pool.

Table 3.1. Calculated forces for water depth of 8 m (SWL Condition).

Fb(kN)	Fz(kN)	Tension(kN)
3619.89	60.33	78.76

Table 3.2. Numerical results of chain forces in the z direction for water depth of 8 m (SWL Condition).

	cable 12	cable 35	cable 15	cable 58	cable 14	cable 36	cable 16	cable 34	Average (kN)
Mean (kN)	-51.25	-70.37	-70.17	-51.22	-51.95	-71.12	-70.91	-51.90	-61.11

Table 3.3. Numerical results of chain tensions for water depth of 8 m (SWL Condition).

	cable 6	cable 12	cable 15	cable 29	cable 32	cable 40	cable 47	cable 58	Average (kN)
Mean (kN)	82.43	67.44	91.84	66.34	94	83.33	91.84	67.48	80.59

When Table 3.1 is compared with Table 3.2 and Table 3.3, the calculated forces in the z direction and tensions using basic equations and numerical results from AQWA are very close to each other.

The same comparison is done for a water depth of 8.4m. The calculated average forces in the z direction and tension are given in Table 3.4. The numerical results obtained from AQWA are given in Table 3.5 and Table 3.6.

Table 3.4. Calculated forces for water depth of 8.4 m (HWL Condition).

Fb(kN)	Fz(kN)	Tension(kN)
7239.78	120.66	157.51

Table 3.5. Numerical results of chain forces in the z direction for water depth of 8.4 m (HWL Condition).

	cable 12	cable 35	cable 15	cable 58	cable 14	cable 36	cable 16	cable 34	Average (kN)
Mean (kN)	-110.99	-129.86	-130.15	-111.03	-111.69	-130.60	-130.88	-111.78	-120.87

Table 3.6. Numerical results of chain tensions for water depth of 8.4 m (HWL Condition).

	cable 6	cable 12	cable 15	cable 29	cable 32	cable 40	cable 47	cable 58	Average (kN)
Mean (kN)	158.90	144.0	168.30	142.80	170.40	159.80	168.30	143.90	157.05

When Table 3.4 is compared with Table 3.5 and Table 3.6, the calculated and numerical results are in good consistency.

Wave force on the same floating structure is numerically obtained by using Ansys AQWA. The wave pressure is caused by wave characteristics such as wave amplitude of 0.125 m, wave period of 4 sec., and wave direction of perpendicular to the floating pool. The accuracy of the wave pressure results from Ansys AQWA is controlled by wave pressure formula which is given equations 3.42 to 3.48 (Goda, 2000, 135-136). Figure 3.20 and Table 3.7 illustrate the description of parameters used in Goda's wave pressure formulas and results according to Goda's Formula, respectively. The pressure is the highest at SWL as it is expected. The results and pressure distribution on the floating structure obtained from Ansys AQWA are given in Table 3.8 and Figure 3.21, respectively.

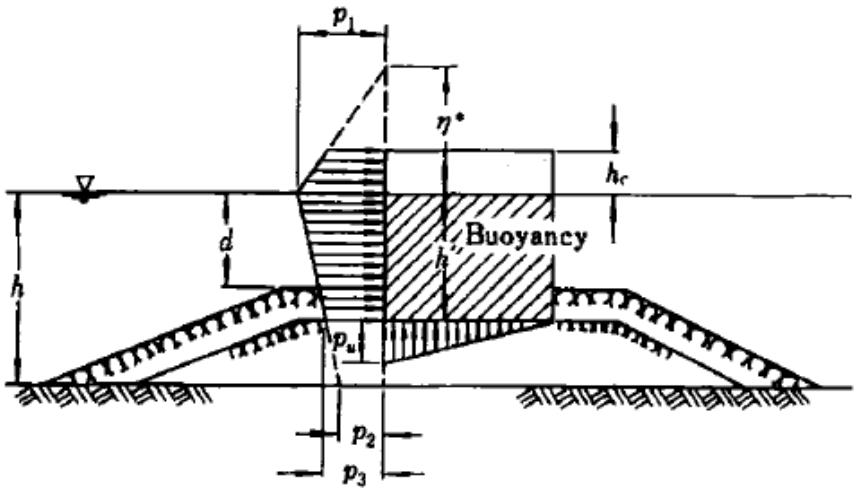

Figure 3.20. Description of parameters using in Goda's wave pressure formulas (Source: Goda, 2000,135).

The elevation that the wave pressure is applied to,

$$\eta^* = 0.75(1 + \cos\beta)H_{max} \tag{3.42}$$

where β represents the angle between the wave direction and normal to the structure.

The wave pressures on the front of the vertical structure,

$$P_1 = \frac{1}{2}(1 + cos\beta)(\alpha_1 + \alpha_2 \cos^2\beta)\rho g H_{max} \tag{3.43}$$

$$P_2 = \frac{P_1}{\cosh 2\pi h/L} \tag{3.44}$$

$$P_3 = \alpha_3 P_1 \tag{3.45}$$

where α_1, α_2 and α_3 are given in the following,

$$\alpha_1 = 0.6 + \frac{1}{2}\left(\frac{\frac{4\pi h}{L}}{\sinh\frac{4\pi h}{L}}\right)^2 \tag{3.46}$$

$$\alpha_2 = min\left\{\frac{(h_b - d)}{3h_b}\left(\frac{H_{max}}{d}\right)^2, \quad 2d/H_{max}\right\} \tag{3.47}$$

$$\alpha_3 = 1 - \frac{h'}{h}\left(1 - \left(1/\cosh\left(\frac{2\pi h}{L}\right)\right)\right) \tag{3.48}$$

Table 3.7. Results from wave pressure calculation by using Goda's wave pressure formula.

Hs(m)	0.25
T(s)	4
Hmax(m)	0.45
Tmax(s)	4
ß	0
d(m)	4.45
h=ds(m)	10
h'(m)	4.45
hc(m)	0.125
ds*(m)	10
hb(m)	10
L0(m)	24.96
h/L0	0.401
a1	0.6
a2	0.189
a3	0,626
P1(Pa)	**3571**
P2(Pa)	571
P3(Pa)	**2236**
η*	0,675
P4(Pa)	75131
hc*(m)	0,125
P(Pa)	17839.58
Pressure on x-z	Force on x-z
9217 Pa	405530N
	405.53kN

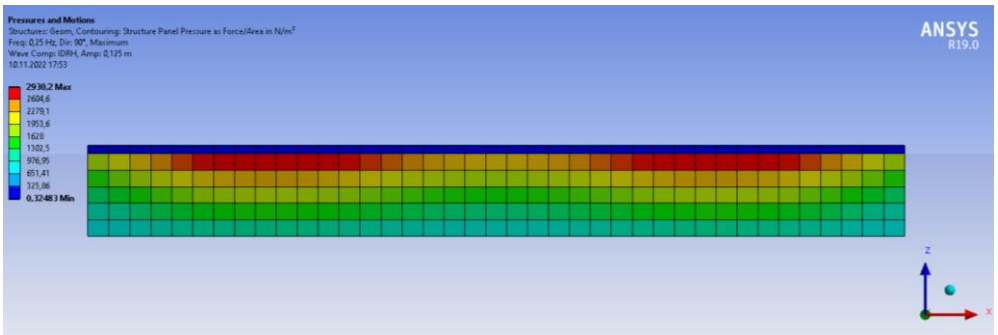

Figure 3.21. Wave pressure distribution on the floating structure (Ansys AQWA).

Table 3.8. Obtained numerical results by using Ansys AQWA.

Total pressure on x-z plane	368.28 kPa
Total force on x-z plane	369.72 kN

According to Table 3.7 and Table 3.8, the results are close to each other, so it verifies the accuracy of the software.

3.6. Modeling of the Floating Pontoons

The geometry of the model is obtained in SpaceClaim and the still water level is defined as a plane where the origin coordinates. The z component of the body is defined in an upward direction. In the study there are multiple floating bodies and all of them is defined as different structure. After the model is created, the mass properties are entered for each structure as seen in Table 3.9 and 3.10. Mass moment of inertias and radius of gyrations for first six pontoons and last (seventh) pontoon are given in Table 3.11 and 3.12, respectively.

Table 3.9. Mass of the pontoons.

Pontoon #	Mass(kg)
Pontoon #1	1179
Pontoon #2	1179
Pontoon #3	1179
Pontoon #4	1179
Pontoon #5	1179
Pontoon #6	1179
Pontoon #7	884,11

Table 3.10. Center of gravities.

Pontoon #	**X(mm)**	**Y(mm)**	**Z(mm)**
Pontoon #1	0	0	331,85
Pontoon #2	11540	0	331,85
Pontoon #3	23080	0	331,85
Pontoon #4	34620	0	331,85
Pontoon #5	46160	0	331,85
Pontoon #6	57700	0	331,85
Pontoon #7	67636,51	0	331,85

Table 3.11. Mass moments of inertia and radius of gyration for first six pontoons.

Ix(kg.mm^2)	Iy (kg.mm^2)	Iz (kg.mm^2)
642390637,9	1,3406E+10	9374734050
Kxx(mm)	Kyy(mm)	Kzz(mm)
738,1467279	3371,99327	2819,82772

Table 3.12. Moments of inertia and radius of gyration for last pontoon.

Ix(kg.mm^2)	Iy (kg.mm^2)	Iz (kg.mm^2)
526715241,2	7702004831	5618678533
Kxx(mm)	Kyy(mm)	Kzz(mm)
745,59488	2851,129	2435,1856

The environmental conditions are composed of the water depth, gravitational acceleration, and density of sea water. The water depth in Teos Marina is 4 meters, the gravitational acceleration, g is 9.81 m/s^2 and the sea water density, ρ is 1025 kg per m^3.

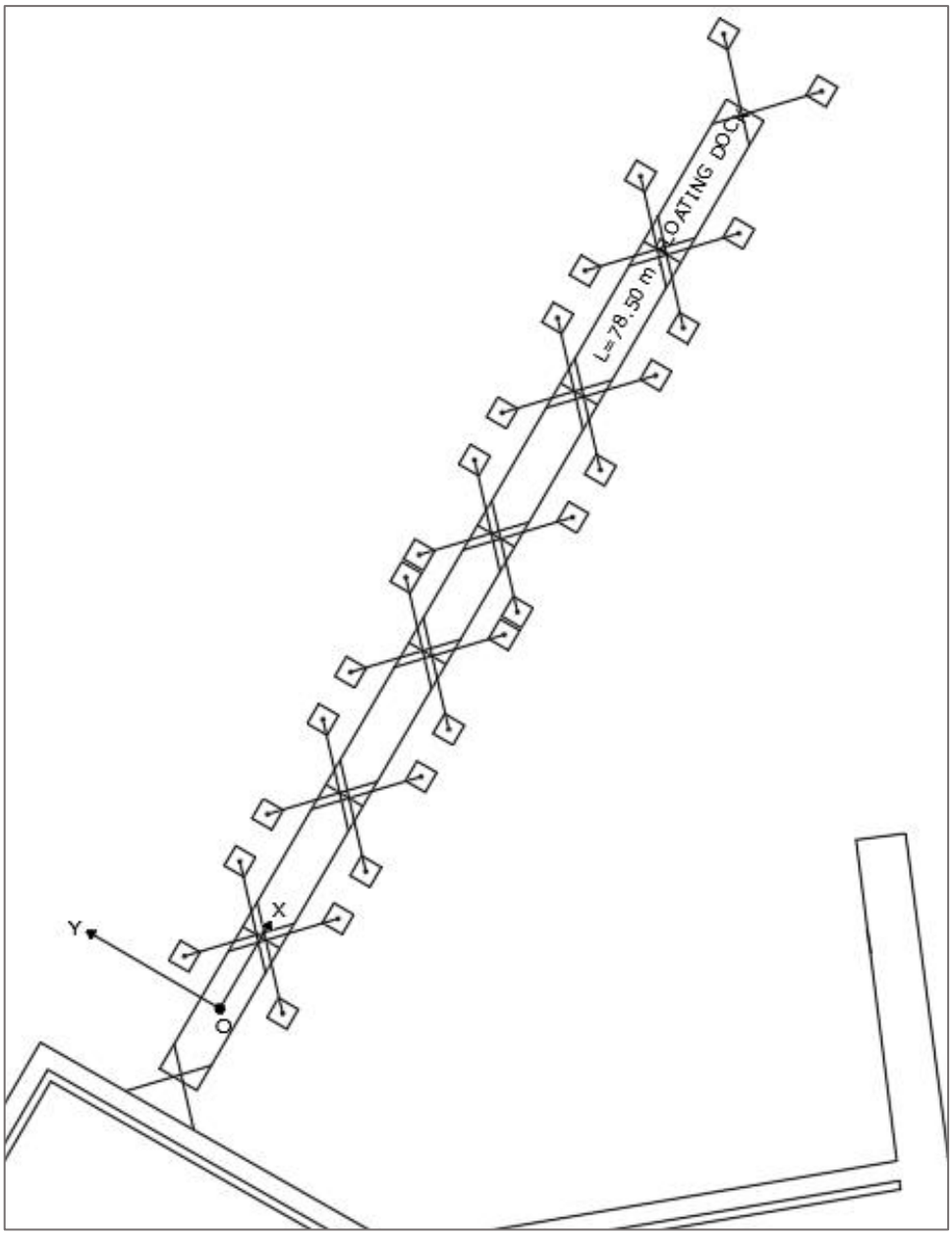

Figure 3.22. Layout of dock A in AutoCAD.

Figure 3.22 shows the AutoCAD drawing of the model. It is provided by the design company. The model geometry in AQWA is obtained based on this drawing, as can be seen in Figure 3.23.

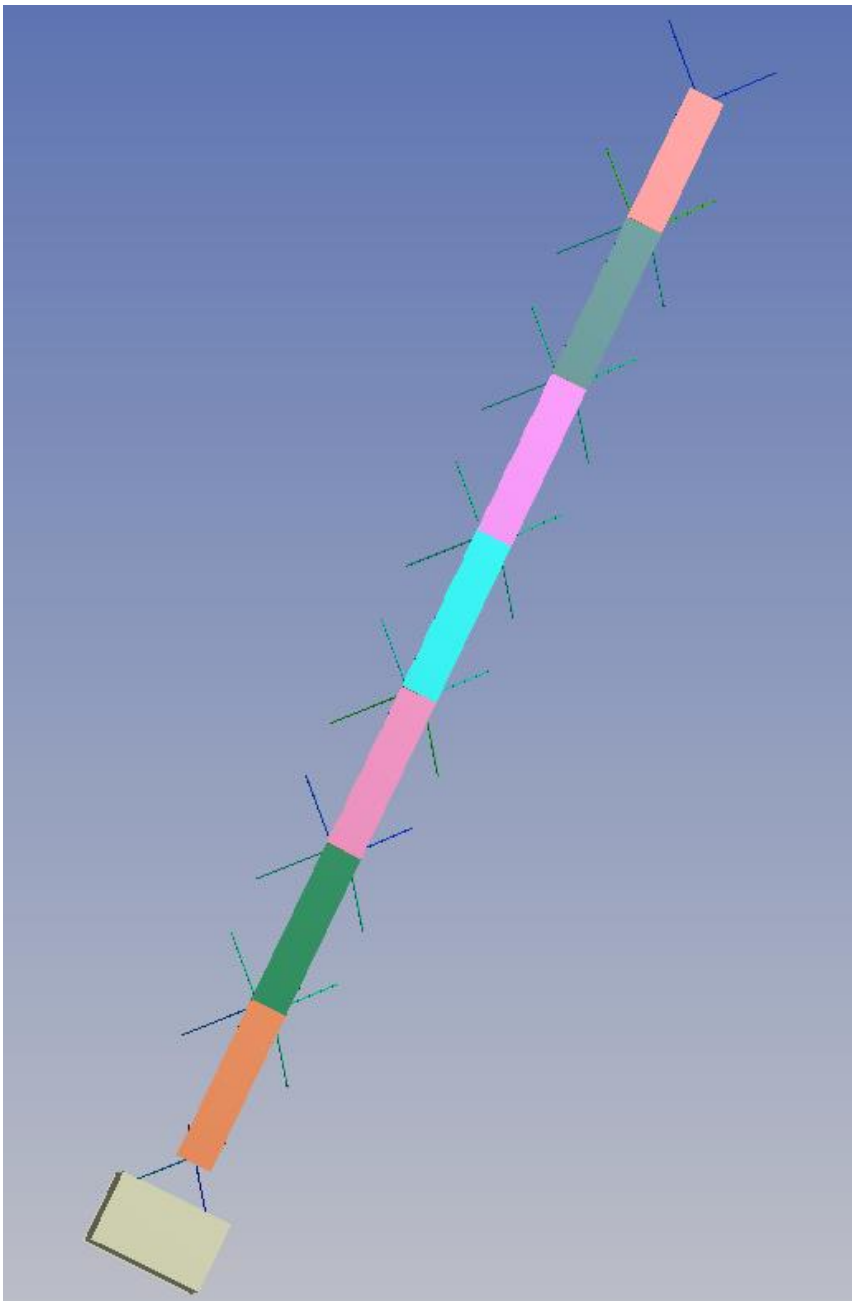

Figure 3.23. Floating pontoons modeled in AQWA.

To form similar conditions with the real application, a quay wall is also modeled, which is connected to the first pontoon by chains as seen in Figure 3.23. Different views of the model are given in Figure 3.24, 3.25 and 3.26 in x, -y, and z directions, respectively.

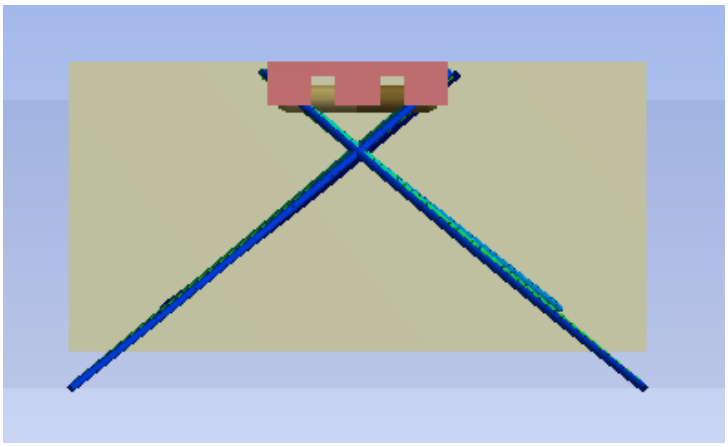

Figure 3.24. View of the model from the x-axis.

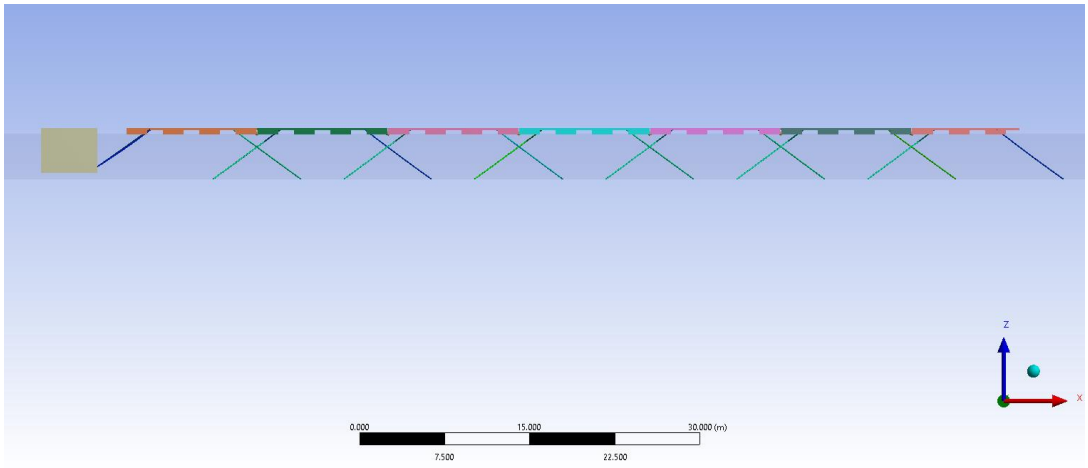

Figure 3.25. View of the model from the y-axis.

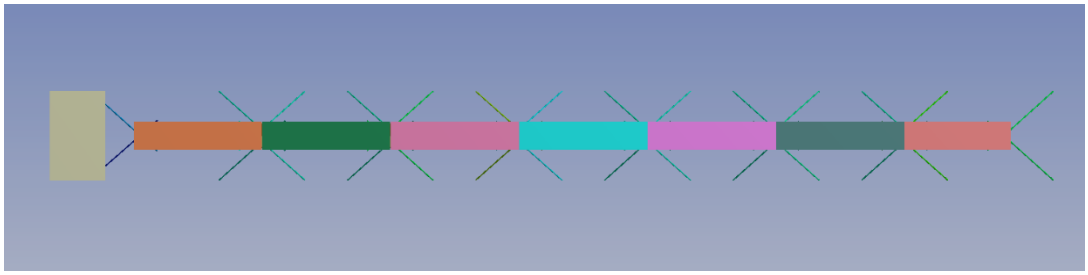

Figure 3.26. View of the model from the z-axis.

As it stated in Section 3.4, the mesh size can influence the hydrostatic and hydrodynamic results. Actual and equivalent volumetric displacements values in hydrostatic analysis can be very different if mesh sizes and properties are not appropriate for the model. The mesh properties using in this project are given in Table 3.13 and 3.14. The maximum element size is taken as 1 m. To get a balance between the computational cost and accuracy in the results, the most appropriate mesh properties are obtained by trial

and error, and entered in the software. The grids on the model can be seen in Figure 3.27. It is ensured that at least one grid is present on every surface of the model to provide accuracy and reliability.

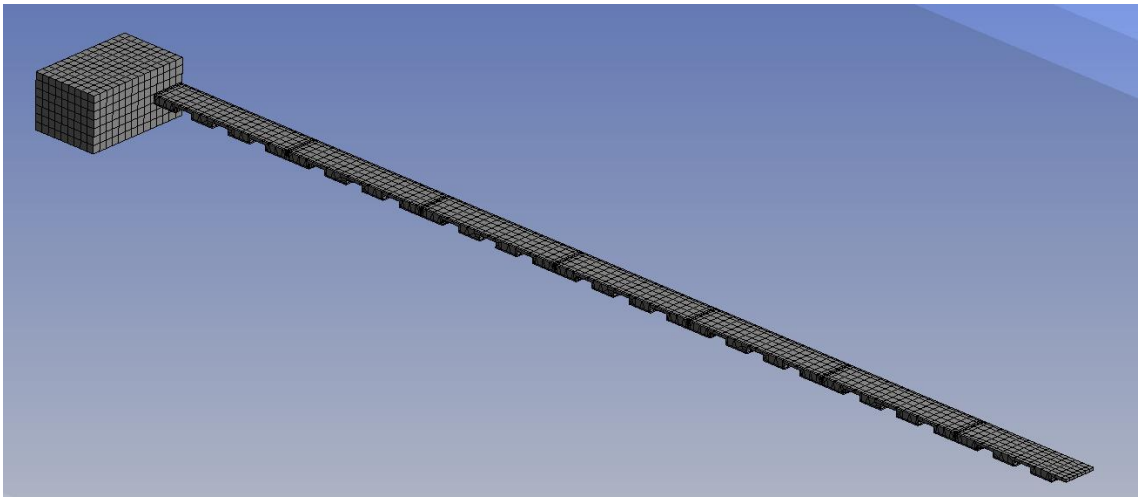

Figure 3.27. Meshed-based model.

Table 3.13. Details of Mesh.

Defeaturing Tolerance	0.5m
Maximum Element Size	1m
Maximum Allowed Frequency	0.619 Hz

Table 3.14. Generated Mesh Information.

Total Nodes	11851
Total Elements	12374
Diffracting Nodes	4868
Diffracting Elements	3953

Hydrostatic Analysis

The fluid loads that are exerted on a body when submerged in still water, which is called the hydrostatic force and moment.

The differentiation of hydrostatic pressure is expressed as,

$$dP_{hys} = \frac{\partial P_{hys}}{\partial x}dx + \frac{\partial P_{hys}}{\partial y}dy + \frac{\partial P_{hys}}{\partial z}dz \tag{3.49}$$

The hydrostatic pressure in x, y and z directions with Taylor series and employing the Newton's Second Law,

$$\begin{aligned} \sum F_x &= P_{hys}dydz - \left(P_{hys} + dP_{hys}\right)dydz = ma_x = (\rho dxdydz)a_x \\ \sum F_y &= P_{hys}dxdz - \left(P_{hys} + dP_{hys}\right)dxdz = ma_x = (\rho dxdydz)a_y \\ \sum F_z &= P_{hys}dxdy - \left(P_{hys} + dP_{hys}\right)dxdy - (\rho dxdydz)g = ma_z \\ &= (\rho dxdydz)a_z \end{aligned} \tag{3.50}$$

where ρ is sea water density, g is gravitational acceleration and a_x, a_y and a_z is acceleration in x, y and z direction, respectively.

The hydrostatic pressure difference in any direction is to be,

$$dP_{hys} = -\rho a_x dx - \rho a_y dy - \rho(g + a_z)dz \tag{3.51}$$

For static case, the acceleration in all components is zero. They can be mathematically shown as,

$$\begin{aligned} \frac{dP_{hys}}{dx} &= 0 \\ \frac{dP_{hys}}{dy} &= 0 \\ \frac{dP_{hys}}{dz} &= -\rho g \end{aligned} \tag{3.52}$$

The z component of Equation 3.45 takes the integral for both sides,

$$\Delta P_{hys} = \rho g \Delta z \tag{3.53}$$

The hydrostatic pressure changes in vertical direction and depends on the unit weight of sea water.

The hydrostatic force is found by integrating the hydrostatic pressure.

$$F_{hys} = \int_A P_{hys}\, dA = \int_A \rho g Z\, dA \tag{3.54}$$

where, Z is vertical coordinate of the wetted surface point and A is the surface area that hydrostatic pressure acting on it. Because it is assumed that the fluid is incompressible the density of sea water does not change. The hydrostatic moment is described as,

$$M_{hys} = \int_A \rho g Z r\, dA \tag{3.55}$$

where r is the moment arm that is distance between resultant force acting point and center of gravity of the pontoon. The hydrostatic moment is calculated with respect to the center of gravity of the body (ANSYS™ AQWA® Theory Manual, 2020).

It is essential to determine appropriate dimensions of pontoons, required freeboard and being stableof pontoons against to external forces and loads for design of the pontoons. These external forces and loads are static load, live load, dead load, hydrostatic pressure, reaction forces of gangways and counterweights due to wind, wave, current.

The freeboard is calculated as,

$$h' = d - \frac{W_1}{\gamma_w A} \tag{3.56}$$

where h' is freeboard, d pontoon height, W_1 is pontoon weight, γ_w is unit weight of water and A is horizontal cross-sectional area of pontoon.

The pontoons transfer the wind load to mooring chains and because of this the pontoons have to be designed to resist the wind load.

The articulations, mooring chains and anchorage or concrete anchorage blocks at the seabed must have required capacity for these loads and forces.

The metacentric height is an important value to determine whether floating structures and vessels are stable or not. It is crucial for stability of free-floating structures, and it is illustrated in Figure 3.28.

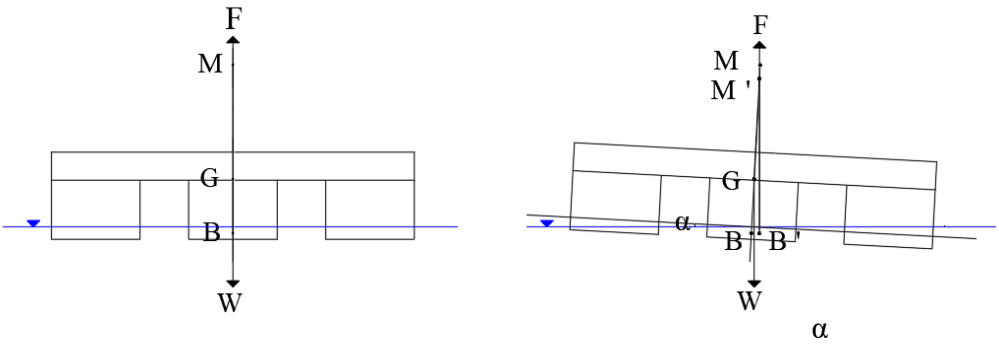

Figure 3.28. Metacentric height illustration on the pontoon.

W the is weight of the pontoon, F is the buoyancy force, G and B letters represent center of gravity and center of buoyancy force of the pontoon and M metacenter height.

As shown in Figure 3.28, the vertical forces are weight of the pontoon and buoyancy force. To satisfy the equilibrium state for the free-floating pontoons the static conditions are satisfied. One of them is that the weight must be equal to the buoyancy force. Displacement water is calculated as,

$$\nabla = (1.829m)(0.610m)(0.0859m)(12) = 1.15m^3 \tag{3.57}$$

The buoyancy force is determined as,

$$F_B = \nabla . \rho . g = (1.15m^3)\left(1.025\frac{t}{m^3}\right)(9.81m/s^2\ ) = 11.56\ tf \tag{3.58}$$

$$W = F_B = 11.56\ tf \tag{3.59}$$

The mass of the pontoon is calculated from the equivalence, and it is determined as 1179 kg.

The other static condition for the equilibrium state is the total moment about the center of gravity of the pontoons is zero. The moment due to buoyancy force can be represented with the hydrostatic moment, M_{hys}. These moments can be described as,

$$M_{hys} + \sum(X_j - X_g)m_{X_j} = 0 \tag{3.60}$$

where X_j is coordinates of j points, X_g is coordinates of center of gravity and m_{X_j} is mass at location X_j.

When the pontoon is tilted a little bit, the new center of buoyancy force is B' and M' is new metacenter which is intersect point of weight and buoyancy force. If the pontoon is more tilted the center of buoyancy is shifted to the right, GM' distance will be smaller and finally it is negative, so the structure is unstable.

According to OCDI (2002), the pontoon is exposed to a uniformly distributed load, if the metacentric height formula is satisfied for stability case, the pontoon is considered to be stable. This formula is given,

$$\frac{\gamma_w I}{W} - \overline{BG} > 0 \tag{3.61}$$

where I is moment of inertia of pontoon's area with respect to water cut plane, W is weight of the pontoon and uniformly distributed load and $\overline{BG}$ is distance between center of buoyancy and gravity.

To determine the geometrical moment of inertia, first the geometrical moment of inertia at center of gravity axis for each pontoon.

$$I_{xG} = \int_{-\frac{a}{2}}^{\frac{a}{2}} y^2 dA = (b)\int_{-\frac{a}{2}}^{\frac{a}{2}} y^2 dy = \frac{(b)y^3}{3} \Big|_{-\frac{a}{2}}^{\frac{a}{2}} = \frac{ba^3}{12} \tag{3.62}$$

When parallel axis theorem is applied, the moment of inertia at water level cut plane is calculated as,

$$I_{x;} = I_{xG} + Ad^2 \tag{3.63}$$

The calculated moment of inertias for all floaters is given in Table 3.15.

Table 3.15. Moment of inertias of area for all floaters.

Floater number	b(m)	a(m)	d(m)	Ad^2 (m^4)	I_x (m^4)
1	1.829	0.61	0.945	0.996	1.031
2	1.829	0.61	0	0	0.035
3	1.829	0.61	0.945	0.996	1.031
4	1.829	0.61	0.945	0.996	1.031
5	1.829	0.61	0	0	0.035
6	1.829	0.61	0.945	0.996	1.031
7	1.829	0.61	0.945	0.996	1.031
8	1.829	0.61	0	0	0.035
9	1.829	0.61	0.945	0.996	1.031
10	1.829	0.61	0.945	0.996	1.031
11	1.829	0.61	0	0	0.035
12	1.829	0.61	0.945	0.996	1.031
				∑	**8.386**

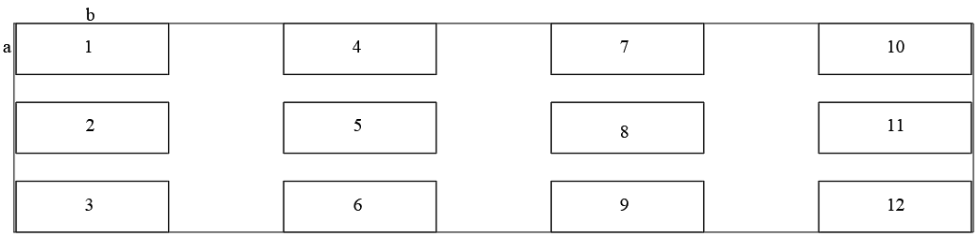

Figure 3.29. Floaters' numbers.

The metacentric height is calculated as 6.92 m which is provided stable of the pontoon. The floater number are illustrated in Figure 3.29.

When the pontoon is exposed to an eccentric load the $\tan\alpha$ provides this formula (OCDI, 2002),

$$(W_1 + P)\left[\frac{b^2 \tan\alpha}{12d\cos^2\alpha)} - \left[\frac{b^2}{24d}\tan^2\alpha + c - \frac{d}{2}\right)\right]\tan\alpha\right] - P[a + (h - c)\tan\alpha] = 0 \quad (3.64)$$

If $\tan\alpha$ is satisfied the below conditions, the pontoon can be considered as stable,

$$\tan\alpha < \frac{2(h-d)}{b} \tag{3.65}$$

$$\tan\alpha < \frac{1}{10} \tag{3.66}$$

where W_1 is weight of the pontoon, P is total eccentric load, b and h is the width and height of the pontoon, respectively, d is the draft of the pontoon when the eccentric load is employed at center of the pontoon, c is the center of gravity of the pontoon from the bottom, a is deviation of the eccentric load from the center axis of pontoon and α is the inclination angle of the pontoon as illustrated in Figure 3.30.

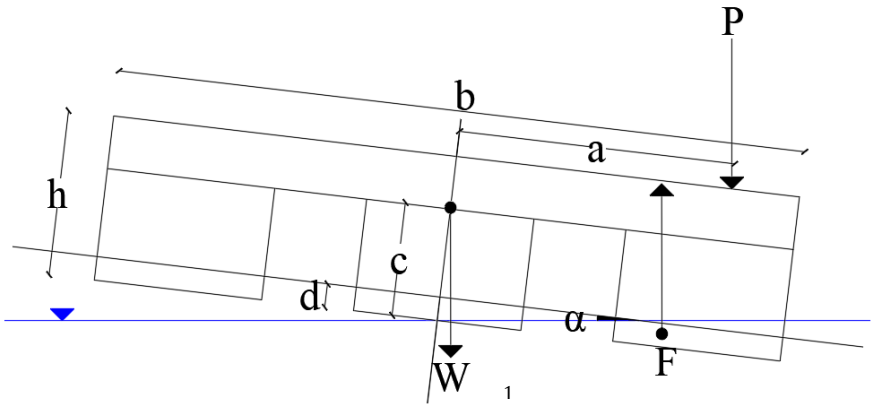

Figure 3.30. Tilted pontoons.

The eccentric load is considered as uniform distributed load that is acting on half of the pontoon. The distributed load is taken 1000 N per meter.

The stability condition according to the inclination angle of pontoon in Table 3.16, α is satisfied.

Table 3.16. Parameters for Equation of 3.64, and result of α.

W_1	11565 N
P	14375 N
b	2.50 m
h	0.60 m
d	0.09 m
c	0.41 m
a	0.53 m
α	**2.97°**
$\tan\alpha$	0.05
$\frac{2(h-d)}{b}$	0.41

It is required that actual volumetric displacement is equal or very close to equivalent volumetric displacement in ANSYS™ AQWA®. The volumetric displacements depend on the mass of the structure. If the entered mass and calculated mass by the software is close these volumetric displacements are close. The software obtains the mass by using displaced water volume because the origin point is on the still water level plane in the project.

The hydrostatic results tell if the structure floats or not for free-floating case without any dynamic effect such as; external forces, wave, wind or current.

3.7. Modeling of Connections Between the Pontoons

Articulations are utilized for connecting the structures which can be floating or fixed in place structures. The structures can connect to each other by hinged, universal, ball and socket and rigid joints in ANSYS™ AQWA® software as seen in Figure 3.31.

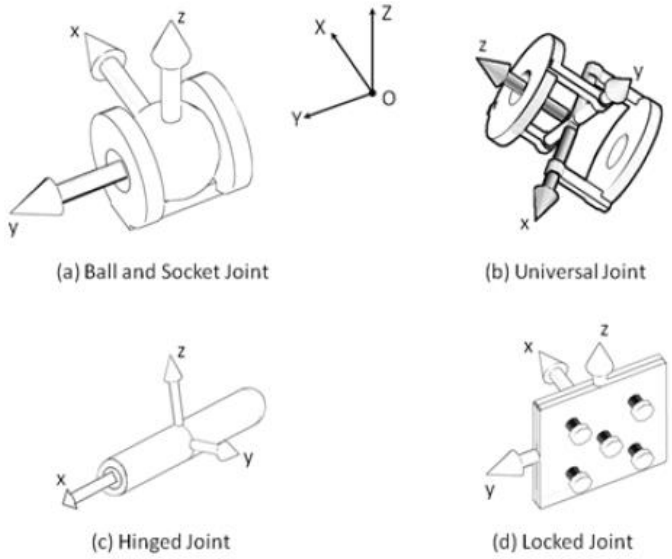

Figure 3.31. Connection types in AQWA (Source: Ansys Inc., 2020).

In the ANSYS™ AQWA® software just rotational freedoms exist for the articulations which are referred to as constraints. At the joint where the connected structures are linked, there is no relative translational motion.

Constrained motions due to the articulations are expressed mathematically in Equations 3.67, 3.68, and 3.69. The vectors between the structure j and k and their connection points, respectively is described as,

$$\vec{r}_j = \vec{X}_p - \vec{X}_{gj} = (x_j, y_j, z_j) \tag{3.67}$$

$$\vec{r}_k = \vec{X}_p - \vec{X}_{gk} = (x_k, y_k, z_k) \tag{3.68}$$

The restriction boundary conditions are mathematically expressed,

$$(\vec{u}_j + \vec{\theta}_j \times \vec{r}_j).\vec{e}_m = (\vec{u}_k + \vec{\theta}_k \times \vec{r}_k).\vec{e}_m \tag{3.69}$$

where $(\vec{u}_j, \vec{\theta}_j)$ and $(\vec{u}_k, \vec{\theta}_k)$ represent translational and rotational motion on structures k and j, the rotational motion at structure k and j equals. $\vec{\theta}_j.\vec{e}_m = \vec{\theta}_k.\vec{e}_m$ and $\vec{e}_m$ is unit vector, m is 1 to 3.

The boundary condition in matrix form is given as,

$$\begin{bmatrix} E^T & E^T R_j \\ 0 & E^T \end{bmatrix} U_j - \begin{bmatrix} E^T & E^T R_k \\ 0 & E^T \end{bmatrix} U_k = 0 \tag{3.70}$$

where E is unit vector, $U_j = (\overrightarrow{u}_j, \overrightarrow{\theta}_j)$ and $U_k = (\overrightarrow{u}_k, \overrightarrow{\theta}_k)$ and R_j and R_k are position vectors for structure j and k, respectively.

The rotation in the y-direction is free for hinged connections in the numerical model with. The boundary condition for hinge-type joint is described as,

$$\begin{bmatrix} E^T & E^T R_j \\ 0 & G^T \end{bmatrix} U_j - \begin{bmatrix} E^T & E^T R_k \\ 0 & G^T \end{bmatrix} U_k = 0 \tag{3.71}$$

where matrix G is given as,

$$G = \begin{bmatrix} 0 & e_{12} & e_{13} \\ 0 & e_{22} & e_{23} \\ 0 & e_{32} & e_{33} \end{bmatrix} \tag{3.72}$$

The rotation in x and y-direction is free for universal connections and it is described as,

$$G = \begin{bmatrix} 0 & 0 & e_{13} \\ 0 & 0 & e_{23} \\ 0 & 0 & e_{33} \end{bmatrix} \tag{3.73}$$

The rotation in all direction is free for ball and socket connections and it is described as,

$$G = \begin{bmatrix} 0 & 0 & 0 \\ 0 & 0 & 0 \\ 0 & 0 & 0 \end{bmatrix} \tag{3.74}$$

The component j in Equation 3.64 is represented with matrix H_j and H_k then the Equation becomes,

$$H_j U_j - H_k U_k = 0 \tag{3.75}$$

The forces and moments on the joints in local axes which represents with R_c are found as,

$$\begin{bmatrix} F_j \\ F_k \\ 0 \end{bmatrix} = \begin{bmatrix} K_{jj} & K_{jk} & -H_j^T \\ K_{kj} & K_{kk} & H_k^T \\ H_j & H_k & 0 \end{bmatrix} \begin{bmatrix} U_j \\ U_k \\ R_c \end{bmatrix} \tag{3.76}$$

where $\begin{bmatrix} F_j \\ F_k \\ 0 \end{bmatrix}$ matrix represents forces and moment on the structure j and k and the total stiffness matrix of the structures j and k is given as $\begin{bmatrix} K_{jj} & K_{jk} \\ K_{kj} & K_{kk} \end{bmatrix}$.

Another type of articulation is rigid joint. It is not allowed to free rotational motion, has fully constrained motion.

In this model ball and socket connections are used for dock A. Stiffness of the connections are calculated as 244.95 kN.m/degree with allowing 10 degrees in rotation y.

3.8. Modeling of Mooring Lines

Mooring lines are utilized to keep the floating structures, and vessels under the extreme environmental conditions. Mooring systems involves suspended lines which can move, and connection parts which is anchor, pile or concrete anchorage blocks to the sea bed. Floating structures can be moored with wire rope, steel linked chain and synthetic fiber rope. The most common and used one is chain because of its durable, having strong resistance for abrasion at the seabed and increasing holding capacity of the anchor or concrete anchorage blocks (Huang and Yang, 2021). The mostly used mooring system is catenary and taut-leg configuration.

In Teos Marina, the floating docks moored by catenary steel chains with diameter of 28 millimeters. The chains are linked aluminum dock on the floating platform to concrete anchorage blocks at the seabed.

Quasi-Static Analysis for Mooring Lines

There are two modeling way in ANSYS™ AQWA® : they are quasi-static and dynamic models. The quasi-static analysis operates with the mooring stiffness curve without taking line dynamics into account, keeping wind and current forces as constant and accounting for the wave-induced vessel forces and reactions in time-domain analysis and a frequency response technique in which the mooring stiffness curve is considered to be linear and low-frequency dynamic responses to wave drift and wind impacts are computed as though for a single degree of freedom system (Brown, 2005).

In quasi-static analysis the hydrodynamic drag forces and inertia forces on the cable are neglected (Alkarem, 2020).

The catenary configuration can be considered as two parts; one of them suspended part and the other part lies part on the seabed. The chain must be resist to external forces which are as seen in Figure 3.32.

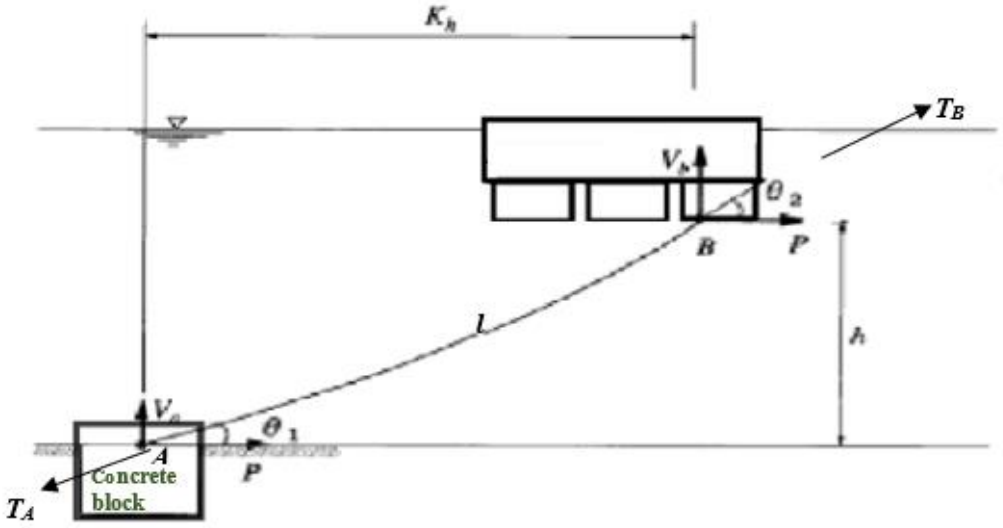

Figure 3.32. Catenary configuration.

The maximum tension on the chain is described as,

$$T = P \sec \theta_2 \tag{3.77}$$

The vertical forces at top and bottom are defined as,

$$V_a = P \tan \theta_1 \tag{3.78}$$

$$V_b = P \tan \theta_2 \tag{3.79}$$

The angles of θ_1 and θ_2 can find by using Equations of 3.4 and 3.5.

$$l = \frac{P}{w}(\tan \theta_2 - \tan \theta_1) \tag{3.80}$$

$$h = \frac{P}{w}(\sec \theta_2 - \sec \theta_1) \tag{3.81}$$

where w is submerged weight per meter (kN/m) and P is horizontal external force (kN).

The horizontal distance between concrete anchorage block and pontoon and chain connection is found as,

$$K_h = \frac{P}{w}(\sinh^{-1}(\tan \theta_2) - \sinh^{-1}(\tan \theta_1) \tag{3.82}$$

The catenary section is considered as straight line in the software. The mathematical expression of this,

$$\theta_1 = \theta_2 = \sin(h/l) \tag{3.83}$$
$$K_h = \sqrt{l^2 - h^2}$$

Dynamic Analysis for Mooring lines

In this study, the dynamic effects on the cables are included in the calculations. The dynamic analysis involves drag forces, elastic tension, bending moment and cable mass effects (ANSYS Inc., 2013). The mooring line is discretized and solve with dynamic analysis by Lumped Mass Method (LMM). The dynamic analyze gives more accurate results than the quasi-static method (Lin and Yang, 2020).

The Lumped Mass Method involves weight, buoyancy force, damping force, internal stiffness, hydrodynamic forces and contact force (Lin and Yang, 2020). The

chains are discretized to N elements in Lumped Mass Method and N+1 nodes are obtained. The all segments have same properties such as equivalent diameter,

Mass matrix at each node is described as,

$$m_i = \frac{\pi}{4} d^2 L \rho I \tag{3.84}$$

where d is equivalent diameter, ρ is density of chain L is unstreched length and I is identity matrix for the element.

The added mass is mathematically defined as,

$$a_i = a_{pi} + a_{qi} = \frac{\pi}{4} d^2 L (C_{an}(I - \hat{q}_i \hat{q}_i^T) + C_{at}(I - \hat{q}_i \hat{q}_i^T)) \tag{3.85}$$

where a_{pi} and a_{qi} are the transverse and tangential added mass, C_{an} and C_{at} are the normal (transverse) and tangential added-mass coefficients. $\hat{q}_i$ represents tangent direction for each node in direction of the line between the two adjacent points. It can be expressed as,

$$\hat{q}_i = \frac{r_{i+1} - r_{i-1}}{|r_{i+1} - r_{i-1}|} \tag{3.86}$$

where r_{i+1} and r_{i-1} represent the position vector of two adjacent node points.

The equation of motion for chains elements is described as (Lin, and Yang, 2020),

$$\begin{aligned} F_M &= \sum_{i=1}^{N} (m_i + a_i)\ddot{r}_i \\ &= \sum_{i=1}^{N} (T_{i+\frac{1}{2}} - T_{i-\frac{1}{2}} + C_{i+\frac{1}{2}} - C_{i-\frac{1}{2}} + W_i + B_i + D_{pi} + D_{qi}) \end{aligned} \tag{3.87}$$

where T_i and C_i represents internal stiffness and damping force at node i, W_i and B_i are the weight of the segments and net buoyancy force at node i and D_{pi} and D_{qi} represents normal (transverse) and normal drag forces at node i.

Generally, the hydrodynamic forces are accounted at mid points like illustrated as above equations then distributed to each node. Hall and Goupee (2015) determine the hydrodynamic forces on the node points. They claimed that the computed drag at the nodes supply damping of line motions.

When ANSYS™ AQWA® software solves the dynamic cable, it is considered as circular cylinder and can be solved by discretization which is illustrated in Figure 3.33. The forces on a discretized element are represented in Figure 3.34. Torsional effect and wave induced force on the cable are neglected in the software for dynamic analysis.

This equation motions on an element are described as,

$$\frac{\partial \vec{T}}{\partial S_e} + \frac{\partial \vec{V}}{\partial S_e} + \vec{w} + \overrightarrow{F_H} = m\frac{\partial^2 \vec{R}}{\partial t^2} \tag{3.88}$$

$$\frac{\partial \vec{M}}{\partial S_e} + \frac{\partial \vec{R}}{\partial S_e} \times \vec{V} = -\vec{q} \tag{3.89}$$

where $\vec{T}$ is the tension, $\vec{V}$ is the shear force vector on the cable element, $\vec{w}$ is the weight of the cable element vector. $\vec{R}$ illustrates position vector at the cable element, $\vec{M}$ is the bending moment vector, m is mass per unit length, and $\vec{q}$ is total moment vector per unit length for the cable element. ΔS_e and D_e represents length of the discretized element and diameter of the element as seen in Figure 3.34. $\overrightarrow{F_H}$ is sum of the hydrodynamic loads vector and is described as,

$$F_H = F_b + F_d - m_a\left[\overrightarrow{a_j}, \overrightarrow{a_{j+1}}\right]^T \tag{3.90}$$

where F_b is the buoyancy, F_d is the drag force and m_a is added mass and $\overrightarrow{a_j}$ and $\overrightarrow{a_{j+1}}$ represent the accelerations at node j and j+1 in the cable element. The current drag force on the chain element is calculated by integrating the drag force along the element length in order to reach accurate result .

The boundary conditions at ends such as,

$$\frac{\partial^2 \vec{R}(0)}{\partial {S_e}^2} = \vec{0} \tag{3.91}$$

$$\frac{\partial^2 \vec{R}(L)}{\partial {S_e}^2} = \vec{0} \tag{3.92}$$

where position of 0 and L represent bottom and top ends of the cable and L is unstreched length.

The software assumes that there are mud springs in the mud layer to determine the reaction forces at the seabed in the mud layer. The mud spring in mud layer ensures the reaction forces at sea bed for every node. The reaction forces, F_{zj} at the seabed are described as,

$$F_{zj} = \begin{cases} 0, & \text{If j node is above the mud layer} \\ \frac{m_{j,net} g}{\hat{z}} \left[-d - z_j + \hat{z} - \frac{\hat{z}}{\pi} (\sin 2\theta) \right], & \text{If j node presents in the mud layer} \\ \frac{m_{j,net} g}{\hat{z}} \left[\hat{z} - 2(d + z_j) \right], & \text{If j node is underneath the seabed} \end{cases} \tag{3.93}$$

$$\theta = -\frac{\pi(d + z_j - \hat{z})}{2\hat{z}}$$

where $m_{j,net}$ is net mass of node j, equals the displaced water mass, $\hat{z}$ is mud layer height and z_j is z component of position vector for node j.

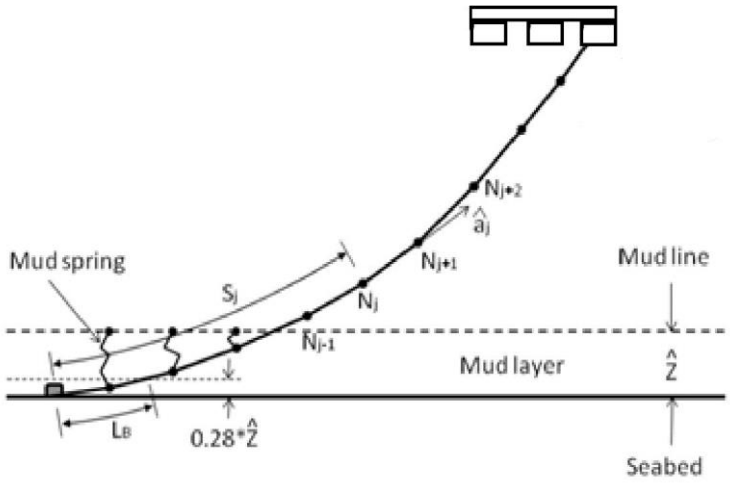

Figure 3.33. Discretization in mooring lines.

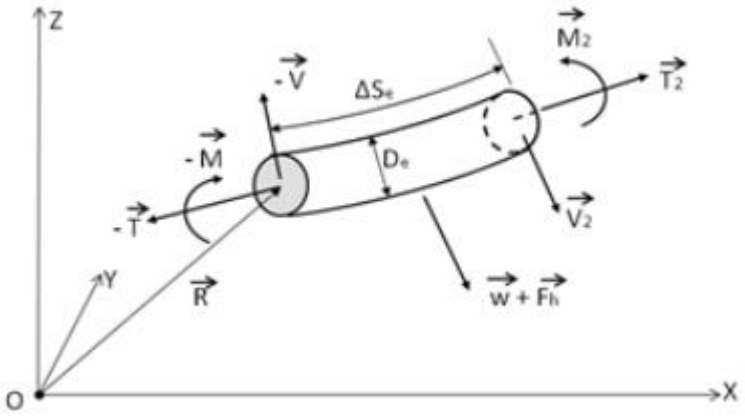

Figure 3.34. Equation motion on an element (Source: ANSYS Inc., 2020).

The catenary section specifications are given in Table 3.17.

Table 3.17. Section properties for DIN763.

Mass per Unit Length (ton/meter)	0.0139
Equivalent Cross-Sectional Area (m^2)	0.002
Stiffness, EA (kN)	66954
Maximum Tension (kN)	300
Added Mass Coefficient	0.5556
Transverse Drag Coefficient	1.2394
Equivalent Diameter (m)	0.0504
Longitudinal Drag Coefficient	0.2034

Mass and load information for this German Standard chain section as seen in Table 3.18 is provided from the company with name of "First Rigging" (German Standard Chain, n.d.).

Table 3.18. Mass and load information for the catenary-shaped chains German Standard Chain, n.d.).

D (mm)	Working load (kg)	Proof load (N)	Breaking load (N)	Approximate mass (kg/m)
28	6000	120000	300000	13.90

The equivalent diameter equals 1.8 times of nominal diameter (OrcaFlex Manual) and the equivalent cross-sectional area is calculated as cut a lobe on the chain. These values important for ANSYS™ AQWA® because the software perceives the studless chain section as cylindrical line so it is vital the convert the equivalent line.

Bending stiffness (EI) assumes zero, it is considered as the discretized chain elements can bend for small moments. Axial stiffness (EA) is calculated with below equation,

$$EA = 0.85 \times 10^8 D^2 \tag{3.94}$$

where D is the nominal diameter and the equation is in kN.

According to OrcaFlex Manual the drag coefficients are calculated from equivalence of the drag forces at the lobe of the chain and overall chain in axial and normal directions. The normal areas for drag forces in axial and normal directions are illustrated in Figure 3.35.

$$\frac{1}{2}\rho V^2 C_{da-chain}(A_{Normal-a}) = \frac{1}{2}\rho V^2 C_{da}(\pi OD) \tag{3.95}$$

$$A_{Normal-a} = 4\left(0.8D^2 + \frac{\pi D^2}{8}\right)\left(\frac{1}{8D}\right) = 0.6D$$

$$C_{da} = (0.106)\, C_{da-chain} \tag{3.96}$$

In OrcaFlex Manual the $C_{da-chain}$ assumes as 0.40.

The normal (transverse) drag coefficient can be find as,

$$\frac{1}{2}\rho V^2 C_{dn-chain}(A_{Normal-n}) = \frac{1}{2}\rho V^2 C_{dn}(OD) \tag{3.97}$$

$$A_{Normal-n} = A_{FACE} + A_{EDGE} = 2.1D$$

$$C_{dn} = \frac{A_{Normal}}{OD} = \frac{2.1D}{1.8D} = 1.17 \tag{3.98}$$

where $OD = 1.8\ D$ is equaivalent diameter, $C_{da-chain}$ is drag coefficient for overall chain and C_{da} is drag coefficient for the lobe of the chain.

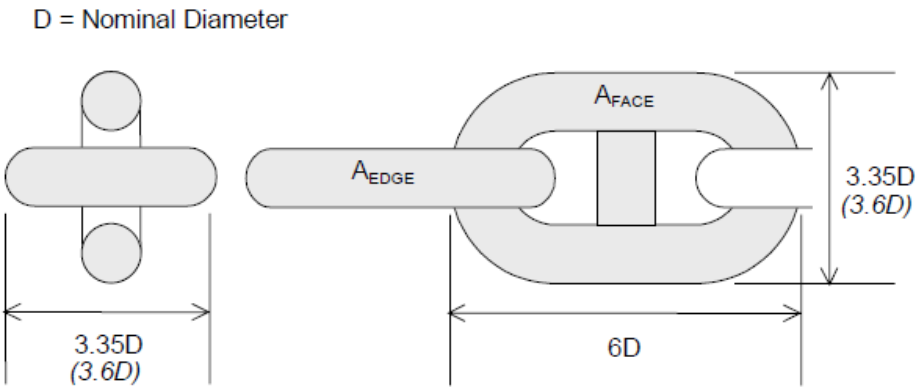

Figure 3.35. Normal chain area definitions (Source: OrcaFlex Manual).

Axial added mass coefficient, C_{aa} in OrcaFlex Manual, is given as 0.08 or 0.07 and normal added mass coefficient C_{an} takes as 1.0 for a circular cylinder value.

The fairlead points of the chains are modeled at the location of the concrete anchorage block. The boats are connected to rope linked by the concrete anchorage blocks and the ropes are further connected to the cleats as illustrated in Figure 3.36. During the tsunami some chains were broken and some of them non-broken, but they drifted away with the concrete anchorage blocks.

Figure 3.36. The cleats on the aluminum dock.

Mooring lines are linked by cross over on x and y axis and catenary. The chains are fixed to the seabed by linking the concrete anchorage blocks.

CHAPTER 4

NUMERICAL MODELING OF FLOATING PONTOONS IN TEOS MARINA UNDER TSUNAMI INDUCED WATER LEVEL CHANGES AND CURRENTS

4.1. Water Level Changes and Current Data of The Tsunami

In this study, tsunami induced water level changes and current speed and direction data are provided by Çiçek (2022) and Doğan (2021). While Doğan (2021) used NAMI-DANCE to model tsunami propagation from the source to the Teos Marina area, XBeach Non-hydrostatic model was used in Çiçek (2022) after coupling NAMI DANCE and XBeach Non-hydrostatic numerical models in the deep water.

To simulate wave dynamics, sediment transport and morphological changes in the nearshore region the XBeach model is commonly utilized. XBeach software offered by Roelvink et al. in 2010, which is proved by field surveys and uses in laboratories. The software can model the morphologic changes under the current and/or wave effects. The new version of the software, XBeach Non-hydrostatic v1.23.5526 (Smit et al., 2010) considers the dispersive behavior of long waves by solving the non-linear shallow water (NSW) equations with non-hydrostatic pressure correction. Unlike conventional hydrostatic model the X Beach Non-hydrostatic model, excels in modeling wave breaking and accompaying turbulence.

It is important to note that XBeach requires high-performance computation and significant computer resources, especially for modeling large areas with high resolution (Li et al., 2012). An alternative software, NAMI DANCE, offers shorter processing times by utilizing Graphics Processing Units (GPU) but lacks the capability to model morphological changes due to its fixed base assumption.

NAMI DANCE focuses on tsunami numerical modeling and utilizes the nonlinear form of long wave equations with appropriate boundary conditions. Multiple numerical solutions have been developed for tsunamis using long wave equations. Generally,

explicit numerical solutions of the NSW Equations are favored due to their reasonable computational time and memory requirements, and their ability to provide results within an acceptable error margins (NAMI DANCE, 2016).

NAMI DANCE which is created by Profs. Zaytsev, Chernov, Yalciner, Pelinovsky and Kurkin is tested with several tsunami model predictions on international scale (Yalçıner vd., 1995; 2002; 2007a, b; Zahibo vd. 2003; Sozdinler vd., 2014; Dilmen vd., 2014; Sozdinler vd. 2015; Zaytsev et al., 2016; Kian vd., 2016; Velioğlu vd., 2016; Aytore vd., 2016; Lynett vd., 2017; Sogut ve Yalciner, 2019; Zaytsev vd., 2019). It obtains crucial tsunami hydrodynamic parameters, including water surface height, flow depth, current velocities, and current directions (Aytore et al., 2016).

Both Çiçek (2022) and Doğan (2021) provided the tsunami water level and current data for some specific points namely components near Dock A, as shown in Figure 4.1. The current data involves current speeds, and current directions.

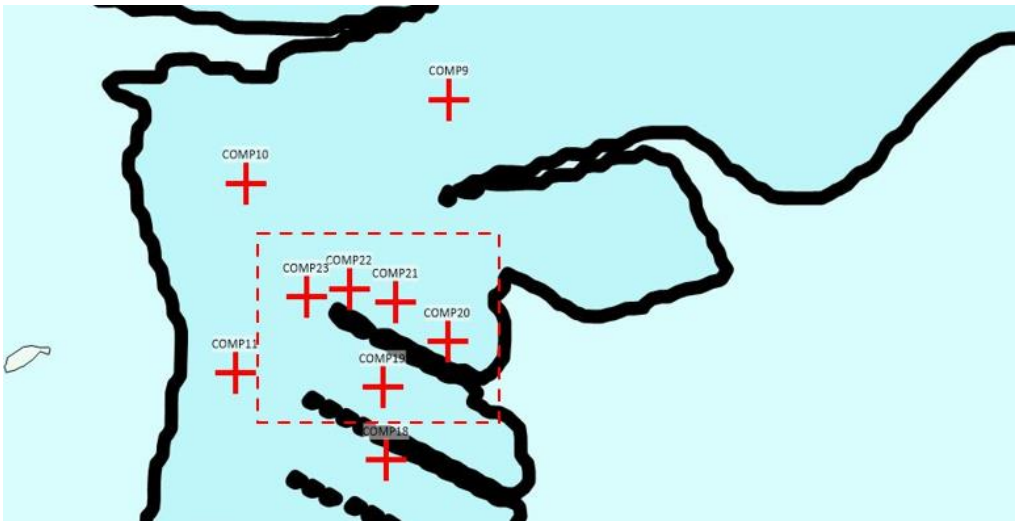

Figure 4.1. Location the current data obtain.

Tsunami induced water level change data in Components 19, 20, 21, 22 and 23 obtained from NAMI-DANCE and XBeach Non-Hydrostatic models are compared in Figure 4.2 and Figure 4.3, respectively.

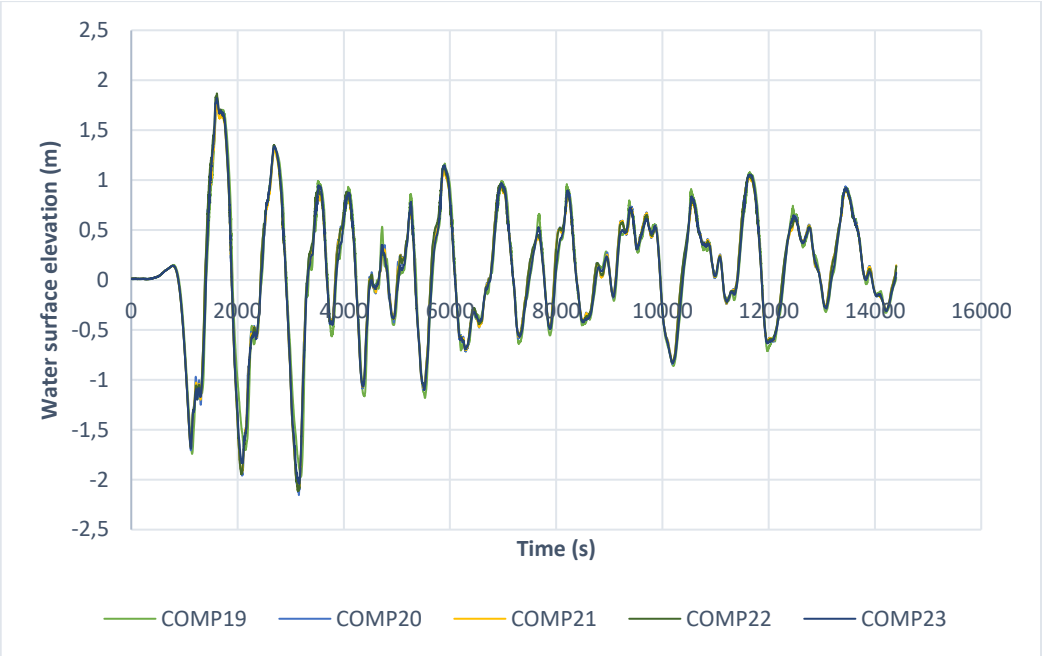

Figure 4.2. Comparison of water surface elevations calculated by NAMI_DANCE at component 19, 20,21,22 and 23.

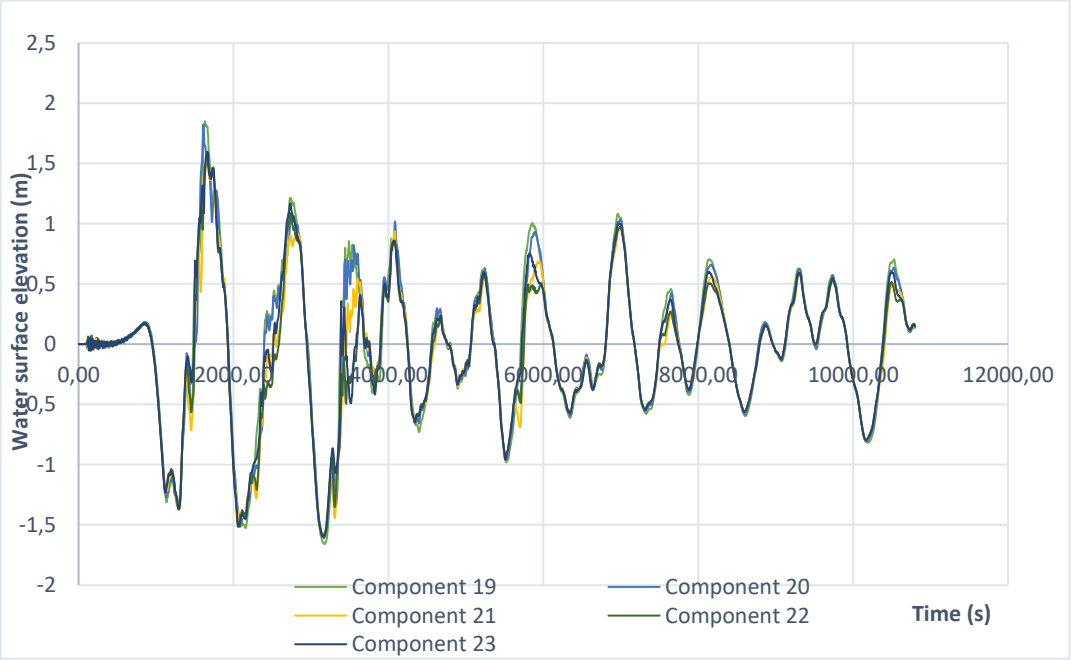

Figure 4.3. Comparison of water surface elevations calculated by XBeach Non-Hydrostatic at component 19, 20,21,22 and 23.

As can be seen in Figure 4.2 and Figure 4.3, water surface elevations are close to each other in all component points. Moreover, water level results of NAMI-DANCE and XBeach Non-Hydrostatic models are similar.

The current speed results of both models for the component points 19,20,21,22 and 23 are compared in Figure 4.4, 4.5, 4.6, 4.7 and 4.8, respectively.

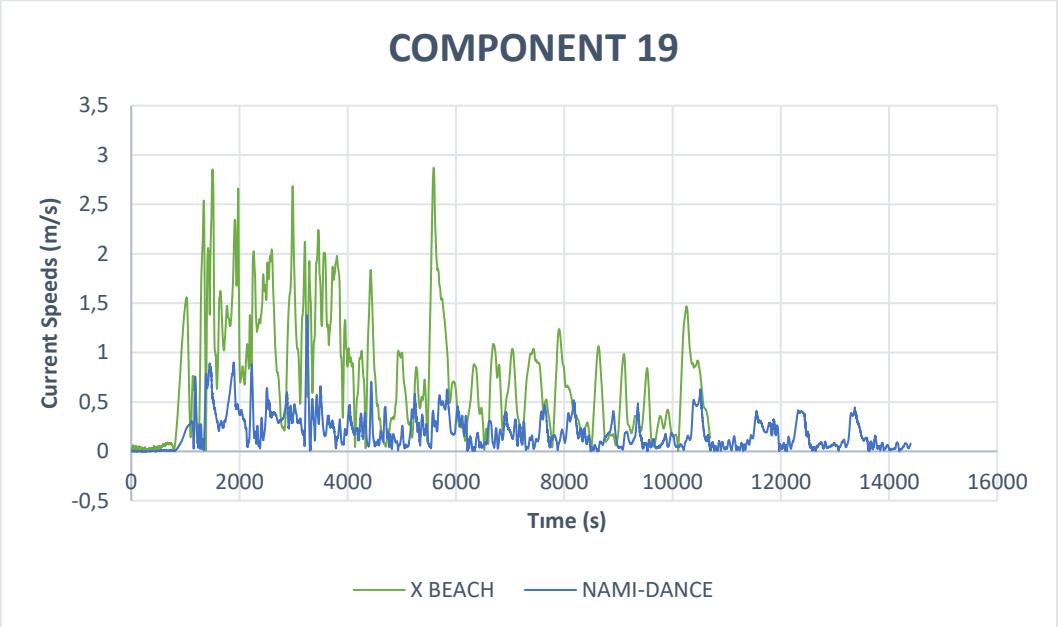

Figure 4.4. Compare the current speed of component 19.

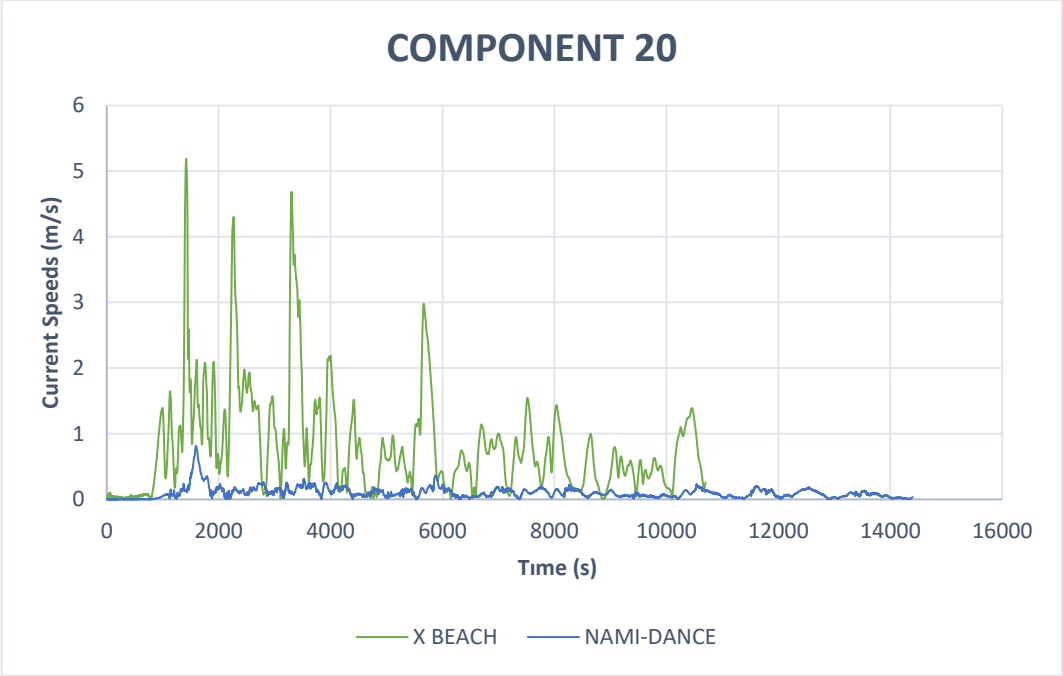

Figure 4.5. Compare the current speed of component 20.

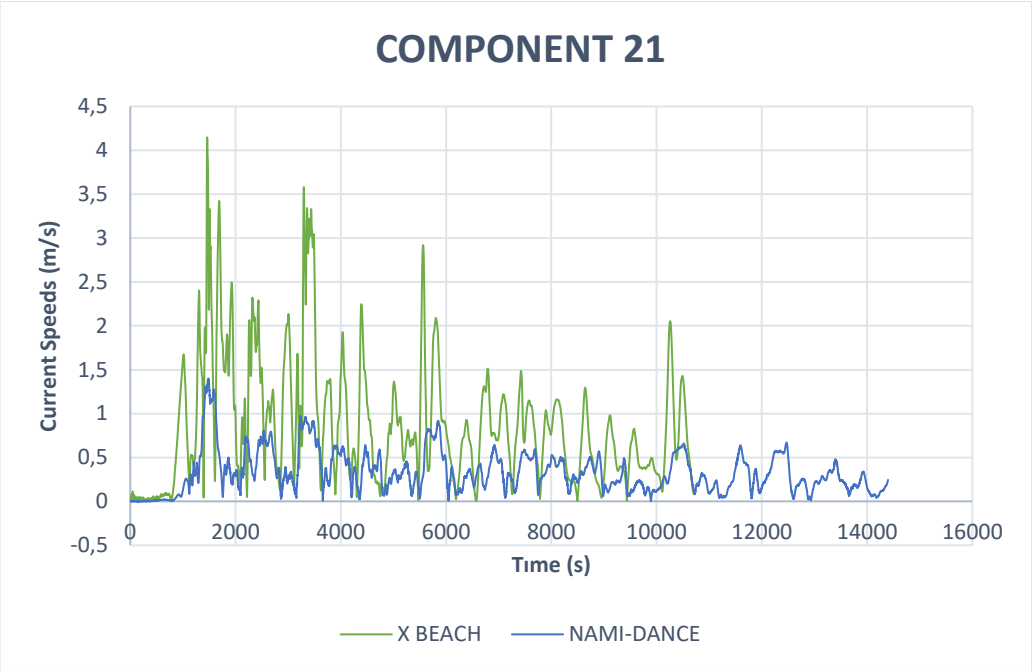

Figure 4.6. Compare the current speed of component 21.

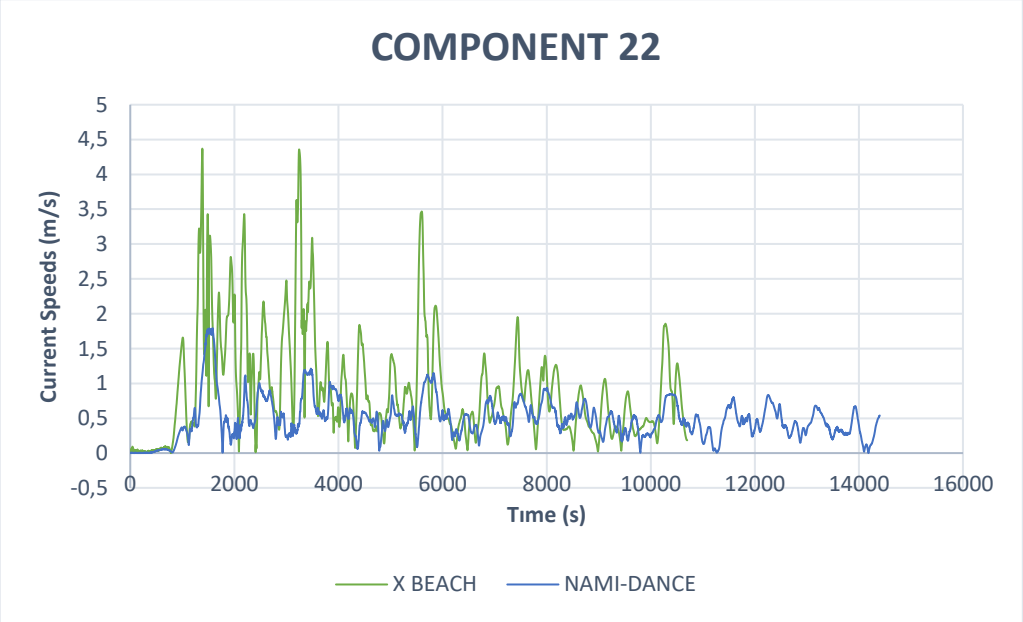

Figure 4.7. Compare the current speed of component 22.

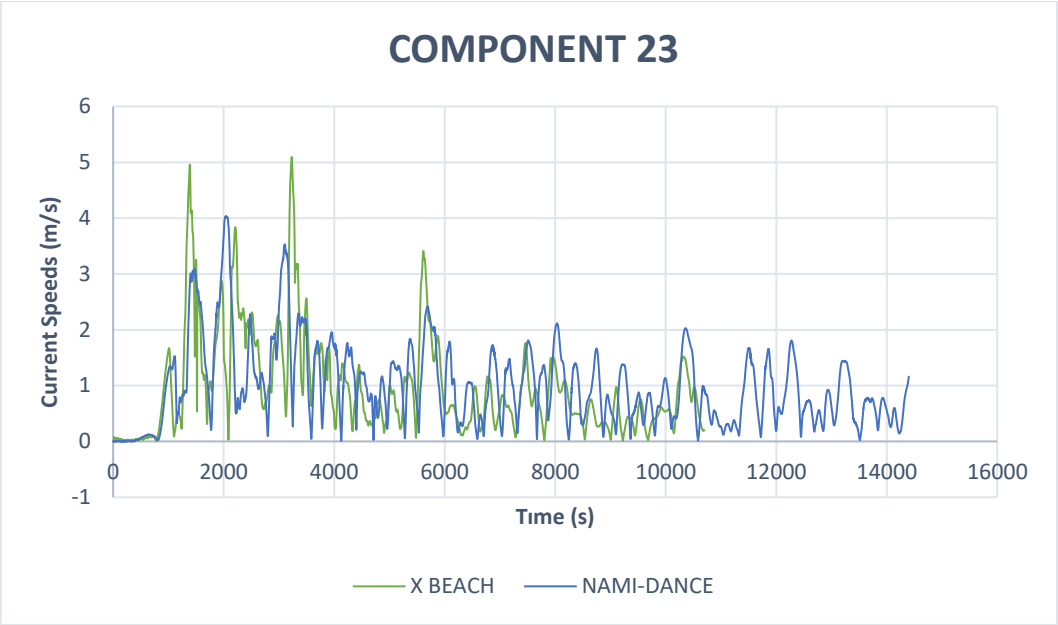

Figure 4.8. Compare the current speed of component 23.

At the points close to the boundary (like 19,20, 21) NAMI-DANCE gives lower current speeds, while XBeach gives similar current speeds for all the component points. Comparison of NAMI-DANCE and XBeach Non-Hydrostatic models in terms of the current speed shows that XBeach calculates higher current speeds. Since there is no measurement during the tsunami event, it is not possible to verify the model results. However, Nami-dance current data is used for this study because it is more logical that the current speeds toward to the shoreline decrease as seen in Fig. 4.4-4.8. A shoreline will experience a succession of successive crests and troughs from a tsunami. Their speed reduces as they approach beaches, bays, or harbors with shallower water (International Information Center. International Tsunami Information Center, A UNESCO/IOC-NOAA Partnership,2023).

As can be seen in Figure 4.2 the water level changes due to the tsunami from Nami-dance are very similar for all components. In that case, water level changes from component 23 as seen in Figure 4.9, are utilized as an input to introduce the water level elevations due to the tsunami to Ansys AQWA.

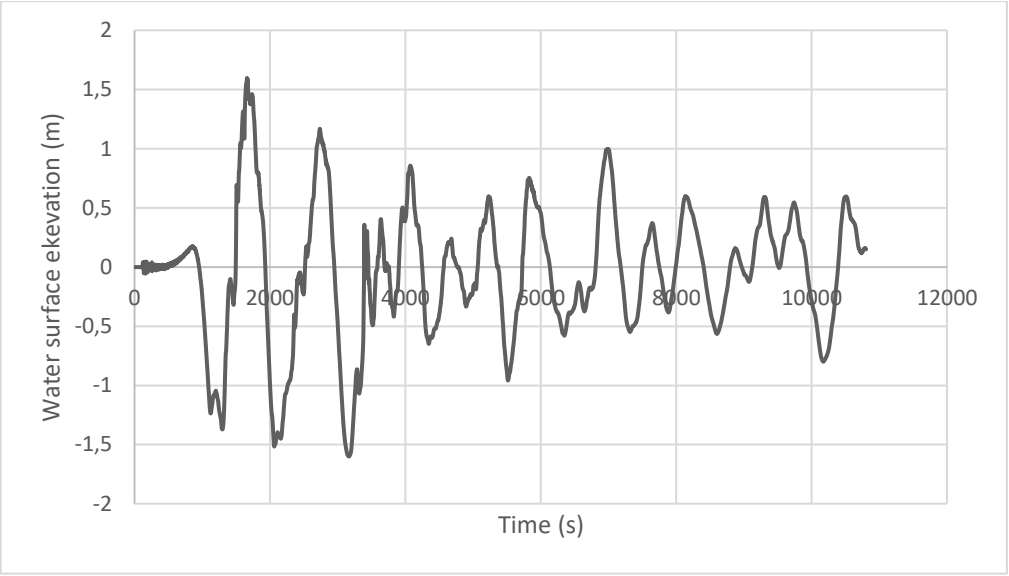

Figure 4.9. Water surface elevation in component 23.

The Nami-Dance current data in comp 23 indicates that the higher current speeds are predominantly in the North (N) and North North East (NNE) directions as can be seen in Figure 4.10.

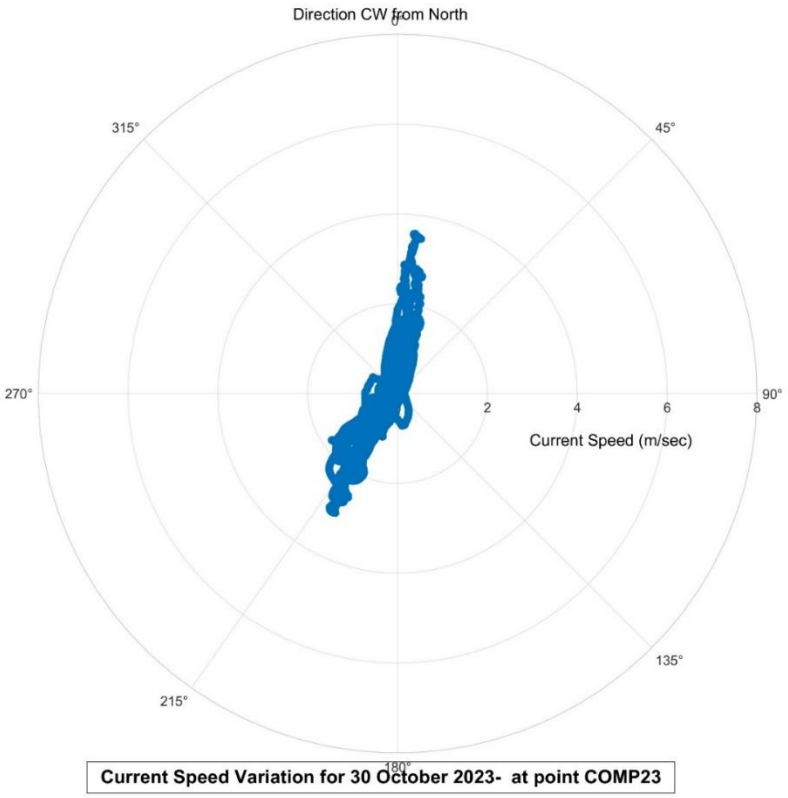

Figure 4.10. Current directions versus current speeds from Nami-dance results.

4.2. Introduction of Tsunami Induced Water Level Changes to Numerical Model in ANSYS™ AQWA®

In ANSYS-AQWA there is no option to define a tsunami wave explicitly. However it is possible to introduce water surface elevation time series as external files (*.wht). In this study, firstly water surface elevation changes due to tsunami obtained in component 23 is converted to wht file and the model is run under the given water elevation data. Unfortunately, AQWA gave error and did not accept the wht file. Because the minimum frequency allowed in a time series in the program is 0.015915 Hz or almost 63 secs (AQWA Theory Manual (2020)), while the tsunami waves have much longer periods. For example, the value of the peak frequency of the tsunami wave is 0.000977Hz (1020 seconds in period).

As it is mentioned in Chapter 3, there is another option to introduce waves in AQWA is to enter a user-defined spectrum. It is possible to convert time based water surface elevation data into frequency based spectrum by employing method of Fast Fourier Transform (FFT).

In this study tsunami waves are introduced to AQWA with a spectrum of the tsunami waves. To control this and validate AQWA, a regular wave that has 1.5 m of wave amplitude and a wave period of 8 seconds, is introduced to the software, and obtained spectrum of the regular wave by using Fast Fourier Method. The spectrum of the regular wave is also entered as input to the software and compare the profiles obtained from the regular wave and its spectrum. Figure 4.11 and Figure 4.12 show the profile of the entered regular wave and the spectrum of the regular wave, respectively. Figure 4.13 illustrates the wave profile of the entered regular waves as the spectrum.

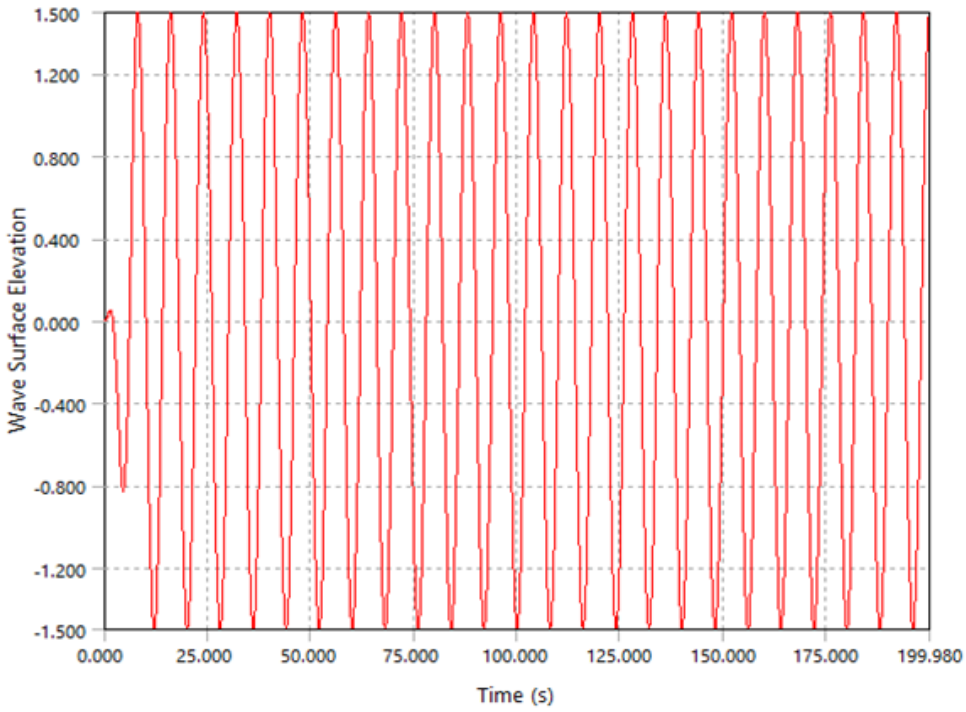

Figure 4.11. Wave profile of the introduced regular wave in AQWA.

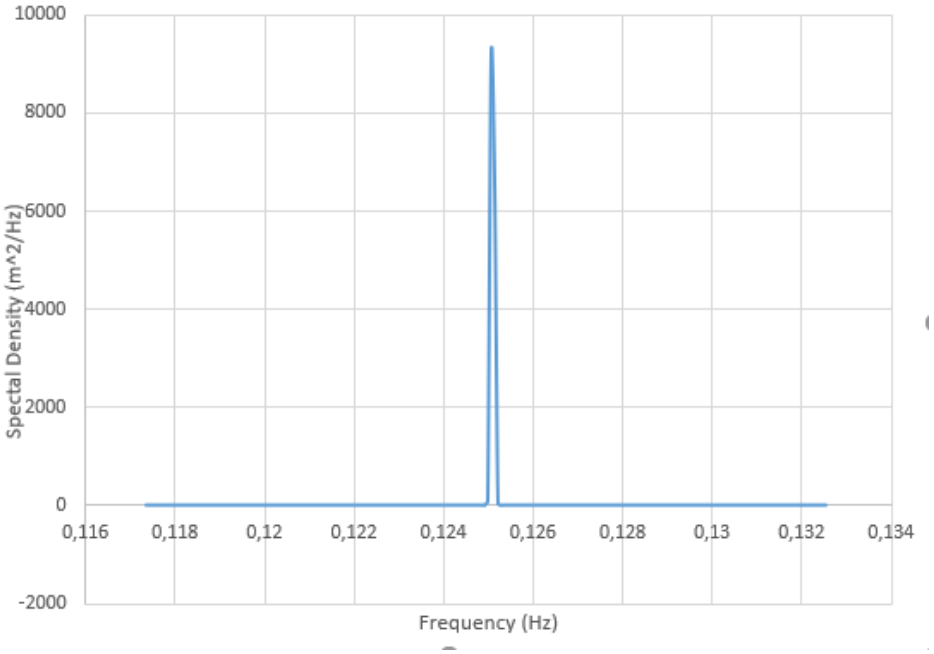

Figure 4.12. Spectrum of the regular wave.

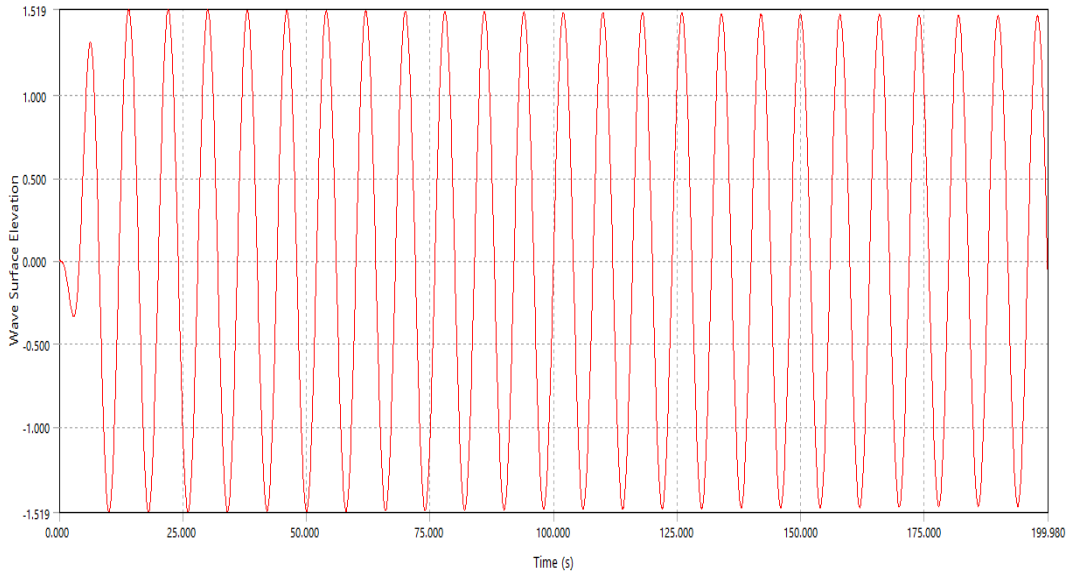

Figure 4.13. Wave profile obtained from spectrum of regular waves in AQWA.

According to Figure 4.11 and 4.13, same profiles are obtained in Ansys AQWA.

To verify this process, the regular wave and the regular wave with the spectrum results on the same floating dock model are investigated. The control provides a comparison of forces on connections between the pontoons in the floating dock. Figure 4.14 shows the forces on the connections in the y direction.

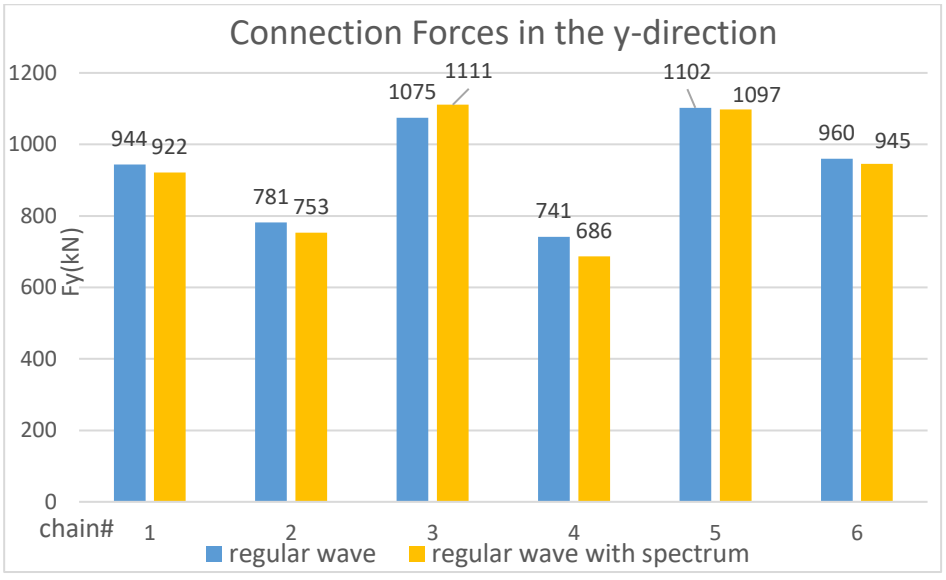

Figure 4.14. Results of connection forces in the y direction from AQWA.

These forces which must be on the connections in the y direction are also calculated using Goda's wave pressure formula. It is determined that 844 kN force must

be on the connections in the y direction. The numerical results are very close to calculated force by using Goda's formula so it is verified the operation in the study for water level changes due to the tsunami.

The frequency spectrum of the tsunami induced water surface elevations is given in Figure 4.15. Spectrum data is converted to an external file with the extension of *.xft including frequency and corresponding spectrum value data which have a maximum size of 200.

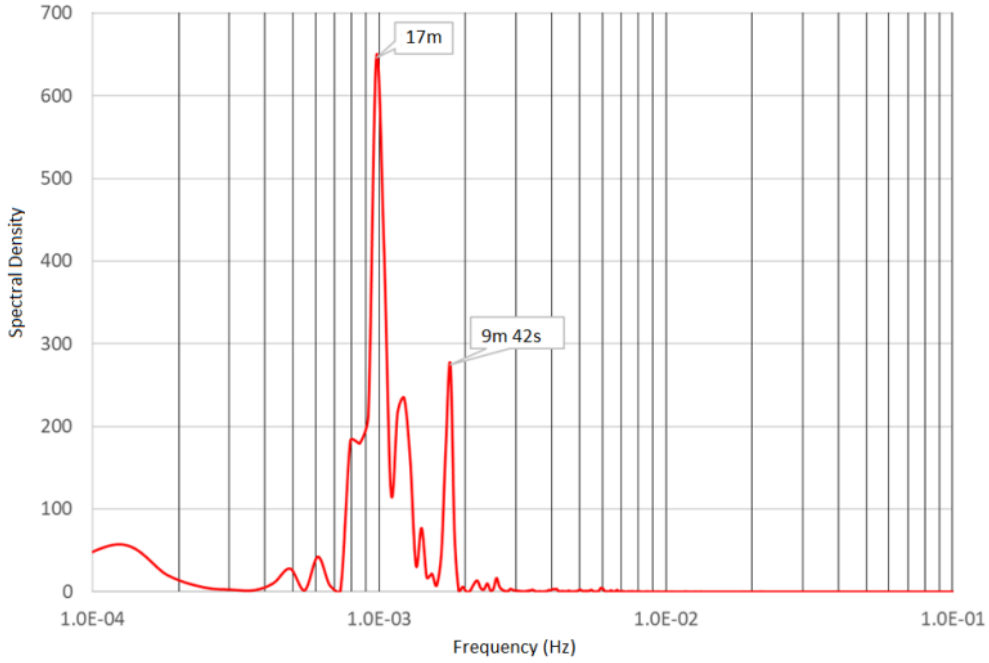

Figure 4.15. The frequency spectrum of tsunami induced water surface elevations.

The non-smoothed spectrum data is used to get rid of the effect of smoothing. Since there are three hours' water level elevation and current data, the model run is conducted for a duration of three hours.

In user defined spectrum option, in addition to spectrum file, direction of the wave, directional spreading and seed number should be defined. The main direction of the tsunami waves are in between N and NNE, as can be seen in Figure 4.16. N and NNE directions make 30 and 7.5 degrees with the orthogonal of the dock A. Therefore, it is assumed that the tsunami wave is perpendicular to dock A to be on the safe side.

Figure 4.16. Main tsunami wave direction (Source: Google Earth, Google Inc.).

For directional spreading, it is assumed that waves are uni-directional. For the seed number, it is first chosen automatically by AQWA. Seed number is used to define the phase of the wave. It is possible to convert spectrum data to time series data by inverse FFT technique and various time series can be obtained by using different seed numbers. When the seed number is chosen by AQWA automatically, as can be seen in Figure 4.17 that the sequence of water level fluctuations is different than the target tsunami water surface elevation data, although the maximum elevations and the number of waves agree each other.

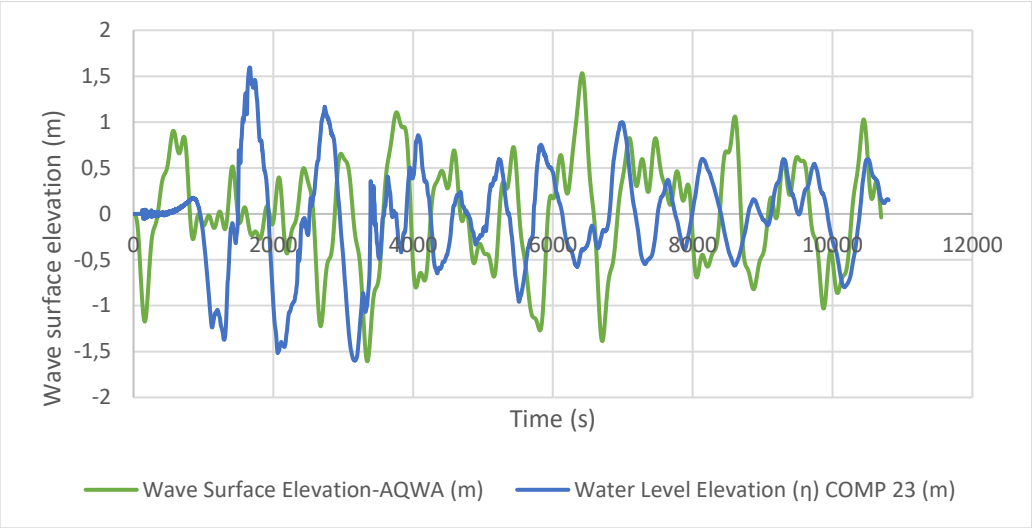

Figure 4.17. Comparison between the surface elevations of target (comp 23) and AQWA with automatic seed number.

Various seed numbers are tried to find appropriate seed numbers and the water level changes are obtained with the different seed numbers. Comparison with target water level changes and the water level changes with some of the different seed numbers are given in between Figure 4.18 and Figure 4.21. To decide the seed number RMSE (Root Mean Square Error) and Mean Squared Error (MSE) are calculated for tried seed number and it is given in Table 4.1.

Table 4.1. RMSE and MSE for tried seed numbers.

SEED no	**Root Mean Square Error (RMSE)**	**Mean Squared Error (MSE)**
1	0.789	0.634
5	0.641	0.514
6	0.768	0.577
7	0.735	0.606
8	0.698	0.552
9	0.809	0.647
10	0.739	0.594
11	0.680	0.543
12	0.760	0.629
13	0.666	0.545
14	0.701	0.545
15	0.695	0.550
17	0.61	0.478
18	0.846	0.659
29	0.726	0.580
31	0.681	0.540
170	0.734	0.595
289	0.724	0.552

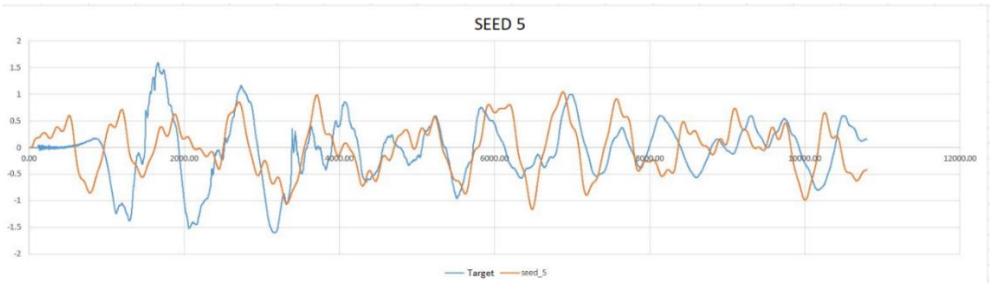

Figure 4.18. Comparison of water level changes with seed number of 5 and target one.

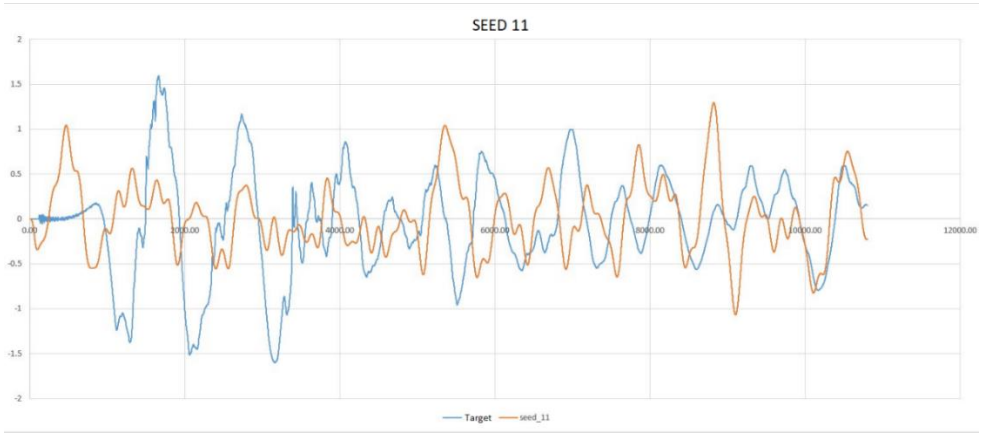

Figure 4.19. Comparison of water level changes with seed number of 11 and target one.

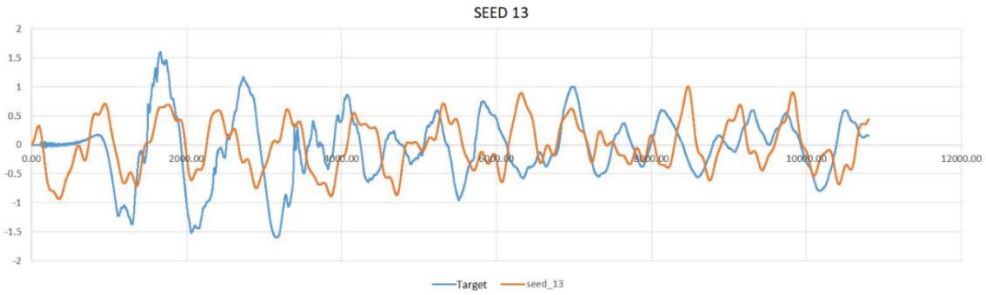

Figure 4.20. Comparison of water level changes with seed number of 13 and target one.

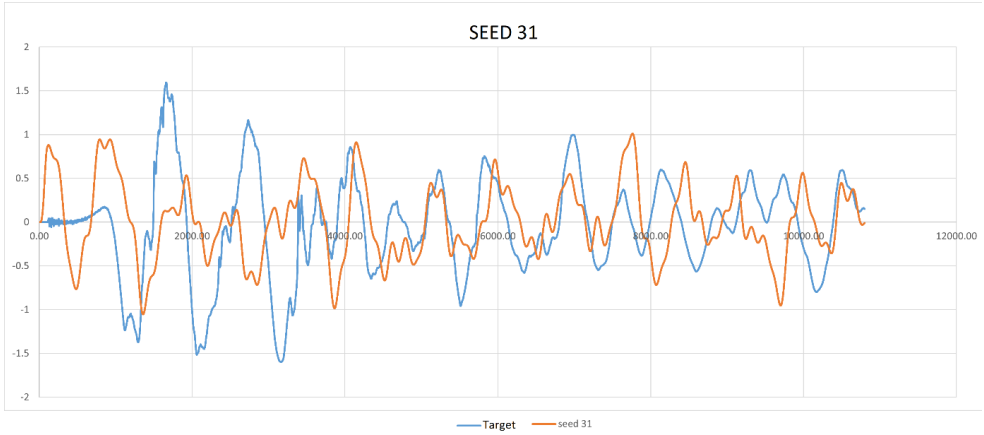

Figure 4.21. Comparison of water level changes with seed number of 31 and target one.

When the seed number is 17, the lowest RMSE and MSE are obtained. It is decided to take the seed number as 17 and it generates time series as close as the target surface elevation time series are obtained as shown in Figure 4.22.

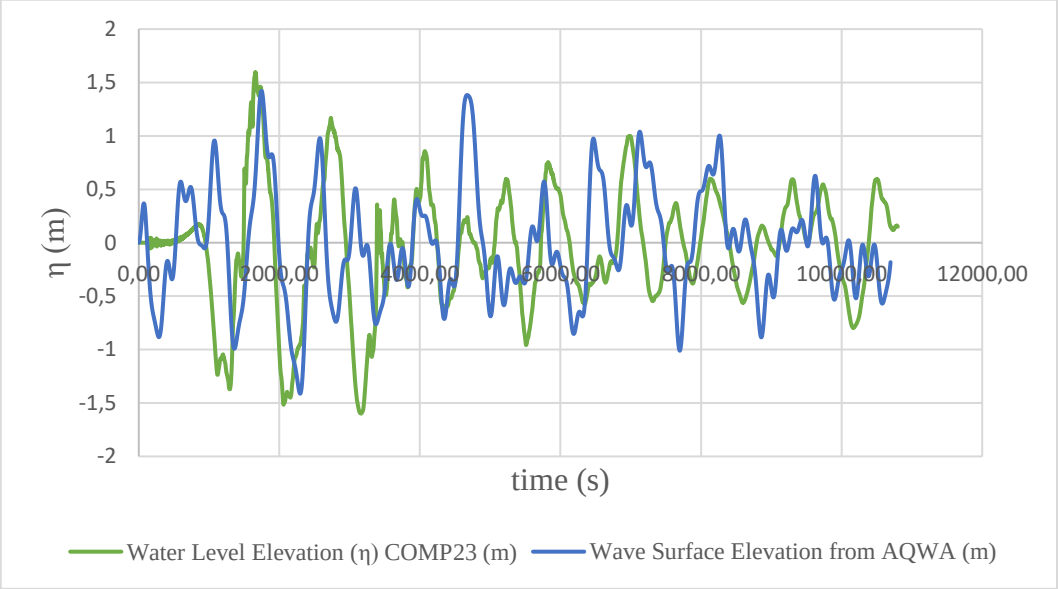

Figure 4.22. Comparison between the surface elevations of target (comp 23) and AQWA with seed number of 17.

To determine impact of the tsunami waves on the numerical model, the wave surface elevation can be obtained from AQWA and compared with actual data. It is crucial that the first peak and second peak tsunami waves occur at the same time with the model, as eyewitness accounts suggest that the second wave caused severe damage to the marina following the initial large tsunami wave. These values closely approximate the real data at the correct time. Figure 4.22 shows a correlation between the peak points and their corresponding times, indicating a successful match between the model and the actual scenario.

4.3. Introduction of Tsunami Induced Current speed and directions to Numerical Model in ANSYS™ AQWA®

Tsunami waves can create severe currents thay may damage vessels and floating structures. Therefore, current speed and direction are significant terms. Borero et al. (2015) state that the currents due to tsunamis apparently take a risk for maritime

operations and their study involves the hazards on ports and harbors because of the tsunami-induced currents.

It is possible to introduce the current by entering the constant depth averaged current speed and direction. Moreover, it is also possible to define depth variable current data. However, current data cannot be introduced as time series. For this reason, firstly, the current data are converted to force and moment acting on floating docks and vessels. Then structure force and moment data can be introduced as time series given as an external file in ANSYS™ AQWA® software.

To obtain the forces due to the currents Equation 4.1 is applied.

$$F_D = \frac{1}{2}\rho C_d V^2 A_n \tag{4.1}$$

where F_D is drag force, C_d is drag coefficient, ρ is sea water density, V is the current speed and A_n is the structure area to the normal flow. The drag coefficients depend on current speed, normal area to the flow, shape and geometry of structure, material roughness and draft.

In this study, tsunami-induced currents are introduced as external forces on the floating dock in a time series. To control this a constant current is entered with a current speed of 4 m/s and the direction perpendicular to the pontoons and the constant current with the same properties is converted to external forces acting on the structure. To comparison of these models connection forces in the y direction are analyzed. When the constant current is entered in AQWA, the average of the forces is 540 N and when the current is entered as external forces in AQWA, the average of the forces is 600 N. Figure 4.23 illustrates the results.

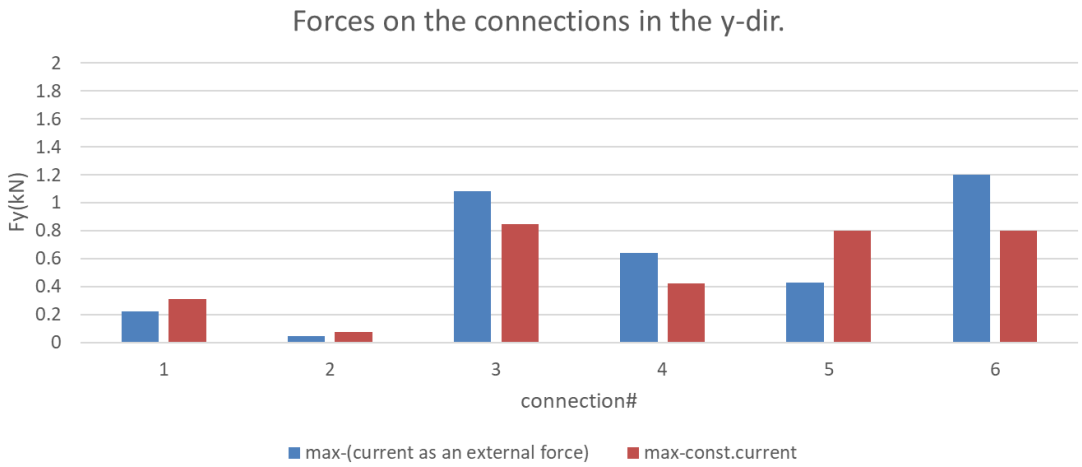

Figure 4.23. Connection forces results of the two models (one includes constant current and the other one is consisted of external forces) in the y direction from AQWA.

As seen in Figure 4.23 the results are close to each other. The current force is calculated as 530 kN force that must be on the connections in the y direction. The calculated one also is similar to the numerical results from AQWA so it is deduced that the software is validated and indicates that a current data can be introduced to AQWA as external forces in a time series with appropriate adjustments.

In this study, the forces and moments are calculated not only on pontoons but also on vessels berthed in docks and then all of them are sum up. Keen et al. (2017) also consider the current force on the vessels to obtain demands of the tsunami induced currents. In their study, the governing drag force equations are obtained from U.S. Army Corps of Engineers (2005), to calculate longitudinal and transverse drag forces due to the current on a vessel. However, U.S. Army Corps of Engineers (2005) recommends the equations for current speeds of 1.5 m/s or below and for boats moored in comparatively big harbors. Since the current velocity data obtained from both of XBeach and NAMIDANCE involves velocities bigger than 1.5 m/s. The formulas given in Britisih standards (BS 6349 - 6: 1989, BS 6349-1: 2000) are used in this study.

4.3.1 Current Forces on Pontoons

The current forces on pontoons are considered longitudinal and transverse axis. The current drag force equation for the pontoons along the longitudinal (in x-axis) and the transverse (in y-axis) are given below:

$$F_x = \frac{1}{2}\rho C_x V^2 A_x \tag{4.2}$$

$$F_y = \frac{1}{2}\rho C_y V^2 A_y \tag{4.3}$$

According to BS6349-6 if the ratio of water depth to the pontoons' draft is smaller than 5, the correction factors must be used. But in this simulation the ratio is about 46.5 so there is no necessary to use the correction factor to calculate force owing to the currents on the floating dock.

To obtain longitidunal and transverse current drag coefficients (Cx and Cy) on pontoons, Figures 4.24 and 4.25 are used.

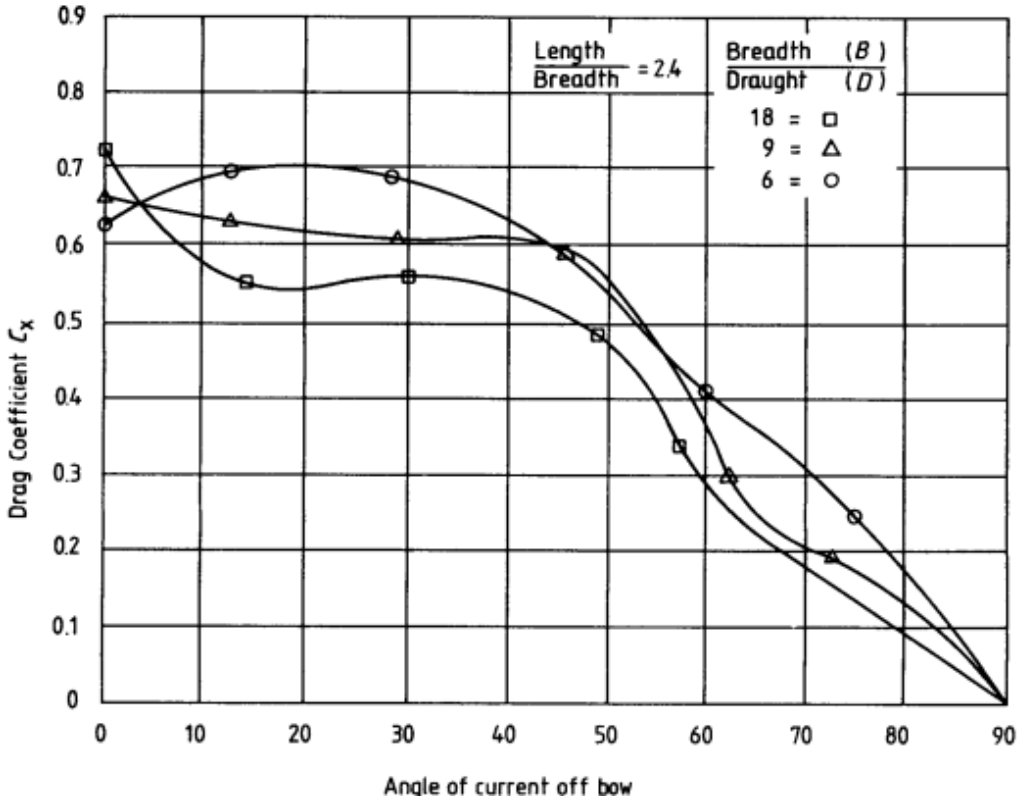

Figure 4.24. Longitudinal drag coefficients for the pontoons (Source: BS 6349 - 6: 1989).

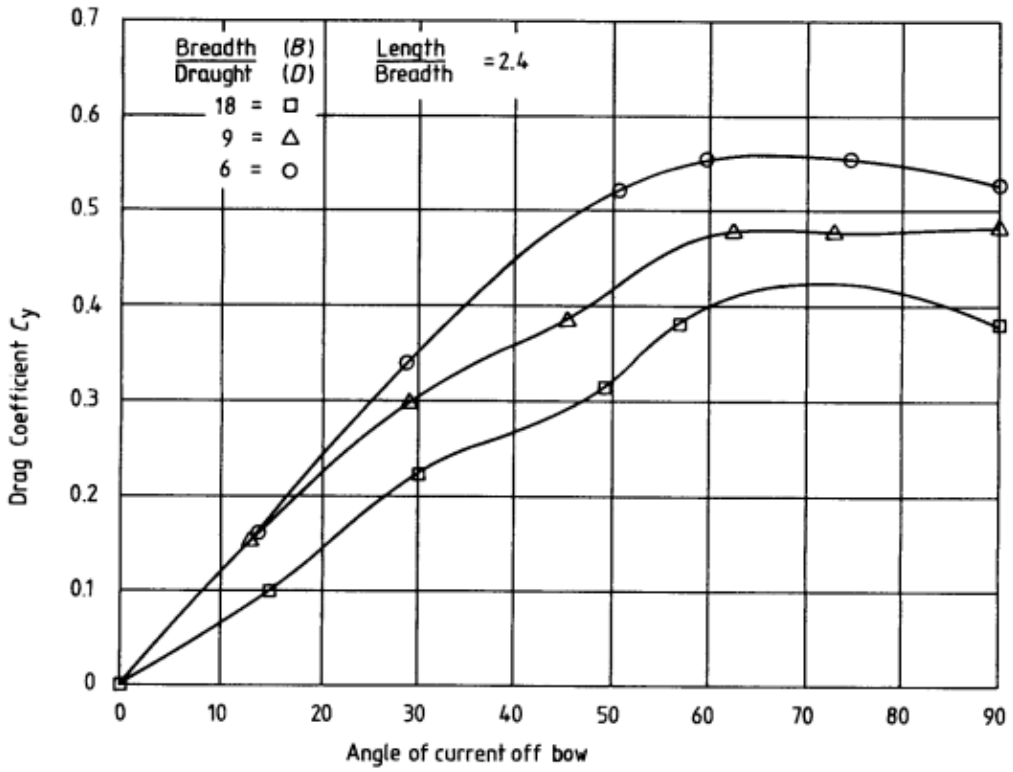

Figure 4.25. Transverse drag force coefficients (Source: BS 6349 - 6: 1989).

4.3.2 Current forces on vessels

Equations 4.4 and 4.5 are used to calculate the transverse and longitudinal current forces on vessels, respectively.

$$F_{TC} = C_{CT} C_{TC} (V_C)^2 L_{BP} D_m \rho \quad (4.4)$$

where; C_{CT} is depth correction factor and C_{TC} is transverse drag force coefficient, L_{BP} is length of the vessels which is perpendicular to the current direction and D_m is draft of the vessels. The drag coefficients for the vessels are obtained from BS 6349 - 6: 1989 as can be seen in Figure 4.26. The depth correction factors are used to obtain force due to the currents on the vessels because the water depth over draft ratio is 2.22. The correction factors for forces in the transverse directions are shown in Figure 4.27. The length and draft of the vessels in Teos Marina are 8 meter and 1,8 meter, respectively as can be seen in Figure 4.28.

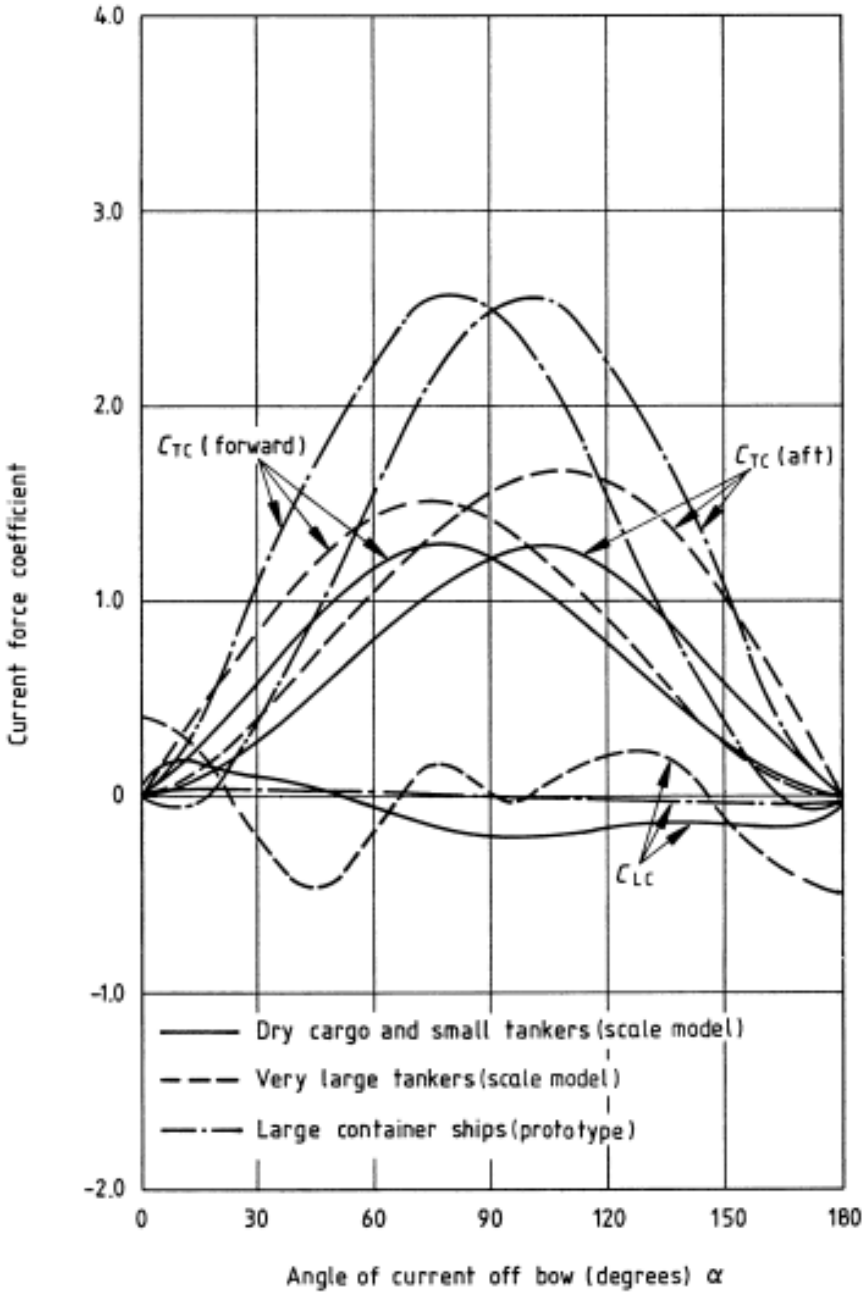

Figure 4.26. Drag force coefficients for vessels (Source: BS 6349 - 6: 1989).

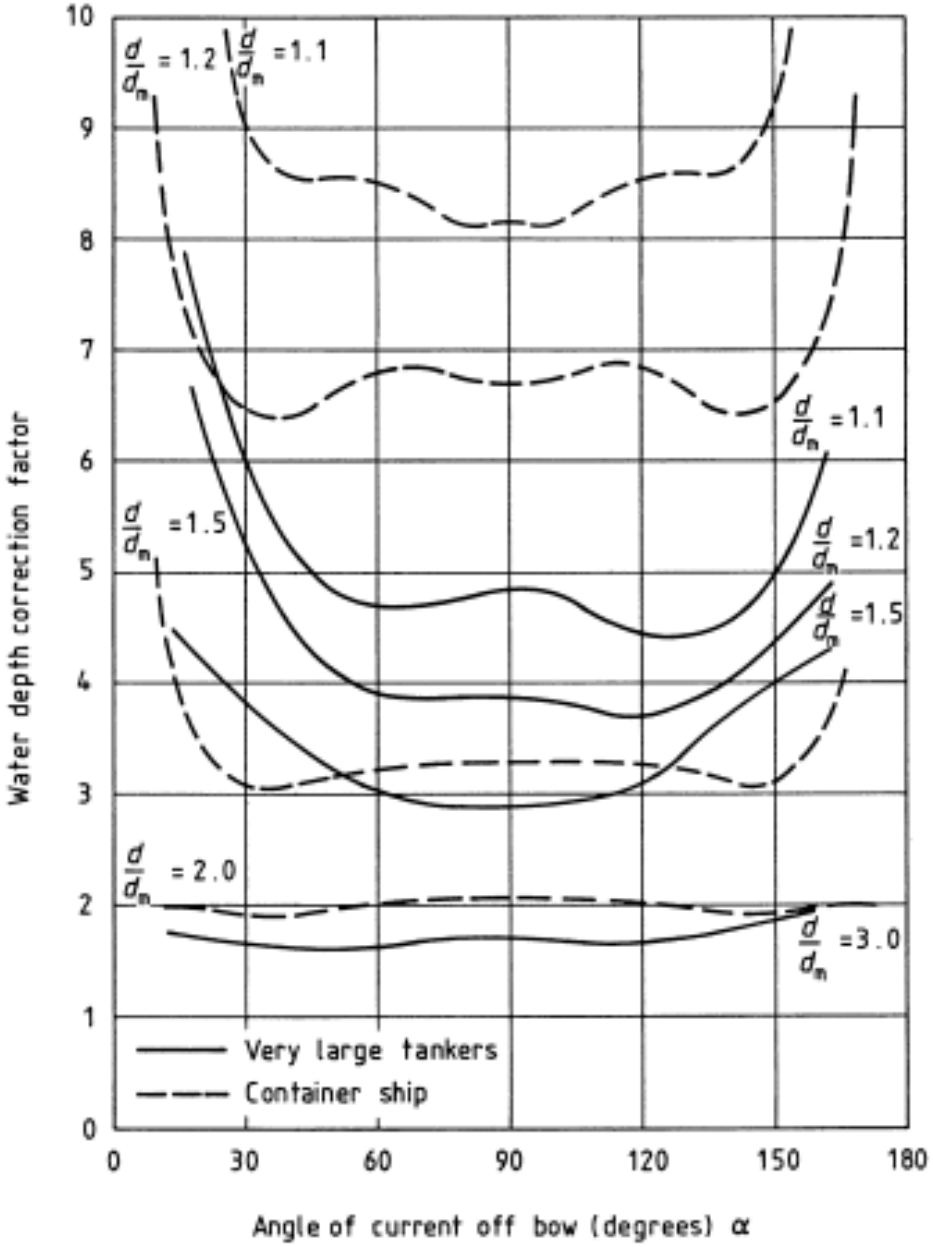

Figure 4.27. Water depth correction coefficients for transverse current force (Source: BS 6349-1: 2000).

Figure 4.28. Draft sizes of the vessels at Teos Marina.

$$F_{LC} = C_{CL} C_{LC} (V_C)^2 L_{BP} D_m \rho \tag{4.5}$$

where; C_{CL} is depth correction factor and C_{LC} is longitudinal drag force coefficient. The depth correction factors are obtained for the study case from BS 6349-1, 2000 as seen in Figure 4.29.

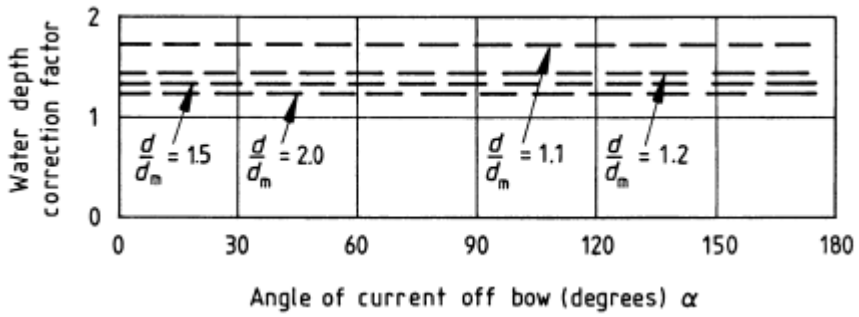

Figure 4.29. Water depth correction coefficients for longitudinal current force (Source: BS 6349-1: 2000).

The longitudinal and tranverse current forces are composed of current forces on the pontoons and vessels, the moments about x and y directions are calculated considering only drag forces on the pontoon, because there is no transfer of the moments from vessel to the pontoon due to berthing of vessel with ropes.

CHAPTER 5

NUMERICAL MODEL RESULTS AND DISCUSSIONS

5.1. Free-Floating Hydrostatic Analysis

The hydrostatic analysis involves volumetric displacement check and metacentric height control. The hydrostatic analysis is examining stability of the free-floating body in still water.

One of the most essential points in the hydrostatic analysis is that the actual and equivalent volumetric displacements should be close to each other. Close results indicate that mesh properties are convenient in the model. In this model, the volumetric displacements are close to each other for all components of the floating dock as seen in table 5.1.

Table 5.1. Volumetric displacements.

Pontoon #	Actual Volumetric Displacement	Equivalent Volumetric Displacement
Pontoon 1	1.1501 m^3	1.1502 m^3
Pontoon 2	1.1501 m^3	1.1502 m^3
Pontoon 3	1.1501 m^3	1.1502 m^3
Pontoon 4	1.1501 m^3	1.1502 m^3
Pontoon 5	1.1501 m^3	1.1502 m^3
Pontoon 6	1.1501 m^3	1.1502 m^3
Pontoon 7	0.8625m^3	0.8625 m^3

Metacentric heights for all pontoons are bigger than the zero as it is calculated, 6.92 m. It means that it is in stable equilibrium in still water. The stability criteria of the metacentric height for the free-floating body are given as small angle stability parameters in AQWA and the results are given in table 5.2.

Table 5.2. Small angle stability parameters.

CoG to CoB (BG)	0.37 m
Metacentric Heights (GM)	6.92 m
CoB to Metacenter (BM)	7.29 m

5.2. Stability Analysis

Determining the stability of the structure without external, waves, current forces, etc. is the purpose of the stability analysis. The stability check examines the responses of the structure for 6 degrees of freedom. The results are shown in Table 5.3 and Table 5.4. To reach more accurate results the software was provided to make more iterations for responses, and this is available with defining maximum error for displacement and rotations iterations which are taken as 10^{-9}m and 10^{-4}°, respectively. The displacements and rotations for all pontoons at these 6 degrees of freedom are close to zero and show that they are stable.

The responses of the pontoons are calculated with respect to the global origin of the model which is at the middle point in the x and y-directions, and water level in the z-direction.

Table 5.3. Displacements of the pontoons in stability analysis.

Pontoon #	X(m)	Y(m)	Z(m)
Pontoon 1	5.27E-04	1.89E-04	-0.03
Pontoon 2	5.24E-04	1.91E-04	-0.04
Pontoon 3	5.23E-04	1.82E-04	-0.04
Pontoon 4	5.22E-04	1.85E-04	-0.05
Pontoon 5	5.21E-04	1.80E-04	-0.05
Pontoon 6	5.20E-04	1.83E-04	-0.05
Pontoon 7	5.17E-04	1.87E-04	-0.05

Table 5.4. Rotations of the pontoon in stability analysis.

Pontoon #	RX(m)	RY(m)	RZ(m)
Pontoon 1	-6.12E-04	5.51E-02	-2.36E-04
Pontoon 2	-6.12E-04	2.81E-02	-2.55E-04
Pontoon 3	-6.12E-04	1.32E-02	-2.23E-04
Pontoon 4	-6.12E-04	-1.79E-03	-2.29E-04
Pontoon 5	-6.14E-04	-1.74E-03	-2.23E-04
Pontoon 6	-6.12E-04	2.40E-03	-2.26E-04
Pontoon 7	-6.10E-04	-1.07E-03	-2.29E-04

5.3. Hydrodynamic Analysis

The hydrodynamic analysis involves determining the responses of the pontoons, forces on the chains and connections and stability controls of the concrete anchorage blocks against sliding and lifting under the tsunami effects. The tsunami impacts are water level changes, current forces, and moments on the floating structure due to the tsunami.

5.3.1 Hydrodynamic Responses

Hydrodynamic responses of the pontoons in six degrees of freedom under the tsunami effect are given in Table 5.5. Pontoon numbers given in Table 5.5 are illustrated in Fig.5.1. Reference points for each pontoon are the same as in the stability analysis.

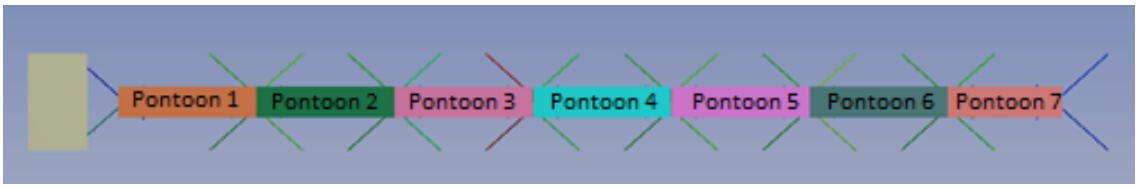

Figure 5.1. Pontoons' numbers.

Table 5.5. Hydrodynamic responses of the pontoons.

	x(m)		y(m)		z(m)	
PONTOON#	min	max	min	max	min	max
1	-0.81	0.97	-0.84	0.90	-2.64	1.64
2	-0.79	0.83	-0.67	0.70	-2.20	1.42
3	-0.78	0.74	-0.67	0.68	-2.12	1.18
4	-0.76	0.72	-0.66	0.66	-2.02	1.11
5	-0.79	0.65	-0.69	0.66	-2.40	1.00
6	-0.86	0.65	-0.71	0.71	-2.58	0.86
7	-1.07	0.65	-0.79	0.78	-2.40	1.06
	RX (°)		RY (°)		RZ (°)	
PONTOON#	min	max	min	max	min	max
1	-43.9	41.6	-11.3	11.6	-5.2	4.6
2	-41.6	40.8	-9.2	9.3	-4.0	3.8
3	-42.0	42.8	-9.0	8.9	-3.7	4.0
4	-41.9	41.7	-8.7	8.8	-4.3	3.8
5	-41.3	40.0	-8.7	9.1	-4.3	4.4
6	-39.8	38.2	-11.2	12.1	-4.9	4.7
7	-38.2	38.4	-12.7	12.1	-5.5	5.5

The pontoons have the most displacement in the z-direction. The reason for that can be the water level changes due to the tsunami.

5.3.2 Forces on the Connections

The numbers of the connections and forces on the connections are given in Figure 5.2 and 5.3, respectively, and the ball and socket joints were broken by the tsunami.

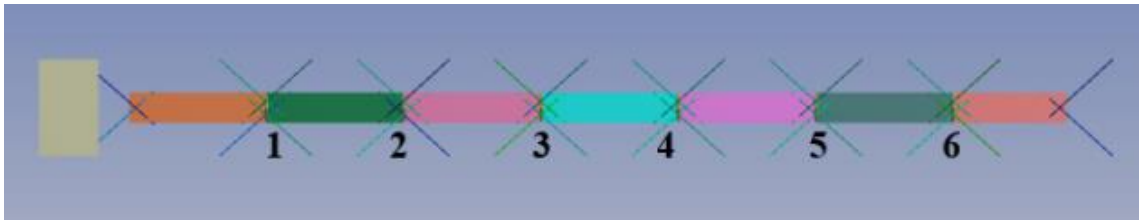

Figure 5.2. Numbered connections.

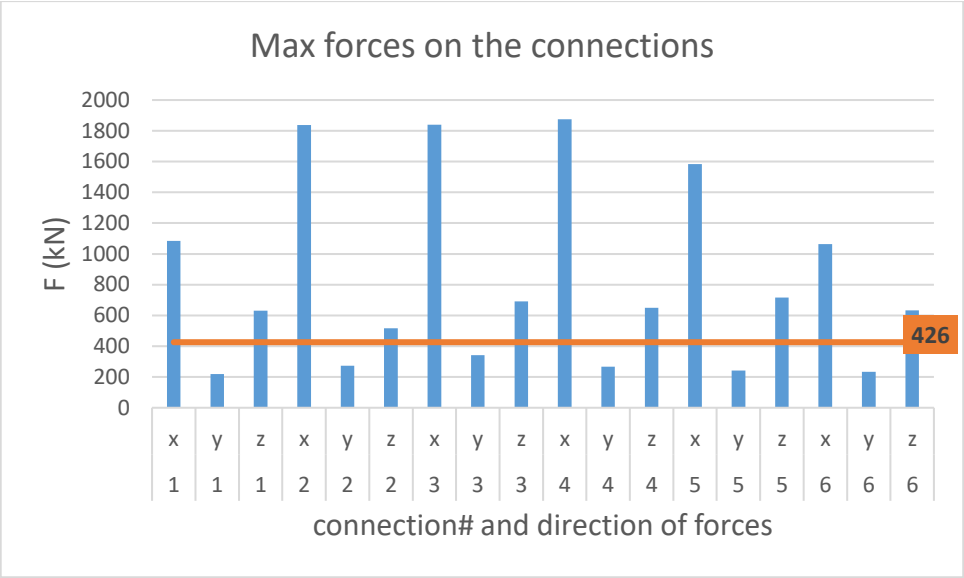

Figure 5.3. Maximum forces on the connections.

Figure 5.3 shows that the forces are higher than the capacity of the connections. The connections are more exposed forces in the x direction as seen in Figure 5.3. The reason may be that forces due to the tsunami-induced currents have stronger components in the x direction rather than the y direction. The tsunami-induced current forces in the x and y direction are given in Figure 5.4 and Figure 5.5, respectively.

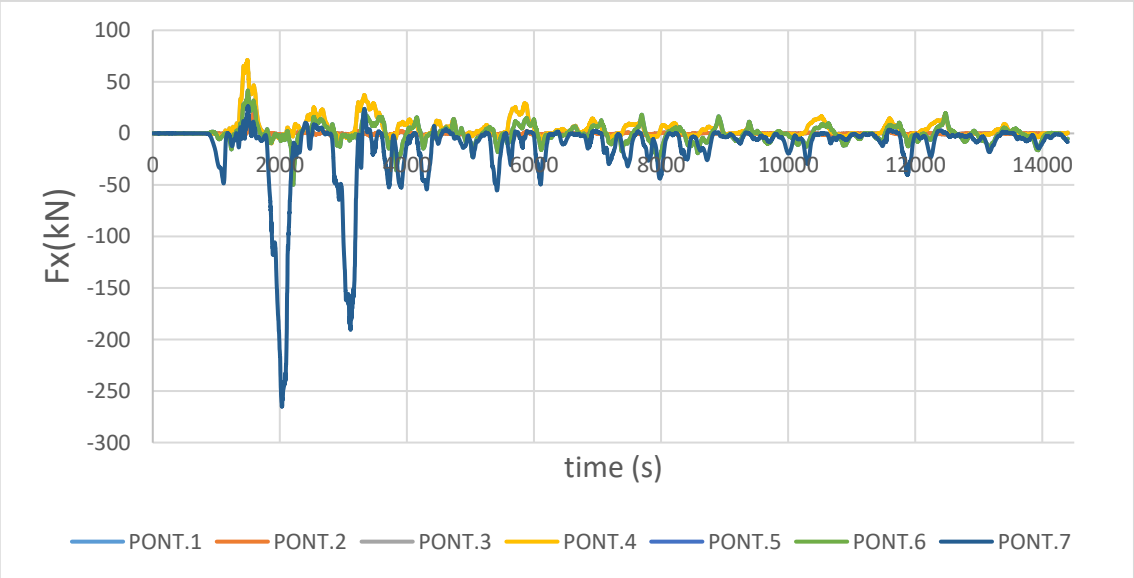

Figure 5.4. Tsunami-induced current forces in the x direction.

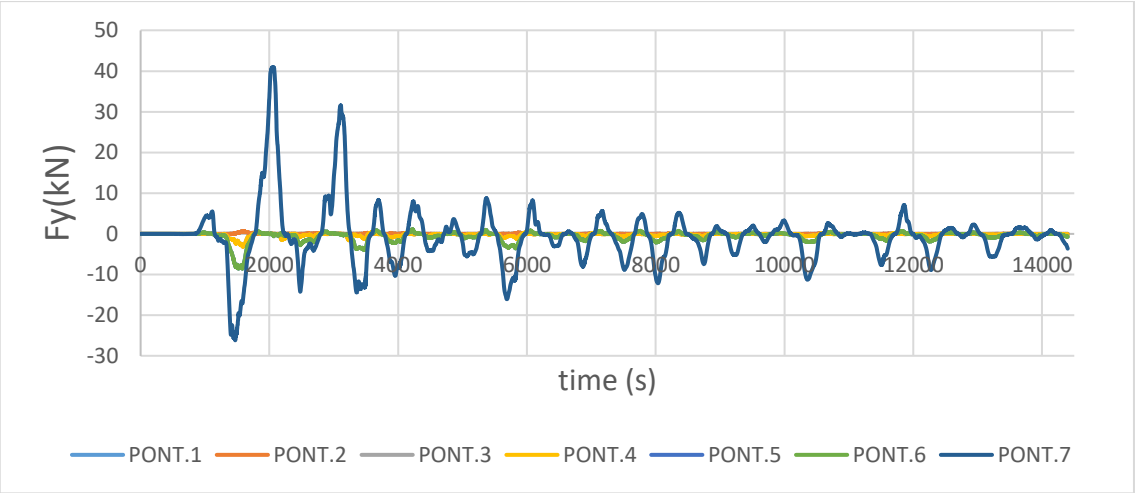

Figure 5.5. Tsunami-induced current forces in the y direction.

The numerical model results show that forces in the x direction creates rotations in y direction. It agrees with what really happened during the tsunami event. A video recorded during the tsunami (TEKNO POLITIK, 2021, 32:43) shows that the first two pontoons started to rotate relative to each other. Moreover, pictures taken during and after the tsunami show that pontoons were split and dragged offshore as shown in Figure 1.2 was mentioned in the Introduction part. As seen in Figure 5.6 the floating dock A was dragged offshore and the pontoons of dock A were split due to the tsunami. This may occur due to the failure of the connections, which are achieved to simulate in the numerical model.

Figure 5.6. Remaining the pontoon of dock A after the tsunami.

5.3.3 Forces on the Chains

The forces on the chains are calculated using cable dynamic option in AQWA under the tsunami effects. Chains are numbered and shown in Figure 5.7. As can be seen in Figure 5.7 chains are oriented to resist against different directions. Calculated tensions in the chains of the floating docks are given in Figure 5.8. The capacity of the chains is also indicated in Figure 5.8.

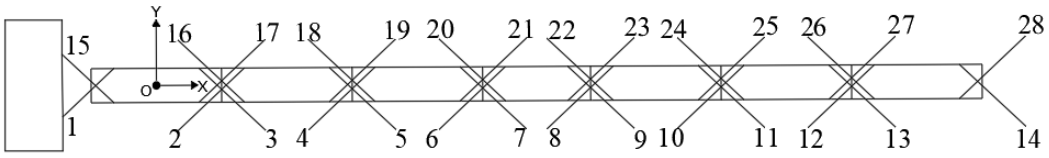

Figure 5.7. Numbered mooring chains.

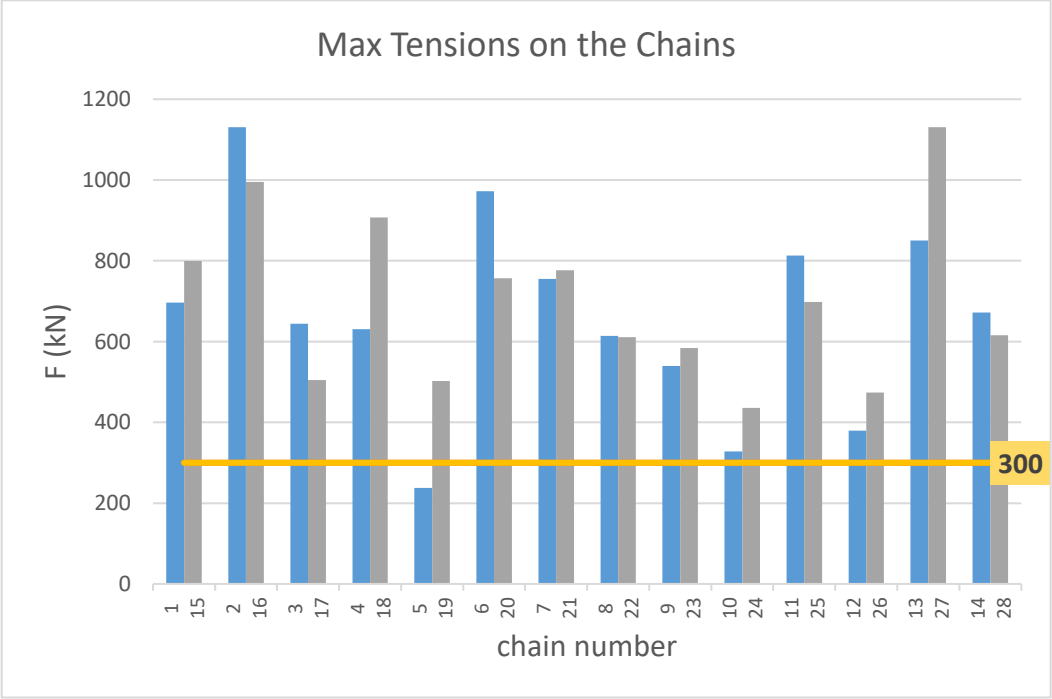

Figure 5.8. Demands from the tsunami and capacity (breaking load) of the chains.

Almost all chains exceeded capacity load which agrees well with the post-tsunami photos showing that pontoons dragged offshore with broken chains. It was realized that the water level changes due to the tsunami have a significant role in chain or fairlead breaking. Figure 5.8 shows that most of the chains were broken due to tsunami loads.

5.3.4 Stability Analysis of Concrete Anchorage Blocks against sliding and uplift

Sliding resistance can be found by the frictional resistance of the concrete anchorage blocks against horizontal pulling force. The horizontal pulling force equals to resultant force on the cable in horizontal directions which are x and y direction.

The sliding of the concrete anchorage block can be controlled by the formula given below:

$$FS_{sliding} = \frac{\sum F_R}{\sum F_D} = \frac{\mu W}{\sqrt{F_x^2 + F_y^2}} \tag{5.1}$$

where $FS_{sliding}$ is factor of safety for sliding and it should not be smaller than 1.5, $\sum F_R$ represents resistance force due to the concrete anchorage block weight, F_x and F_y are forces on chain in x and y direction, respectively. μ is friction coefficient of the seabed and it is taken as 0.5 because the sea bottom material around dock A is sand. It is confirmed by sieve analysis test on a sample taken in the Teos Marina, at the Soil Laboratory of İzmir Institute of Technology. The results of the sliding check for each concrete anchorage block are given in Table 5.6 and Figure 5.9 illustrates the concrete anchorage blocks' numbers.

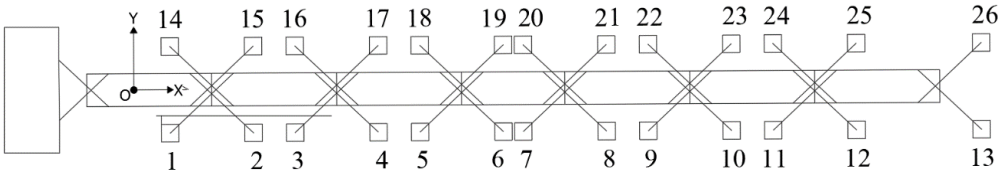

Figure 5.9. Numbered concrete anchorage blocks.

Table 5.6. Sliding controls for each concrete anchorage blocks.

Concrete Block#	Fr(kN)	Fd(kN)	F.S.-sliding	Check
1	23.56	924.72	0.03	*not safe for sliding*
2	23.56	535.76	0.04	*not safe for sliding*
3	23.56	546.92	0.04	*not safe for sliding*
4	23.56	273.41	0.09	*not safe for sliding*
5	23.56	788.99	0.03	*not safe for sliding*
6	23.56	654.50	0.04	*not safe for sliding*
7	23.56	548.95	0.04	*not safe for sliding*
8	23.56	451.98	0.05	*not safe for sliding*
9	23.56	308.46	0.08	*not safe for sliding*
10	23.56	762.21	0.03	*not safe for sliding*
11	23.56	307.32	0.08	*not safe for sliding*
12	23.56	740.81	0.03	*not safe for sliding*
13	23.56	525.40	0.04	*not safe for sliding*
14	23.56	674.16	0.03	*not safe for sliding*
15	23.56	892.11	0.03	*not safe for sliding*
16	23.56	437.81	0.05	*not safe for sliding*
17	23.56	793.46	0.03	*not safe for sliding*
18	23.56	361.57	0.07	*not safe for sliding*
19	23.56	726.27	0.03	*not safe for sliding*
20	23.56	695.19	0.03	*not safe for sliding*
21	23.56	542.51	0.04	*not safe for sliding*
22	23.56	524.36	0.04	*not safe for sliding*
23	23.56	330.50	0.07	*not safe for sliding*
24	23.56	566.71	0.04	*not safe for sliding*
25	23.56	363.96	0.06	*not safe for sliding*
26	23.56	951.76	0.02	*not safe for sliding*

Table 5.6 shows that all the concrete anchorage blocks are sliding under tsunami loads. Sliding results of the numerical model agree well with observations and measurements in the marina after the tsunami. It is also observed that some concrete anchorage blocks uplifted and floated during the tsunami. Therefore, it is also checked that uplift of the anchorage blocks could be simulated or not in the numerical model.

In the case of up-lifting, there are three forces to be considered on a concrete anchorage block. These are weight of the concrete anchorage block, buoyancy force on a concrete anchorage block and tension in the mooring chain in the vertical (z) direction. If the weight of the concrete anchorage block is bigger than the summation of both

buoyancy and chain tension forces in Z direction, up-lift will not occur. It can be mathematically expressed as,

$$W - F_B > |F_Z| \tag{5.2}$$

where F_B and F_Z are the buoyancy force on the concrete anchorage block and chain tension force in the z-direction, respectively. Table 5.7 shows the uplift results of concrete anchorage blocks during the tsunami.

Table 5.7. Uplift check for each concrete anchorage blocks.

Concrete Block#	W(kN)	Fb(kN)	Fz(kN)	Control
1	47.13	18.23	-439.34	*uplift*
2	47.13	18.23	-373.27	*uplift*
3	47.13	18.23	-319.19	*uplift*
4	47.13	18.23	-147.38	*uplift*
5	47.13	18.23	-492.38	*uplift*
6	47.13	18.23	-452.00	*uplift*
7	47.13	18.23	-353.32	*uplift*
8	47.13	18.23	-183.88	*uplift*
9	47.13	18.23	-108.96	*uplift*
10	47.13	18.23	-322.75	*uplift*
11	47.13	18.23	-191.54	*uplift*
12	47.13	18.23	-339.80	*uplift*
13	47.13	18.23	-322.44	*uplift*
14	47.13	18.23	-444.74	*uplift*
15	47.13	18.23	-279.32	*uplift*
16	47.13	18.23	-459.80	*uplift*
17	47.13	18.23	-358.22	*uplift*
18	47.13	18.23	-266.40	*uplift*
19	47.13	18.23	-420.03	*uplift*
20	47.13	18.23	-421.22	*uplift*
21	47.13	18.23	-318.28	*uplift*
22	47.13	18.23	-218.58	*uplift*
23	47.13	18.23	-375.98	*uplift*
24	47.13	18.23	-254.89	*uplift*
25	47.13	18.23	-591.38	*uplift*
26	47.13	18.23	-280.72	*uplift*

As can be seen in Table 5.7 all the concrete anchorage blocks floated. According to the eyewitnesses of the tsunami in the marina, the concrete anchorage blocks floated, and this case is confirmed with uplift controls for the concrete anchorage.

CHAPTER 6

CONCLUSIONS

The most recent tsunami occurred on 30 October 2020 in the Aegean Sea, which was generated by an Mw 6.6 normal-faulting earthquake, between Izmir and Samos Island. The tsunami severely damaged the Turkish and Greek coasts and killed one person in Seferihisar. Especially, floating docks in Teos Marina, Seferihisar were highly damaged due to tsunami hydrodynamic forces. It was observed that the mooring chains and fairleads were broken, and the pontoons were dragged offshore. Moreover, the aluminum frames of docks and the moored ships were damaged. This thesis focused on examining the tsunami-induced damage on the floating docks, specifically Dock A which was the most damaged in Teos Marina. A numerical model was used to investigate the hydrodynamic behavior of the floating pontoons under tsunami-induced forces. After checking the stability of the pontoons without any external forces such as wave, wind, or currents, etc., hydrodynamic responses of the pontoons, forces on the mooring chains and forces on the connections and anchorage blocks were calculated. Results were compared with the post-tsunami surveys, photos, records, and eyewitness testimonies.

The following conclusions were derived from the numerical model results:

1. The literature survey shows that mid-fidelity hydrodynamic numerical models based on potential flow theory solved in the time domain have not been used in tsunami-induced damages on the floating docks. Since mid-fidelity hydrodynamic tools enable to simulate nonlinear subsystems like the joints and mooring chains, they have advantages in modeling floating docks. In this study, for the first time, water level changes and currents due to the tsunami could be introduced to a mid-fidelity model, Ansys-AQWA, by coupling the frequency spectrum of tsunami-induced water surface elevations and the time series of the current forces. Agreement between the water surface elevations of the target and the model, especially for the biggest tsunami wave in the time series showed that it was achieved to simulate the tsunami impacts in the numerical model.

2. The demand tension loads due to the tsunami calculated by the numerical model exceeded the capacity load for almost all the tensioned chains, which agrees well with the post-tsunami photos showing that pontoons dragged offshore with broken chains.
3. Calculations based on the numerical model indicated that many of the concrete blocks used as mooring anchors were dragged and uplifted due to the tsunami. Eyewitness observations support this result. The main reason for the uplift is water level changes due to the tsunami.
4. The connections between the pontoons experienced rotations and forces exceeding their capacity in the numerical model that agrees with the post-tsunami records showing that relative rotations and split of the pontoons dragged offshore.
5. It can be suggested that if all the floating docks in Teos Marina can be modeled, more accurate results might be obtained. However, it was not possible due to high computer cost.

Consequently, the tsunami-induced damage to floating dock A in Teos Marina were examined successfully in this study. The numerical analysis results are well-matched with the actual event. The inferences of the study can contribute to a better understanding of the hazards on the floating pontoons due to tsunamis, especially in ports, and highlight the prominence of further research on the improved strength of coastal structures and resistance to tsunami-like extreme conditions.

REFERENCES

AFAD. 2020. Disaster and Emergency Management Authority (AFAD), Ministry of Interiors, Ankara-Turkey. http://deprem.afad.gov.tr.

Aktaş Kadir, Al Karem Ruwad Adnan , Öztunalı Özbahçeci Bergüzar, Özkol Ünver. n.d. "Hydrodynamic Modeling Of Floating Offshore Wind Turbines." 9. Kıyı Mühendisliği Sempozyumu. 788-801.

Alkarem, Y.R., Ozbahceci B.O. 2021. "A Complemental Analysis Of Wave Irregularity Effect On The Hydrodynamic Responses Of Offshore Wind Turbines With The Semi-Submersible Platform." Applied Ocean Research 113. https://doi.org/10.1016/j.apor.2021.102757.

Alpar Bedri, Kuran Uğur, Yalçıner Ahmet C., and Altınok Yıldız. 2005. "Türkiye Çevresi Denizlerde Depreşim Dalgası Oluşma Olasılığı Bulunan Bazı Bölgeler." *Türkiye Mühendislik Haberleri Sayi 438*.

Altendorf Christine T., Curfman David, Balkus Nancy J., and Mcandrew Michael. 2020. *Unified Facilities Criteria (Ufc) Approved For Public Release; Distribution Unlimited Moorings*. Washington, DC.: UFC 4-159-03.

Altinok, Y, and S Ersoy. 2000. "Tsunamis Observed on and Near the Turkish Coast." *Natural Hazards*. Vol. 21.

Altınok Yıldız. 2005. "Türkiye Çevresinde Tarihsel Tsunamiler." *Türkiye Mühendislik Haberleri Sayi 438* .

Altınok Yıldız, and Ersoy Şükrü. 1994. "Türkiye Kıyıları ve Yakın Çevresini Etkileyen Tsunamiler." *İstanbul Üniv. Müh. Fak. Yerbilimleri Dergisi* 9: 111–23.

Ambraseys, N. N. 1962. Data for the investigation of the seismic sea-waves in the Eastern Mediterranean, Bull. Seism. Soc. Am. 52, 895–913.

Ambraseys, N. 2002. "The Seismic Activity of the Marmara Sea Region over the Last 2000 Years." *Bulletin of the Seismological Society of America*. Vol. 92.

Agency,Anadolu.2020.Accessed 2023. https://www.aa.com.tr/tr/yasam/kismitsunamide-olen-kadinin-oglu-ile-torunu-yasadiklarini-anlatti/2030786#.

Ansys Inc. 2020. “Aqwa Theory Manual Third-Party Software.” http://www.ansys.com.

Antonopoulos, J. 1979. “Catalogue of Tsunamis in the Eastern Mediterranean from Antiquity to Present Times.”

Aytore, Betul, Ahmet Cevdet Yalciner, Andrey Zaytsev, Zeynep Ceren Cankaya, and Mehmet Lütfi Suzen. 2016. “Assessment of Tsunami Resilience of Haydarpaşa Port in the Sea of Marmara by High-Resolution Numerical Modeling.” *Earth, Planets and Space* 68 (1). https://doi.org/10.1186/s40623-016-0508-z.

Baptista, M A, * S Heitor, J M Miranda,’, P Miranda134, and L Mendes Victor’. 1998. “The 1755 Lisbon Tsunami; Evaluation Of The Tsunami Parameters.” *J. Geodynamics*. Vol. 25.

Barthe ́lemy Eric. 2004. “Nonlinear Shallow Water Theories For Coastal Waves.” *Surveys in Geophysics* 25.

Borrero, Jose C., and Derek G. Goring. 2015. “South American Tsunamis in Lyttelton Harbor, New Zealand.” *Pure and Applied Geophysics* 172 (3–4): 757–72. https://doi.org/10.1007/s00024-014-1026-1.

Borrero, Jose C., Patrick J. Lynett, and Nikos Kalligeris. 2015. “Tsunami Currents in Ports.” *Philosophical Transactions of the Royal Society A: Mathematical, Physical and Engineering Sciences*. Royal Society of London. https://doi.org/10.1098/rsta.2014.0372.

British Standards Institution. 2003. *Maritime Structures. Part 1, Code of Practice for General Criteria.* British Standards Institution.

Brown, David T. 2005. "Chapter 8: Mooring Systems ." In *Handbook of Offshore Engineering*. London UK: Elsevier Ltd.

Chandrasekaran Srinivasan. n.d. *Ocean Engineering & Oceanography*. Edited by Florida Atlantic University SeaTech, Dania Beach, USA Nikolas I. Xiros, New Orleans, USA Manhar R. Dhanak. Vol. 9. Springer Nature. http://www.springer.com/series/10524.

Çekirdekçi, Burak Tunç. 2015. “ANSYS AQWA Ile Gemi ve Açık Deniz Yapıları Dizaynına Yönelik Çözümler,” 30–36.

Çekirdekçi, Burak T. 2015. "Science Engineering And Technology Cfd Applications For Seakeeping Calculations Of Floating Bodies." Master's thesis, Istanbul Technical University.

Çiçek, Yağiz Arda. 2022. “Coupling Of Nami Dance And Xbeach Numerical Models To Simulate Tsunami Induced Morphological Changes: Case Study In Siğacik Bay.” Master's thesis, Middle East Technical University.

Costas Emmanuel Synolakis, By, and James Eric Skjelbreia. n.d. “Evolution Of Maximum Amplitude Of Solitary Waves On Plane Beaches.”

Dean Robert G., and Dalrymple Robert A. 1984. *Water Wave Mechanics For Engineers And Scientists*. Vol. 2. Farrer Road, Singapore: World Scientific Publishing Co. Pte. Ltd.

Dengler, L., B. Uslu, A. Barberopoulou, S. C. Yim, and Annabel Kelly. 2009. “The November 15, 2006 Kuril Islands-Generated Tsunami in Crescent City, California.” In *Pure and Applied Geophysics*, 166:37–53. https://doi.org/10.1007/s00024-008-0429-2.

Dogan, Gozde Guney, Alessandro Annunziato, Gerassimos A. Papadopoulos, Hasan Gokhan Guler, Ahmet Cevdet Yalciner, Tarık Eray Cakir, Ceren Ozer Sozdinler, et al. 2019. “The 20th July 2017 Bodrum–Kos Tsunami Field Survey.” *Pure and Applied Geophysics* 176 (7): 2925–49. https://doi.org/10.1007/s00024-019-02151-1.

Dogan, Gozde Guney, Efim Pelinovsky, Andrey Zaytsev, Ayse Duha Metin, Gulizar Ozyurt Tarakcioglu, Ahmet Cevdet Yalciner, Bora Yalciner, and Ira Didenkulova. 2021. “Long Wave Generation and Coastal Amplification Due to Propagating Atmospheric Pressure Disturbances.” *Natural Hazards* 106 (2): 1195–1221. https://doi.org/10.1007/s11069-021-04625-9.

Dogan, Gozde Guney, Ahmet Cevdet Yalciner, Yalcin Yuksel, Ergin Ulutaş, Orhan Polat, Işıkhan Güler, Cihan Şahin, Ahmet Tarih, and Utku Kânoğlu. 2021. “The 30 October 2020 Aegean Sea Tsunami: Post-Event Field Survey Along Turkish Coast.” *Pure and Applied Geophysics* 178 (3): 785–812. https://doi.org/10.1007/s00024-021-02693-3.

Fritz, Hermann M., Jose C. Borrero, Costas E. Synolakis, and Jeseon Yoo. 2006. “2004 Indian Ocean Tsunami Flow Velocity Measurements from Survivor Videos.” *Geophysical Research Letters* 33 (24). https://doi.org/10.1029/2006GL026784.

GEER, Hellenic Association of Earthquake Engineering, Earthquake Engineering Association of Turkey, Earthquake Foundation of Turkey, and Earthquake Engineering Research Institute (USA). 2020. “Seismological and Engineering Effects of the M 7.0 Samos Island (Aegean Sea) Earthquake.” https://doi.org/10.18118/G6H088.

German Standard Chain. Accessed 2023. http://www.firstrigging.com/1-5-German-standard-chain.html#seds .

Ghafari Hamidreza, Dardel Morteza. 2018. "Parametric study of catenary mooring system on the dynamic response of the semi-submersible platform." Ocean Engineering 153: 319–332. https://doi.org/10.1016/j.oceaneng.2018.01.093.

Goda, Yoshimi. 2000. *Random Seas and Design of Maritime Structures (Advanced Series on Ocean Engineering 15)*. Vol. 15. World Scientific Publishing Co. Pte. Ltd. .

González Frank I. 1999. “TSUNAMI!” *Scientific American* 280 (May): 56–65. https://doi.org/10.2307/26058242.

Gumusay, Mustafa Umit, Gokalp Koseoglu, and Tolga Bakirman. 2016. “An Assessment of Site Suitability for Marina Construction in Istanbul, Turkey, Using GIS and AHP Multicriteria Decision Analysis.” *Environmental Monitoring and Assessment* 188 (12). https://doi.org/10.1007/s10661-016-5677-5.

Gupta, Harsh K, and Vineet K Gahalaut. 2013. “Springer Briefs In Earth Sciences.” http://www.springer.com/series/8897.

Hall, Matthew, and Andrew Goupee. 2015. “Validation of a Lumped-Mass Mooring Line Model with DeepCwind Semisubmersible Model Test Data.” *Ocean Engineering* 104 (June): 590–603. https://doi.org/10.1016/j.oceaneng.2015.05.035.

Horikawa K. 1961. “Tsunami phenomena in the light of engineering viewpoint. Report on the Chilean tsunami of May 24, 1960, as observed along the coast of Japan.“ Tokyo, Japan: University of Tokyo

Huang, Wei Hua, and Ray Yeng Yang. 2021. “Water Depth Variation Influence on the Mooring Line Design for Fowt within Shallow Water Region.” *Journal of Marine Science and Engineering* 9 (4). https://doi.org/10.3390/jmse9040409.

International Information Center. International Tsunami Information Center, A UNESCO/IOC-NOAA Partnership. 2023. "What Determines how Destructive a Tsunami Will Be near the Origin and at a Distant Shore?" http://itic.ioc-unesco.org/index.php?option=com_content&view=article&id=1206:what-determines-how-destructive-a-tsunami-will-be-near-the-origin-and-at-a-distant-shore&catid=1340&Itemid=2051#:~:text=Tsunamis%20arrive%20at%20a%20coastline,50%2D60%20km%2Fh.

Kânoğlu, Utku, V. Titov, E. Bernard, and C. Synolakis. 2015. “Tsunamis: Bridging Science, Engineering and Society.” *Philosophical Transactions of the Royal Society A: Mathematical, Physical and Engineering Sciences*. Royal Society of London. https://doi.org/10.1098/rsta.2014.0369.

Keen, Adam S., Patrick J. Lynett, Martin L. Eskijian, Aykut Ayca, and Rick Wilson. 2017. “Monte Carlo–Based Approach to Estimating Fragility Curves of Floating Docks for Small Craft Marinas.” *Journal of Waterway, Port, Coastal, and Ocean Engineering* 143 (4). https://doi.org/10.1061/(asce)ww.1943-5460.0000385.

Kian, Rozita, Deniz Velioglu, Ahmet Cevdet Yalciner, and Andrey Zaytsev. 2016. “Effects of Harbor Shape on the Induced Sedimentation; L-Type Basin.” *Journal of Marine Science and Engineering* 4 (3). https://doi.org/10.3390/jmse4030055.

Koshimura, Shunichi, Satomi Hayashi, and Hideomi Gokon. 2014. “The Impact of the 2011 Tohoku Earthquake Tsunami Disaster and Implications to the Reconstruction.” *Soils and Foundations* 54 (4): 560–72. https://doi.org/10.1016/j.sandf.2014.06.002.

Kundu Anjan. 2007. *Tsunami and Nonlinear Waves*.

Lander, James F, Lowell S Whiteside, and Patricia A Lockridge. 2002. “A Brief History Of Tsunamis In The Caribbean Sea.” *Science of Tsunami Hazards*. Vol. 20.

Levin Boris, and Nosov Mikhail. 2009. *Physics of Tsunamis*.

Li, Linlin, Qiang Qiu, and Zhenhua Huang. 2012. “Numerical Modeling of the Morphological Change in Lhok Nga, West Banda Aceh, during the 2004 Indian Ocean Tsunami: Understanding Tsunami Deposits Using a Forward Modeling Method.” *Natural Hazards* 64 (2): 1549–74. https://doi.org/10.1007/s11069-012-0325-z.

Lin, Yu Hsien, Shin Hung Kao, and Cheng Hao Yang. 2019. “Investigation of Hydrodynamic Forces for Floating Offshore Wind Turbines on Spar Buoys and Tension Leg Platforms with the Mooring Systems in Waves.” *Applied Sciences (Switzerland)* 9 (3). https://doi.org/10.3390/app9030608.

Lin, Yu Hsien, and Cheng Hao Yang. 2020. “Hydrodynamic Simulation of the Semi-Submersible Wind Float by Investigating Mooring Systems in Irregular Waves.” *Applied Sciences (Switzerland)* 10 (12). https://doi.org/10.3390/app10124267.

Lost Christchurch. 2012. The earthquake wave at Lyttelton, 1868. See http://lostchristchurch.org.nz/the-earthquake-wave-at-lyttelton-1868 (accessed 15 March 2015).

Lynett, Patrick J., Jose C. Borrero, Robert Weiss, Sangyoung Son, Dougal Greer, and Willington Renteria. 2012. “Observations and Modeling of Tsunami-Induced Currents in Ports and Harbors.” *Earth and Planetary Science Letters* 327–328 (April): 68–74. https://doi.org/10.1016/j.epsl.2012.02.002.

Lynett, Patrick J., Kara Gately, Rick Wilson, Luis Montoya, Diego Arcas, Betul Aytore, Yefei Bai, et al. 2017. “Inter-Model Analysis of Tsunami-Induced Coastal Currents.” *Ocean Modeling* 114 (June): 14–32. https://doi.org/10.1016/j.ocemod.2017.04.003.

Mori, Nobuhito, Tomoyuki Takahashi, Tomohiro Yasuda, and Hideaki Yanagisawa. 2011. “Survey of 2011 Tohoku Earthquake Tsunami Inundation and Run-Up.” *Geophysical Research Letters*. Blackwell Publishing Ltd. https://doi.org/10.1029/2011GL049210.

Nami Dance. 2016. “Nami Dance User_Manual_5.9.”

National Renewable Energy Laboratory (NREL), Sandia National Laboratories. 2023. "Next-Generation Marine Energy Software Needs Assessment."

Nistor Ioan, Palermo Dan , Cornett Andrew , and Al-Faesly Taofiq. 2010. "Experimental And Numerical Modeling Of Tsunami Loading On Structures."

OCDI. 2002. *Technical Standards and Commentaries for Port and Harbor Facilities in Japan*. *Japan Ports and Harbours Association*. Japan.

Orcina Ltd. n.d. “OrcaFlex Manual.”

Özbahçeci Öztunalı Bergüzar, Al Karem Ruwad Adnan , İren Ümit, 2018 "Yüzer Dalgakiranlarin Performansinin Sayisal Modelle İncelenmesi." 9. Kıyı Mühendisliği Sempozyumu. 776-787.

Özer, Ceren, and Ahmet Cevdet Yalçıner. 2011. “Sensitivity Study of Hydrodynamic Parameters During Numerical Simulations of Tsunami Inundation.” *Pure and Applied Geophysics* 168 (11): 2083–95. https://doi.org/10.1007/s00024-011-0290-6.

Özkan, Özgür. 2008. “İstanbul Teknik Üniversitesi Fen Bilimleri Enstitüsü Türkiye’de Marinalarin Kamusal Kullanima Etkileri Ve Öneriler.”

Papazachos B. C., Koutitas, Hatzıdımıtrıou P. M., Karacostas B. G., and Papaıoannou A. 1986. “Tsunami Hazard in Greece and the Surrounding Area.” *Annales Geophysicae*, 79–90.

Pringgana Gede, Cunningham Lee S. , Rogers Benedict D. 2016. "Modeling of tsunami-induced bore and structure interaction." Engineering and Computational Mechanics 109-125.

Regina, M. Yasmin, and E. Syed Mohamed. 2022. “Modeling Study of Tsunami Wave Propagation.” *International Journal of Environmental Science and Technology*. Institute for Ionics. https://doi.org/10.1007/s13762-022-04484-2.

Roelvink, Dano, Ad Reniers, Ap Van Dongeren, Jaap Van Thiel De Vries, Jamie Lescinski, and Robert Mccall Report. 2010. “XBeach Model Description and Manual Version 6 XBeach Model Description and Manual.”

Samaei, Seyed Reza, Azarsina Farhood , Ghahferokhi Mohammad Asadian. 2016. "Numerical Simulation of Floating Pontoon Breakwater with ANSYS AQWA Software and Validation of the Results with Laboratory Data." Bulletin de la Société Royale des Sciences de Liège 85: 1487 - 1499.

Shuto, N. 1991. “Numerical Simulation of Tsunamis-Its Present and Near Future.” *Natural Hazards*. Vol. 4.

Sievers HA, Villegas GC, Barros G. 1963. The seismic sea wave of 22 May 1960 along the Chilean coast. Bull. Seismol. Soc. Am. 53, 1125–1190.

Smit, P B, G S Stelling, D Roelvink, J Van Thiel De Vries, R Mccall, A Van Dongeren, C Zwinkels, and R Jacobs. 2010. “XBeach: Non-Hydrostatic Model.”

Sumer, B Mutlu, Atilla Ansal, ; K Önder Çetin, Jesper Damgaard, ; A Riza Gunbak, Niels-Erik Ottesen Hansen, Andrzej Sawicki, et al. 2007. “Earthquake-Induced Liquefaction around Marine Structures.” https://doi.org/10.1061/ASCE0733-950X2007133:155.

Tekno Politik,. 2021. *30 Ekim Samos Depremi ve Tsunamisinde Teos Marinada neler oldu?* Accessed 2023. https://www.youtube.com/watch?v=74V-fMvRwhM&t=1962s&ab_channel=TEKNOPOLITIK.

Teosmarina.com.tr. “Technical Services.” Teos Marina: The address of peace and trust. Accessed July 1, 2023. https://www.teosmarina.com.tr/en/teknik-hizmetler.html.

Teosmarina.com.tr. “About Us.” Teos Marina: The address of peace and trust. Accessed July 1, 2023. https://www.teosmarina.com.tr/en/kurumsal.html.

Velioğlu Söğüt, Deniz, and Ahmet Cevdet Yalçıner. 2019. “Performance Comparison of Nami Dance and FLOW-3D® Models in Tsunami Propagation, Inundation and Currents Using NTHMP Benchmark Problems.” *Pure and Applied Geophysics* 176 (7): 3115–53. https://doi.org/10.1007/s00024-018-1907-9.

Watson, David G. M. 1998. *Practical Ship Design*. Elsevier.

Whitham, G. B. (Gerald Beresford). 1974. *Linear and Nonlinear Waves*. Wiley.

Williams, A N, H S Lee, and Z Huang. 2000. “Floating Pontoon Breakwaters.” *Ocean Engineering*. Vol. 27. www.elsevier.com/locate/oceaneng.

Wilson, Rick I., Amanda R. Admire, Jose C. Borrero, Lori A. Dengler, Mark R. Legg, Patrick Lynett, Timothy P. McCrink, et al. 2013. “Observations and Impacts from the 2010 Chilean and 2011 Japanese Tsunamis in California (USA).” *Pure and*

Applied Geophysics 170 (6–8): 1127–47. https://doi.org/10.1007/s00024-012-0527-z.

Wiśniewski, Bernard, and Tomasz Wolski. 2012. “The Safety of the Shipping and Ports in the Aspect of the Tsunami Events.” *Scientific Journals* 30 (102): 150–57.

Wood, Nathan J., and Jeff Peters. 2015. “Variations in Population Vulnerability to Tectonic and Landslide-Related Tsunami Hazards in Alaska.” *Natural Hazards* 75 (2): 1811–31. https://doi.org/10.1007/s11069-014-1399-6.

Yalçıner, A C, Kuran, U., Akyarli, A., & Imamura, F. 1995. An Investigation on the Propagation of Tsunamis in the Aegean Sea by Mathematical Modeling BT - Tsunami: Progress in Prediction, Disaster Prevention and Warning (Y. Tsuchiya & N. Shuto, Eds.). https://doi.org/10.1007/978-94-015-8565-1_4

Yalçıner Ahmet C. 1999. “1999 İzmit Tsunamisi.” *Bilim ve Teknik.*

Yalçıner A. C. Alpar B., Altınok Y., Özbay I., Imamura F. 2002. "Tsunamis in the Sea of Marmara: Historical Documents for the Past, Models for Future" Special Issue of Marine Geology, V: 190, (2002) 445-463.

Yalçıner, A. C., Pelinovsky, E., Zaitsev, A., Kurkin, A., Özer, C., Karakuş, H., & Özyurt, G. 2007. Modeling and visualization of tsunamis: Mediterranean examples. In Tsunami and Nonlinear Waves (pp. 273-283). Springer, Berlin, Heidelberg.

Yalçıner A. C., and Synolakis C. E. 2007. Tsunamis and their impacts on Marine Structures, Guidelines on seismic-induced liquefaction around marine structures" in LIMAS Special Issue in ASCE Journal of Waterway, Port, Coastal and Ocean Engineering (Editor Mutlu Sumer). Volume: 133 Issue: 1 Pages: 55-82 Published: JAN-FEB 2007

Zahibo, Narcisse, Efim Pelinovsky, Ahmet Yalçıner, Andrey Kurkin, Andrey Koselkov, and Andrey Zaitsev. 2003. “The 1867 Virgin Island Tsunami: Observations and Modeling.” *Oceanologica Acta* 26 (5–6): 609–21. https://doi.org/10.1016/S0399-1784(03)00059-8.

Zaytsev, A. I., E. N. Pelinovsky, A. Yalçıner, H. Susmoro, G. Prasetya, R. Hidayat, G. I. Dolgikh, et al. 2019. “Generation of the 2018 Tsunami on Sulawesi Island:

Possible Sources." *Doklady Earth Sciences* 486 (1): 588–92. https://doi.org/10.1134/S1028334X19050295.

Zheng Yanna, Li Jiafan , Mu Yingna , Zhang Yu , Huang Siyao , Shao Xiran. 2023. "Numerical Study on Wave Dissipation Performance of OWC-Perforated Floating Breakwater under Irregular Waves." Edited by Francesco Riganti Fulginei. Sustainability 15 (14). https://doi.org/10.3390/su151411427.

Zhang, Yinglong J., Robert C. Witter, and George R. Priest. 2011. "Tsunami-Tide Interaction in 1964 Prince William Sound Tsunami." *Ocean Modeling* 40 (3–4): 246–59. https://doi.org/10.1016/j.ocemod.2011.09.005.